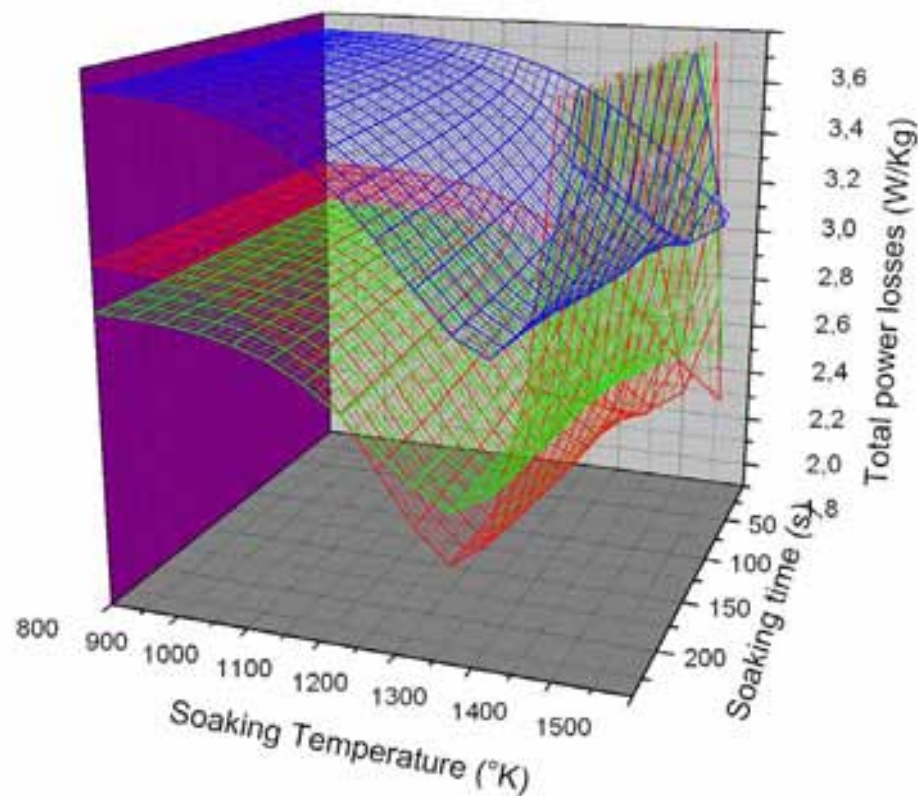




Study of the Influence of Grain Size and Precipitates on the Electromagnetic Losses in different grades of Non-Oriented Fully Processed Electrical Steel



Speciality: **Engineering of Materials**

Director: **Dra M^a Dolors Baró**

Author: **Margarita Miranda**

Co-Director: **Marc De Wulf**

February, 2008

Dolors Baró Mariné, Catedràtica de Física Aplicada del Departament de Física de la Universitat Autònoma de Barcelona.

FA CONSTAR:

Que ha fet el seguiment mitjançant tutories del treball de final de carrera concloent a la titulació d' Enginyeria de Materials titulat "Study of the influence of grain size and precipitates in different grades of non-oriented fully processed electrical steel" de l'alumna Margarita Miranda.

Al mateix temps considerem que és apte i autoritzem la seva presentació i posterior defensa.

I per què així consti, signem el present escrit.

M. D. Baró

Bellaterra, 24 de gener de 2008

OCAS NV

John Kennedylaan 3

B-9060 Zelzate

Tel : +32 9 345.12.11

Fax: +32 9 345.12.04

www.ocas.be

Zelzate, 28 January 2008

CERTIFICATION FOR PROJECT PRESENTATION AND DEFENCE

Margarita Miranda De La Torre has been working in OCAS on the project "Study of the influence of grain size and precipitates in different grades of non-oriented fully processed electrical steels."

She was closely followed-up and supervised, and meetings on a regular basis showed that she was progressing very well with this project.

I consider that Margarita is suitable and well prepared, and I hereby authorize her presentation and the subsequent defence.



Marc De Wulf
Program Manager Electrical Steels

AGREEMENTS

This work has been done with the collaboration of all the people of the Steel Researcher Center in Gent, OCAS, especially **Marc De Wulf** and **Daniel Ruiz Romera** from the Substrates and Metallic Coatings Development Departament, who were in continuous dedication, and **Chris Xoffer**, giving the TEM lessons. Moreover, I have to be agreed with **Wahib Saikaly**, from the Centre Pluridisciplinaire de Microscopie électronique et de Microanalyse, in the Faculté des Sciences de Saint Jérôme, in Marseille, for the TEM technical support. Previous knowledge about microscopy was acquired in the Servei de Microscòpia de la Universitat Autònoma de Barcelona, with **Emma Rossinyol**. Finally, this work would not be possible without the collaboration of **M^a Dolors Baró**, project director, whom I am agreed very much for this opportunity.

The project is dedicated to my parents, my brothers and my boyfriend, who were together with me during all the way of my degree.

Margarita Miranda de la Torre, 2008

MEMORY

MEMORY INDEX:

1. INTRODUCTION	3
2. SAMPLE IDENTIFICATION	6
2.1. Samples with different annealing parameters (grain size analysis)	6
2.2. Samples of different composition to analysis precipitates	8
3. METODOLOGY	10
3.1. Thermal treatments	10
3.2. Measurements of grain size	10
3.2.1. Sample preparation for metallography	10
3.2.2. Optical microscope observation	12
3.2.3. Intercept procedure	12
3.2.4. Statistics of grain size	15
3.3. Precipitates characterization	20
3.3.1. Sample preparation for TEM	20
3.3.2. Transmission Electron Microscope observation	28
3.4. Measurement of magnetic properties and loss separation	30
3.4.1. Total energy losses (P_{tot})	30
3.4.2. Quasi-static hysteresis losses (P_{hys})	31
3.4.3. Classical Foucault losses (P_F)	31
3.4.4. Excess losses (P_e)	32
3.4.5. Magnetic induction (B)	32
4. RESULTS AND DISCUSSION	33
4.1. Grain size as a function of annealing parameters. Grain size modelling	33
4.1.1. Soaking temperature	33
4.1.2. Soaking time	34
4.1.3. Grain size modelling	38
4.2. Effect of grain size on magnetic induction	42
4.3. Foucault losses, Hysteresis losses and Excess losses in function of grain size	45
4.3.1. Foucault losses	45
4.3.2. Hysteresis losses	47
4.3.3. Excess losses	48
4.3.4. Total power losses	49
4.4. Optimum annealing parameters	50
4.4.1. Effect of grain size on total power losses	50
4.4.2. Optimum annealing parameters	51
4.4.3. Total power losses as a function of annealing parameters	53
4.5. The role of precipitates on grain size and power losses	55
4.5.1. Effect of precipitates on grain size	56
4.5.2. Effect of precipitates on power losses	60
4.5.3. Effect of steel composition	62
4.5.4. Precipitates observations by TEM	66
5. SUMMARY AND CONCLUSIONS	76
6. BIBLIOGRAPHIC REFERENCES	78

APPENDICE INDEX:

1. Results of grain size.....	81
2. Correlations ASTM number for uniform, randomly oriented and equiaxed grains.....	94
3. Statistical results for grain size.....	96
4. Marseille TEM images.....	100
5. Guide for TEM observation procedures.....	144
6. Photographic gallery.....	148

1. INTRODUCTION

The development of new steel grades is one of the main goals of ArcelorMittal. The material under study is non-oriented fully processed electrical steel (soft ferromagnetic material). Steels for electrical use are important materials with relevance for industry. Non-oriented fully processed electrical steels are iron-silicon alloys that have similar magnetic properties in all directions in the plane of the sheet (Ref. 1). Particularly, the material is a high magnetic efficiency steel, with a very low magnetic losses level. This kind of steel is used mainly in electrical engines and transformers in a lot of electrical devices. Its function in electrical engines is to amplify the magnetic field. Thus, the magnetization forces and the engine power increase. Because the engine is magnetized and demagnetized 60-400 times per second, depending on the frequency applied, the steel gets strongly heated. The magnetic energy is transformed in thermal energy and dissipated. This effect is not desirable in the behavior of electrical engines, and it is called magnetic hysteresis losses (Ref. 2).

In order to certificate the electrical steel quality, the maximum hysteresis losses values are established in EN 10106:95 standard. There is a difference between the guaranteed maximum loss of the steel grade ordered and the typical loss of the steel supplied. All the relations between the losses and the different parameters affecting the material should be studied in order to reduce this difference. In this report, an overview of the results concerning microstructural properties (grain size and precipitates) and magnetic properties is given. The power loss in the behavior of non-oriented electrical steel is strongly influenced by microstructural features, such as grain size, precipitates, or inclusions. There are other important parameters like the material composition or the material texture, not included in the range of the present report.

The prediction of magnetic properties is connected with the grain size and shape, and with the grain boundaries movement, it means, with the grain growth process (Ref. 3). In addition, the diameter, shape and composition of precipitates can have influence also in the movement of domain walls, it means, in the power losses. During the magnetization of electrical steels, both grain boundaries and precipitates are a barrier to the movement of the domain walls. Grain boundaries and precipitates inhibit the rotation of magnetic vectors and increase the power losses. Consequently, a maximum grain size and a minimum precipitates level are desirable. (Ref. 4) For a similar grain size, the losses differences could be explain with a study of precipitates.

The most important parameters on the final power losses of electrical steels are related to the microstructure, especially to the grain boundaries and precipitates. The relations between magnetic losses and both microstructural properties have been attempted to explain. The presence of precipitates and grain boundaries restrain the movement of domain walls and increase the magnetic losses. In addition, precipitates and grain size are related due to the fact that fine precipitates can hinder the grain growth. All these features are closely linked to the processing parameters.

The mentioned characteristics are directly linked to the processing parameters. To produce thin sheets of steel with the minimum core loss, a carefully processing should be carried. The steel sheet is unrolled from the coil, annealed, varnished, and re-coiled, all in a continuous process. During this process various parameters such as temperature, speed, etc. affect the electromagnetic properties of the final product (Ref. 5). The reduced losses achieved are mainly a result of a modified final annealing cycle (Ref. 3). Sixty samples had been given varying annealing parameters in order to simulate continuous annealing conditions on the product line.

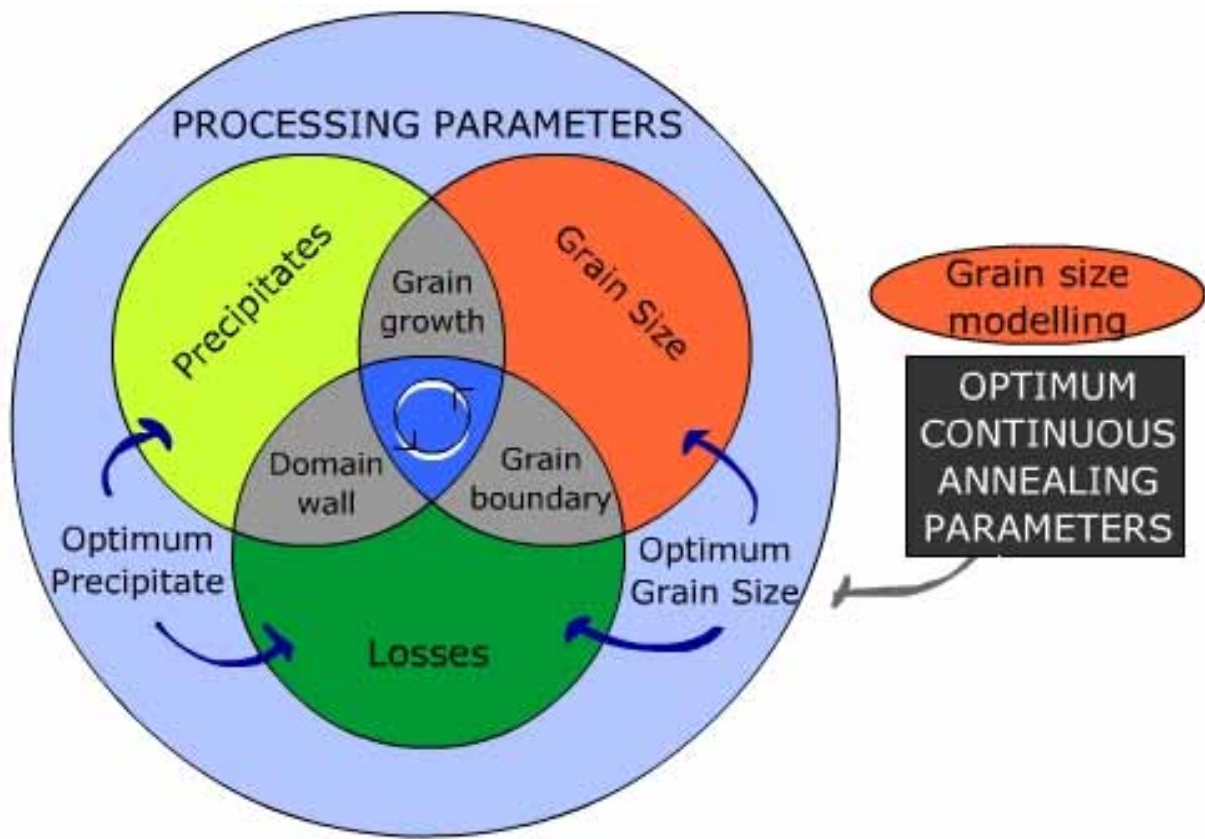


Fig. 1: Scheme of different properties affecting the final electrical steel quality.

2. SAMPLE IDENTIFICATION

2.1. Samples with different annealing parameters (grain size analysis)

The characterized materials were produced in St-Chély and their main properties are displayed in Table 1. They are fully processed electrical steels based on the M32 chemical composition, cold rolled down to three different thickness, and continuous annealed with different parameters (soaking time and line speed) (Table 2).

An overview of the processing history of the samples is given by Fig. 2. After continuous casting, the slab is reheated at between 1100 and 1200°C (slab reheating). Then it is hot rolled down to 2mm and coiled. Hot band annealing, or batch annealing at 800°C is carried out afterwards. An additional annealing cycle prior to cold rolling has the effect to producing a more homogeneous microstructure. (Ref. 4).The following step is to cold roll the strip down to the desired thickness (0.35, 0.50 and 0.65mm). After cold rolling, the coil is subjected to continuous annealing treatment. The treatments have been applied during different conditions.

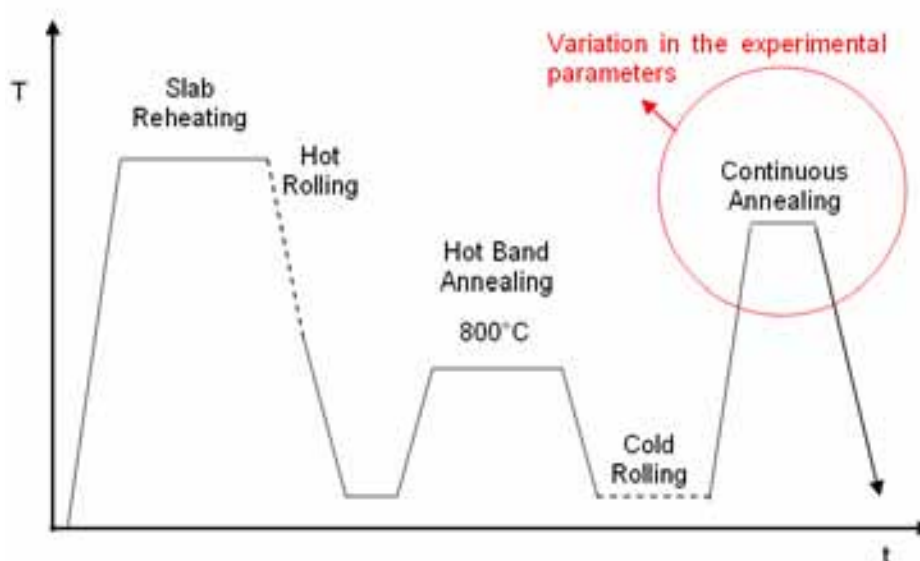


Fig. 2: Processing diagram

Sample	Thickness (mm)	EN 10106:1995	Composition (M32)
F01514	0,35	M 235-35 A AFCS	3.25% Si 0.92% Al 0.19% Mn
F01494	0,50	M 250-50 A AFCS	
F98843	0,65	M 310-65 A AFCS	

Table 1: Samples characterized for grain size analysis

Annealing temperatures (°C)	Annealing times (s)	Annealing speed (m/min)
950	120	25
1000	100	30
1020	80	35
1050	60	40
	40	50

Table 2: Test parameters

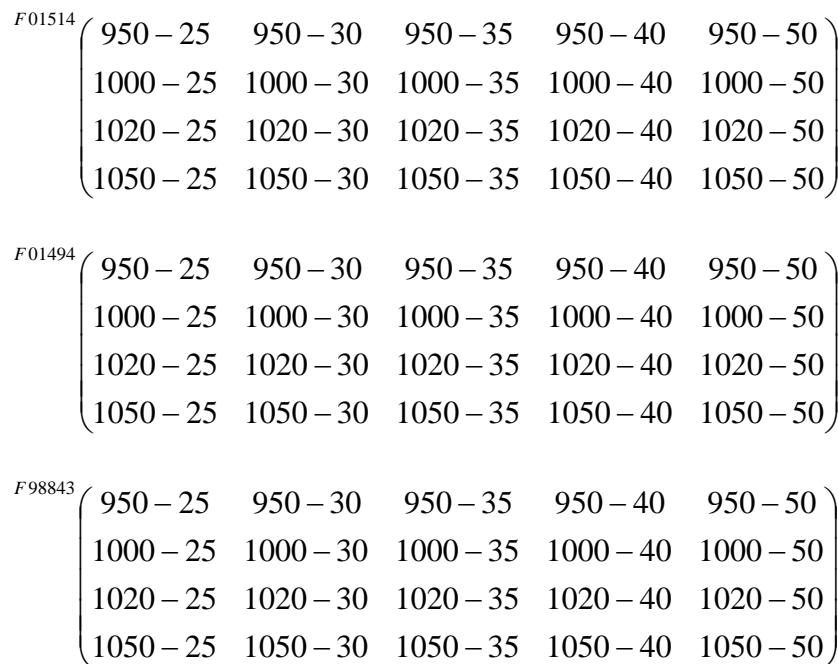
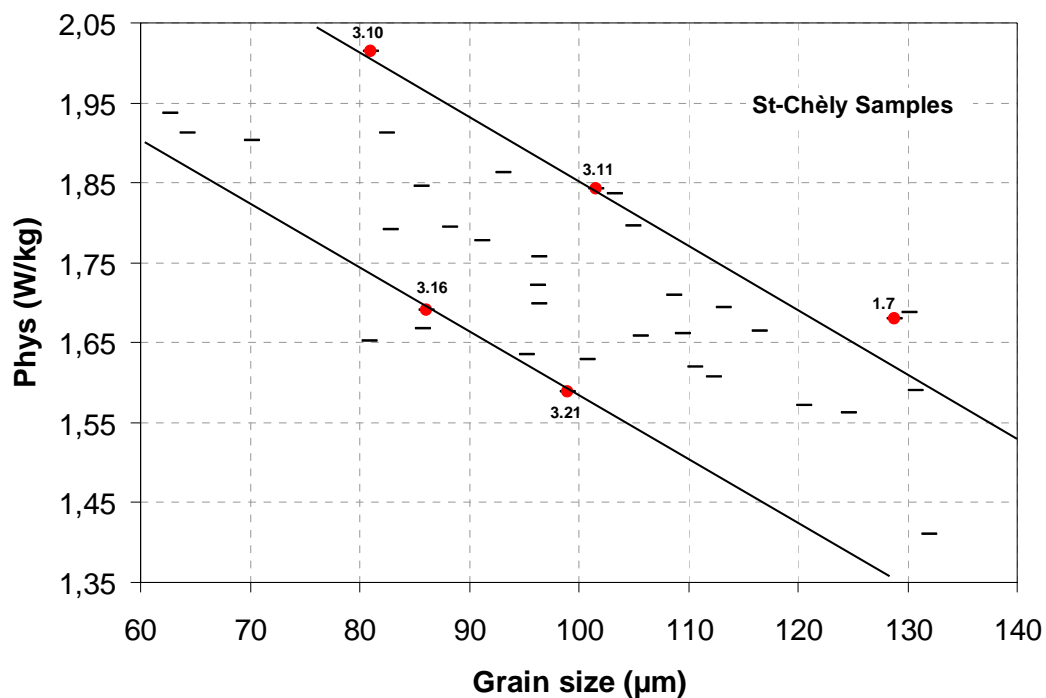


Fig. 3: Representative matrix of test samples for 0.35, 0.50 and 0.65 mm.

2.2. Samples of different composition to analysis precipitates

Five samples of a M250-50 electrical steel grade (0.5 mm thick) were selected in order to make a precipitates characterization. The reasons to choose these samples come from Graph 1. For an equal grain size, differences in hysteresis loss of up to 0.3 W/kg are seen. The chemical composition and the texture of these samples are rather similar so we might expect precipitates to be the reason for this strong variation.



Graph 1: St Chély samples analysis of hysteresis losses and grain size

These samples come from finished coiled produced in St-Chély. Their chemical composition and the main properties are shown in Table 3. The composition analysis was made in OCAS (Ref. 6).

Sample	Thickness (mm)	Hysteresis losses (W/Kg)	Alloys ¹ (ppm)			Characteristics	EN 10106:1995	Comp
			C	Ti	N			
F00790A (3.11)	0,50	1.84	35	147	10	High titanium, high loss	M 250-50 A AFCS	3.2%Si 0.9%Al 0.2%Mn
F99406D (3.21)	0,50	1.59	23	70	14	Low titanium, low loss		
F94266A (1.7)	0,50	1.68	31	85	21	High nitrogen, high loss		
F00712A (3.10)	0,50	2.02	45	86	14	High titanium, high sulphur, high loss		
F00440B (3.16)	0,50	1.69	25	67	14	Low titanium, low sulphur, low loss		

Table 3: Samples selected for precipitates analysis

¹ The exact composition is not available for commercial protection reasons.

3. METODOLOGY

3.1. Thermal treatments

Continuous annealing treatments were performed using a pilot line, at St-Chély installations, France. The device consists in a furnace, which is provided by different heating zones to simulate the industrial process.

3.2. Measurements of grain size

The grain size measurements were performed following the ASTM E 112-96 standard with the lineal intercept method (Ref. 7).

To determine grain size, a cross section across the longitudinal section was examined using optical microscopy. The samples were embedded, polished and etched with Nital 4% during approximately 8 seconds in order to get all the grain boundaries visible. The sample preparation is explained because the small thickness and the high silicon composition of this kind of materials make difficult a good sample preparation.

3.2.1. Sample preparation for metallography

The following methodology was used for thin samples with high silicon composition. The steps can be related in four steps:

- **CUTTING:** If the sample is thinner than 1.5 mm, it should be cut by the guillotine (Gerver). If not, it can be cut by the power saw (Struers).

- EMBEDDING: The sample is embedded in a special resin to give an easier manipulation. There were tried different ways to avoid any damage in the samples.

- *Cold embedding without pressure*: the samples were straight, but the resin was not fixed very well to the sample. This gave less quality in the pictures after etching.

- *Embedding without pressure with preheating*: is the best way to prepare this kind of samples. The preheating (140°C) is for 4 minutes without pressure. The heating is with 180°C (resin melting point) during 8.5 minutes, and the cooling is 4 minutes. In the heating and cooling the pressure is 15 kN, to fix the sample with the resin. The resin employed is "durofast".

- POLISHING: Firstly, the samples are grinded with plates of 80 and 220 numbers (grains of SiC by square inch). As a lubricant, water can be used. After each grinding step, the samples should be cleaned with water in order to avoid the contamination of the following plates. It is necessary also to clean the sample holder. Secondly, the samples are polished in three steps with water-solution of suspension diamond particles of sizes 9 µm, 3 µm and 1 µm consecutively. As a lubricant, DP-Lubricant Blue (Struers) is used. Even for better results, is suggested to make the last two steps of polishing with alcohol-based suspension solution and DP-Lubricant Yellow (Struers). In this case, the surface is cleaner, probably with less oxide contamination. After each polishing step, the samples must be cleaned with methanol, in order to avoid possible surface oxidation, dried with compressed air and finally softly cleaned with acetone.

- ETCHING: To avoid oxidation, the sample has to be etched immediately after polishing. The etching used is Nital (4%) and ethanol (96%). First it is etched during approx. 4 seconds and then the sample is turned in order to allow the etching to penetrate into the grain boundaries, approx. 3 seconds. The time of

etch exposure depends of the amount of aluminum. Higher %Al means more time to etch. After etching, the sample is cleaned with methanol and dried with compressed air. Finally, it is cleaned very soft with acetone, to remove possible stains produced with the methanol.

3.2.2. Optical microscope observation

Five different fields were analyzed for each sample using the same magnification (x160) with the optical microscope, *Reichert Jung*.

The pictures were printed and carefully examined following the intercept procedure.

3.2.3. Intercept procedure

There are three basic procedures for grain size estimation of a metals consisting of a single phase: comparison, planimetric and intercept procedure. For higher degrees of accuracy in determining average grain size, the intercept or planimetric procedures may be used. (Ref. 7)

The specimen should be large enough in area to permit measurement of at least five images at the desired magnification. Also has to show most of the grain boundaries.

In the intercept procedure, the average grain size is estimated by counting the number of grains intercepted by one or more straight lines sufficiently long to yield at least 50 intercepts. The precision of grain size estimates is a function of the number of grain interceptions counted.

When counting intercepts it should be following the follow rules:

- Segments at the end of a test line which penetrate into a grain are scored as a $\frac{1}{2}$ intercepts.
- When counting intersections, the end points of a test line are not intersections and are not counted except when the end appears to exactly touch a grain boundary. In this case should be scored $\frac{1}{2}$ intersections.
- A tangential intersection with a grain boundary should be scored as one intersection. An intersection apparently coinciding with the junction of three grains should be scored as $\frac{1}{2}$.

The information about grain size measurements is shown in the appendix 1.

The following procedure was used to the grain size calculus.

Linear length: $L = H + V + D1 + D2$ (mm)

Mean linear length: $\bar{L} = \frac{\sum X_i}{n} = \frac{\sum L_i}{5}$

Intersections number: $I = IH + IV + ID1 + ID2$

Mean intersection number: $\bar{I} = \frac{\sum X_i}{n} = \frac{\sum I_i}{5}$

Number of intercepts per unit length: $N_L = \frac{I}{L}$

Mean number of intercepts per unit length: $\bar{N}_L = \frac{\sum X_i}{n} = \frac{\sum N_{Li}}{5}$

Using these results the nominal diameter can be determined. It is in fact the distance between two interceptions:

Nominal diameter: $D_n = \frac{\bar{L}}{\bar{I}}$ ($\mu\text{m/int}$)

The relationship between the ASTM grain size number, G , and the mean lineal intercept procedure is the equation:

$$\text{ASTM number grain size: } G = -3,2877 + 6.643856 \log_{10}(\overline{N_L})$$

From here on, the mean diameter was calculated. This is the normalized distance between two grain boundaries. The equation corresponds with a regression obtained by the correlations between ASTM number for uniform, randomly oriented and equiaxed grains (appendix 2). This value is the grain size measured in μm , which is showed in the graphics of this report, and it corresponds with equiaxial grains.

$$\text{Mean diameter: } D_M = 359,08 \cdot \exp(-0.3464G)$$

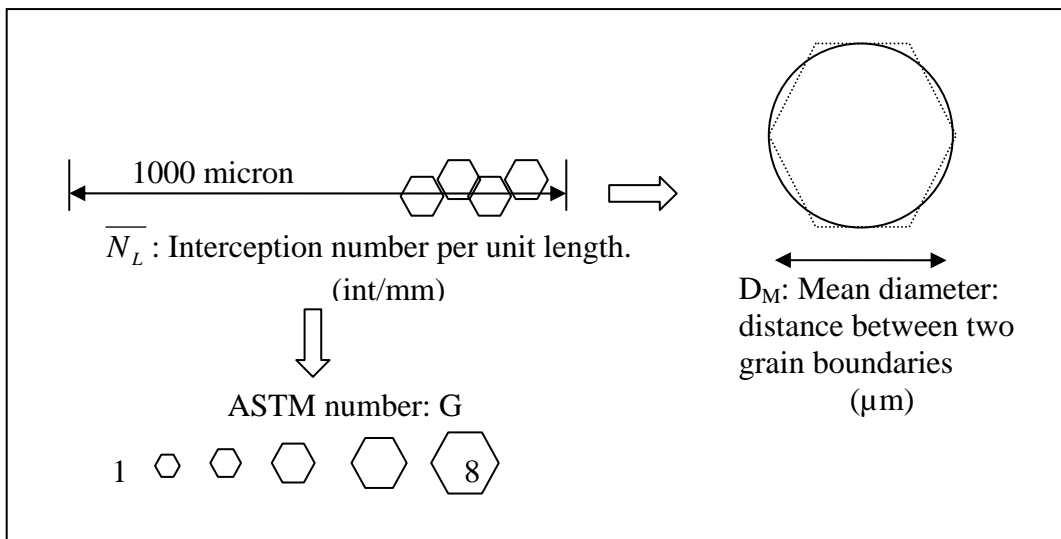
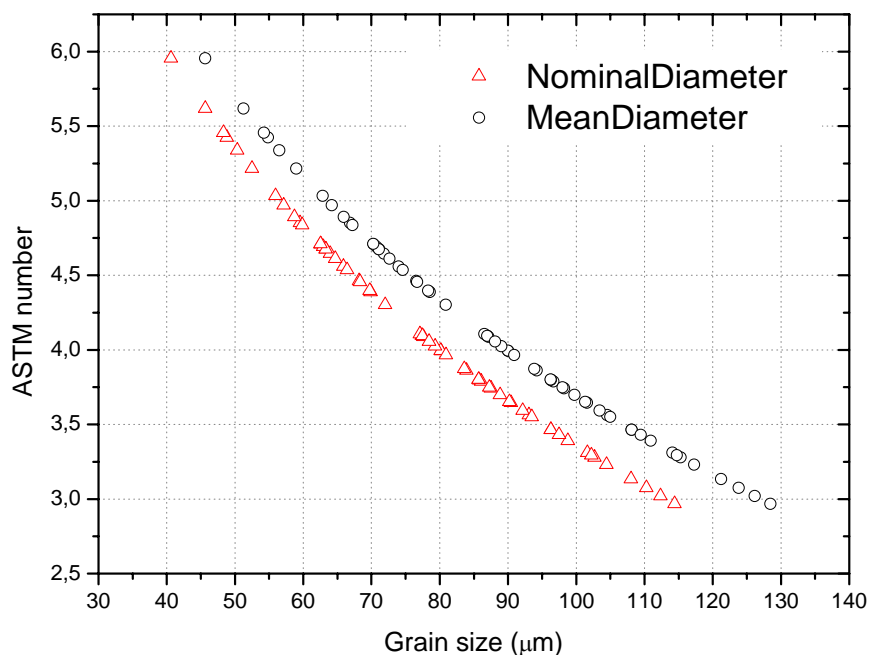


Fig. 4: Intercept procedure: relation between grain size and ASTM number

The mean diameter is always bigger than the nominal diameter, as is showed in Graph 2:



Graph 2: Comparison between nominal diameter and mean diameter

3.2.4. Statistics of grain size

3.2.4.1. According with ASTM standard

The estimation of average grain size is not a precise measurement. A metal structure is an aggregate of three dimensional crystals of varying sizes and shapes. As a general rule, a 10% of Relative Accuracy (or lower) is considered to be an acceptable precision. According with Ref. 7 ASTM E 112-96: Standard Test Methods for Determining Average Grain Size, the calculus of this parameter is made using the equations of Table 5.

For the intercept method, 10% RA (or less) is obtained with about 400 intercept or intersection counts. In our case, around 250 were counted. The mean number of interceptions per millimeter was statistically analyzed to determine the relative accuracy in the results obtained. In Table 4, the number of

interceptions scored per millimeter corresponds with the average for each sample. The value of relative accuracy mentioned (RA) changes between 23.56% and 2.39% (Appendix 3).

Sample F01514	0.35mm
Standard deviation	1,43
95% confidence interval	1,7761233
Percent relative accuracy, %RA	12,883521
Sample F01494	0.50mm
Standard deviation	1,2469185
95% confidence interval	1,5480838
Percent relative accuracy, %RA	12,072674
Sample F98843	0.65mm
Standard deviation	1,0157647
95% confidence interval	1,2610362
Percent relative accuracy, %RA	10,239496

Table 4: Percent relative accuracy in the number of interceptions scored per millimeter

Mean value of N_L	$\bar{X} = \frac{\sum X_i}{n}$																																				
Standard deviation	$s = \left[\frac{\sum (X_i - \bar{X})^2}{n-1} \right]^{1/2}$																																				
95% confidence interval	$95\% CI = \frac{t \cdot s}{\sqrt{n}}$																																				
	<table border="1"> <thead> <tr> <th>N° of fields, n</th> <th>t</th> <th>N° of fields, n</th> <th>t</th> </tr> </thead> <tbody> <tr> <td>5</td> <td>2.776</td> <td>13</td> <td>2.179</td> </tr> <tr> <td>6</td> <td>2.571</td> <td>14</td> <td>2.160</td> </tr> <tr> <td>7</td> <td>2.447</td> <td>15</td> <td>2.145</td> </tr> <tr> <td>8</td> <td>2.365</td> <td>16</td> <td>2.131</td> </tr> <tr> <td>9</td> <td>2.306</td> <td>17</td> <td>2.120</td> </tr> <tr> <td>10</td> <td>2.262</td> <td>18</td> <td>2.110</td> </tr> <tr> <td>11</td> <td>2.228</td> <td>19</td> <td>2.101</td> </tr> <tr> <td>12</td> <td>2.201</td> <td>20</td> <td>2.093</td> </tr> </tbody> </table>	N° of fields, n	t	N° of fields, n	t	5	2.776	13	2.179	6	2.571	14	2.160	7	2.447	15	2.145	8	2.365	16	2.131	9	2.306	17	2.120	10	2.262	18	2.110	11	2.228	19	2.101	12	2.201	20	2.093
	N° of fields, n	t	N° of fields, n	t																																	
	5	2.776	13	2.179																																	
	6	2.571	14	2.160																																	
	7	2.447	15	2.145																																	
	8	2.365	16	2.131																																	
	9	2.306	17	2.120																																	
	10	2.262	18	2.110																																	
	11	2.228	19	2.101																																	
12	2.201	20	2.093																																		
<i>95% CI multipliers, t</i>																																					
Percent relative accuracy, %RA	$\% RA = \frac{95\% CI}{\bar{X}} \cdot 100$																																				

Table 5: Statistical analysis

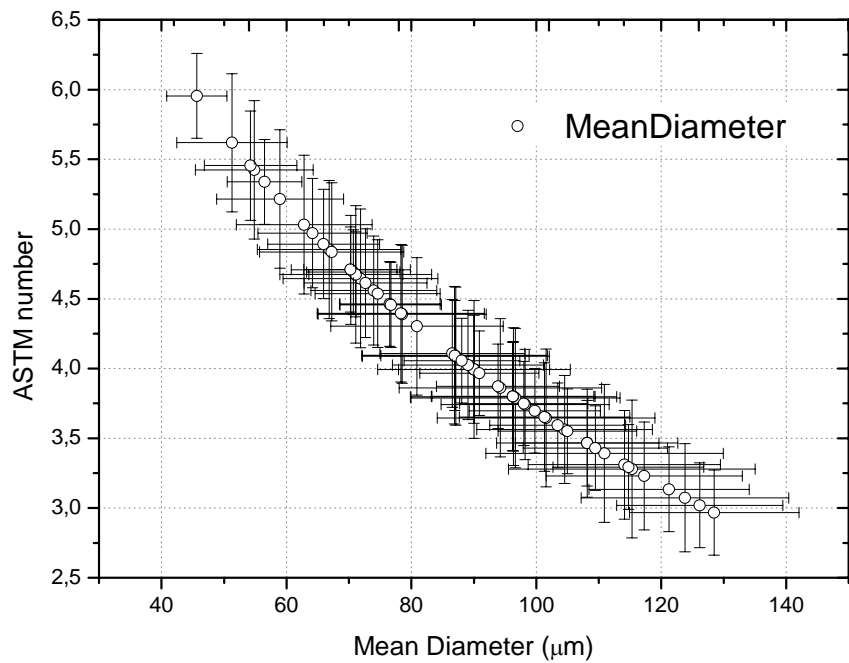
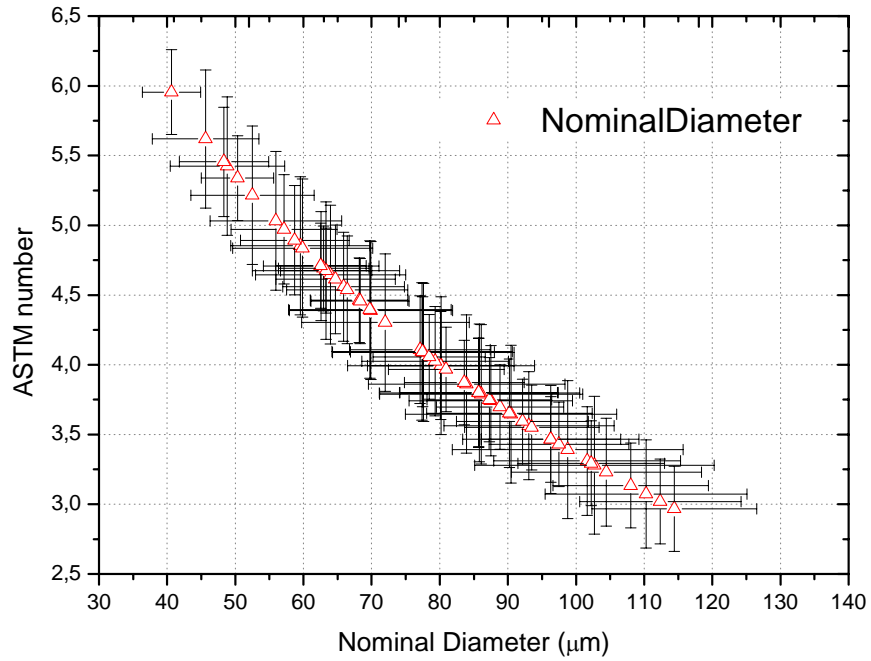
3.2.4.2. Calculated error

Using the propagated error formula, shown below, it is possible to calculate the error in the grain size value. In Table 6 is shown the maximum and the minimum deviation value. In order to give an accuracy range, the average for each thickness was calculated. The values of propagated error for each sample are shown in appendix 3.

$$F = F(x, y, z, \dots) \Rightarrow \Delta F = \sqrt{\left(\frac{\partial F}{\partial x} \cdot \Delta x\right)^2 + \left(\frac{\partial F}{\partial y} \cdot \Delta y\right)^2 + \left(\frac{\partial F}{\partial z} \cdot \Delta z\right)^2 + \dots}$$

sample		Nominal diameter (±ΔD _n) μm	ASTM grain size (±ΔG)	Mean diameter (±ΔD _M) μm
F01514	MAX	17,58	0,50	19,74
	MIN	7,84	0,49	8,83
	AVERAGE	12,39	0,50	13,92
F01494	MAX	14,81	0,39	16,61
	MIN	6,56	0,39	7,38
	AVERAGE	10,75	0,39	12,08
F98843	MAX	12,10	0,31	13,57
	MIN	4,29	0,30	4,83
	AVERAGE	8,71	0,30	9,78
TOTAL AVERAGE		10,62	0,40	11,93

Table 6: Calculated error results: mean values for each thickness



Graph 3: Statistical Results of Grain size: a) nominal diameter, b) mean diameter

3.3. Precipitates characterization

In order to characterize the precipitates, a comparison between different techniques of Transmission Electron Microscope sample preparation has been made (Table 7).

The samples were prepared using the carbon replica method, if thin foils are used, the magnetic properties of the material increase the beam deflection of the electron beam in the microscope. It means that the magnetic field of the sample degrades de image quality. A lower resolution in the micrographs is not desired, especially in the observation of the smallest precipitates ($\leq 10\text{nm}$). (Ref. 8, Ref. 9, Ref. 10)

Samples were also prepared in Marseille using electrochemical etching to remove the carbon layer. (Sample 3.21 and Sample grain oriented)

3.3.1. Sample preparation for TEM

A description of carbon replica sample preparation for Transmission Electron Microscope was made especially for the selected samples, which contains high-Si and posses a low thickness making the procedure especially difficult.

Table 8 is a summary of the parameters that has to be established for the preparation of the samples analyzed.

Technique	Preparation	Observation	Analysis results	Storage	
Thin foil by electrochemical etching	<ul style="list-style-type: none"> ✓ The sample can be prepared with simple equipments. ✓ Window technique: large thin area ✓ Electropolishing: Unnecessary stopping etching after perforation 	<ul style="list-style-type: none"> ✓ The sample microstructure is preserved 	<ul style="list-style-type: none"> ✓ Qualitative precipitates analysis: surface observation 	<ul style="list-style-type: none"> ✓ Sample robustness ✓ Possibility of re-etching 	✓
	<ul style="list-style-type: none"> * Chemical etching: Necessary stopping etching after perforation. * Necessary to begin with a thin piece of material (<100µm). A lot of prepolishing. * Not easy determination of the etching parameters 	<ul style="list-style-type: none"> * Necessary to achieve a thickness less than 50nm * Very high thickness * Topography roughness * Unsuitable for ferromagnetic materials, because of the magnetic field of the specimen the electron beam is deflected and resolution is degraded. 	<ul style="list-style-type: none"> * The precipitates shape can be changed by the etching * Some precipitates can be dissolved by the etching * Strongly oxidizing etchings can change the particles composition. * Due to the sample size, it is not possible the quantitative analysis 	<ul style="list-style-type: none"> * Surface oxidation * They have to be stored in a vacuum desiccator or in liquid free of water 	*
Thin foil by FIB	<ul style="list-style-type: none"> ✓ Fast 	<ul style="list-style-type: none"> ✓ The sample microstructure is preserved ✓ High homogeneity through the thickness 	<ul style="list-style-type: none"> ✓ Qualitative precipitates analysis: surface observation ✓ Due to homogeneity throughout the thickness is possible the quantitative analysis 	<ul style="list-style-type: none"> ✓ Sample robustness ✓ Re-thinning possible 	✓
	<ul style="list-style-type: none"> * Special equipment necessary 	<ul style="list-style-type: none"> * Unsuitable for ferromagnetic materials, because of the magnetic field of the specimen the electron beam is deflected and resolution is degraded. 	<ul style="list-style-type: none"> * May occur specimen heating, ion damage or ion implantation in the sample surface 	<ul style="list-style-type: none"> * Surface oxidation * They have to be stored in a vacuum desiccator or in liquid free of water 	*
Thin foil by PIPS	<ul style="list-style-type: none"> ✓ The sample can be prepared in the first steps with simple equipments. 	<ul style="list-style-type: none"> ✓ The sample microstructure is preserved 	<ul style="list-style-type: none"> ✓ Qualitative precipitates analysis: surface observation 	<ul style="list-style-type: none"> ✓ Sample robustness ✓ Re-thinning possible 	✓
	<ul style="list-style-type: none"> * Special equipment necessary * Necessary to begin with a thin piece of material (<20µm). A lot of prepolishing. * Not easy determination of the etching parameters 	<ul style="list-style-type: none"> * Necessary to achieve a thickness lower than 50nm * High thickness * Topography roughness * Unsuitable for ferromagnetic materials, because of the magnetic field of the specimen the electron beam is deflected and resolution is degraded. 	<ul style="list-style-type: none"> * May occur specimen heating, ion damage or ion implantation in the sample surface * Due to the sample size, is not possible the quantitative analysis 	<ul style="list-style-type: none"> * Surface oxidation * They have to be stored in a vacuum desiccator or in liquid free of water 	*
Carbon replicas	<ul style="list-style-type: none"> ✓ The sample can be prepared with simple equipments. 	<ul style="list-style-type: none"> ✓ Low thickness ✓ Good resolution at high magnification 	<ul style="list-style-type: none"> ✓ Qualitative precipitates analysis ✓ In some cases it is possible the quantitative analysis 	<ul style="list-style-type: none"> ✓ Sample durability. 	✓
	<ul style="list-style-type: none"> * Not easy determination of the etching parameters * Strongly oxidizing etchings can change the particles composition. 	<ul style="list-style-type: none"> * The sample microstructure is not always preserved * Carbide precipitates difficult to analyze. * Not possible to see the matrix. 	<ul style="list-style-type: none"> * Due to precipitates deep removed in the etching, and the sample size, only is possible the qualitative analysis * The precipitates shape can be changed by the etching * Some precipitates can be dissolved by the etching 	<ul style="list-style-type: none"> * Sample robustness 	*

Table 7: TEM sample preparation comparison for precipitates analysis in electrical steels

<p>Power saw or Guillotine</p> <p>Angle: depends of the material</p> <p>Velocity: depends of the material</p> <p>Size</p>
<p>Micrometer</p>
<p>Embedding</p> <p>Bakelite diameter</p> <p>Resin</p> <p>Preheating temperature, time and force</p> <p>Heating temperature, time and force time</p> <p>Cooling temperature, time and force</p>
<p>Polishing</p> <p>Suspension and lubricant: alcohol or water based</p> <p>Plate: (special for TEM)</p> <p>Steps to grind: normally 80 and 220</p> <p>Steps to polish: normally 9, 3 and 1 μm</p> <p>Time in each step</p> <p>Force in each step</p>
<p>Etching</p> <p>Reactive solution</p> <p>Time etching</p>
<p>Carbon evaporator</p> <p>Carbon thickness desired</p> <p>Voltage</p> <p>Emission</p> <p>Deposition rate</p>
<p>Electrochemical etching (to remove the carbon replica)</p> <p>Electrolyte</p> <p>Current</p> <p>voltage</p> <p>Time etching</p>
<p>Chemical etching (to remove the carbon replica)</p> <p>Reactive solution</p> <p>Time etching</p>

Table 8: Equipment and parameters used for the carbon replica preparation

CUTTING

The first step is to measure the thickness of the sample with a micrometer. It is important to take the replica in the middle of the sample.

A guillotine (*Gerver*) was used to cut the samples, with 90° angles. This was possible due to the fact that the samples thickness was lower than 1.5mm. If the samples are thicker, it should be cut by another guillotine (*LVD*), using 91.5° angles, not to damage the guillotine edge.

The size of the samples has to be bigger than 1 cm x 1 cm, due to the etching equipment. It should not be very big for an easier manipulation. A suitable size is 1.5cm x 1.5cm.

EMBEDDING

To embed the sample a special program is used with a special resin. The sample is placed to analyze the longitudinal section, taken free the big area of the sample (not the cross section like in the grain size samples). Due to the thickness of the samples, they have to be stuck to another piece of thicker material; otherwise, it can be lost in the grinding step. The used sticker is thermosetting and it should be during 30 min at 180°C in a furnace (*Memmert*)

The embedding machine is ProntoPress-10, of *Struers*. It used the following parameters to the thin samples with transparent resin (*Specifast*, of *Struers*): without preheating, the samples of 30mm diameter are heating with 180°C (resin melting point) during 6 minutes. The pressure is 20KN. After this, the cooling is 8 minutes at a slow rate.

GRINDING AND POLISHING

The final surface has to be specular (mirrorlike). The follow steps in the polishing machine (Multidoser, of *Struers*) are necessary for that purpose:

Grinding:

Grind with plates of 80 and 220 number (grains of SiC by square inch) for approx. 3 min each one. It depends on the sample thickness because it should be removed until de middle of the sample. In our case, due to the thickness we use the first steps only to remove the superficial surface of the samples. The pressure in the sample holder arm must be approximately 30 N. As lubricant and refrigerant, water can be used. After each grinding step, the samples should be cleaned with water in order to avoid contamination from the nearby plates. It is also necessary to clean the sample holder. For these steps, another automatically polishing machine can be used, *Prepamatic* of *Struers*.

Polishing:

To avoid contaminating samples with external particles, new polishing plates should be used. It is necessary to polish in three steps with a water based solution of suspension diamond particles of sizes 9, 3 and 1 μm consecutively. As a lubricant and refrigerant, DP-Lubricant Blue (*Struers*) is used. After each polishing step, the samples must be cleaned with methanol, in order to avoid possible surface oxidation, dried with compressed air and finally softly cleaned with acetone. The time and the force are the same than before, 30 N, 3 minutes.

ETCHING

To avoid oxidation, the sample has to be etched immediately after polishing. The solution used is HNO₃ (Nital) (4%) and ethanol (96%). First, it is etched during approx. 4 seconds and then the sample is turned in order to allow the etching to penetrate into the grain boundaries, approx. 3 seconds.

The time of etch exposure depends of the amount of aluminum. Higher %Al means more time to etch. After etching, the sample is cleaned with methanol and dried with compressed air. Finally, it is cleaned very soft with acetone, to remove possible stains produced with the methanol.

It is important to note that Nital can dissolve the MnS precipitates for very long exposure times.

When the sample is ready, it should be removed from the bakelite. This step can be performed by a small electrical saw. The transparent resin makes visible the sample and therefore the process easier.

CARBON LAYER DEPOSITION

The carbon deposition is made with a carbon evaporator (*BAL-TEC MED 020 Coating System*). This equipment should be cleaned every two times. It is also necessary to put the carbon bar in the middle of the filament to obtain a correct flow.

Sometimes it is important to cover with a carbon layer only a specific sample area. In this case, it is possible to put tape on the rest of the sample.

One time the sample is inside, the steps to follow are:

- 1- Start
- 2- Make vacuum during 5-10 min., until approx. 5.9×10^{-5} bars, pressing the “pump/vent” button.
- 3- Start to turn the sample with a medium speed. In our case, it has to keep pressed the “rotary on” button until two lines.
- 4- Select program 1 in the screen.
- 5- Select carbon, C, in the screen, and the thickness desired. In our case it is necessary between 10-20 nanometers (100-200Å).
- 6- Switch on the power turning to ON, and move the selectors of “voltage” until approximately 1.75 and “emission” until approx. 0.74.
- 7- Push the button “process on” and immediately, push “measure”
- 8- Move the selectors “voltage” and “emission” to change the deposition rate until 0.2-0.3 nm/sec, and wait.
- 9- Move the selectors of “voltage” until approximately 1.75 and “emission” until approx. 0.74, to come back to the initial situation, and switch off the power turning to OFF.
- 10- Stop to turn the sample pressing “rotary off” button.
- 11- Break the vacuum pressing “pump/vent” and “full speed”.
- 12- Switch off.

REMOVING THE CARBON LAYER

Before remove the carbon layer is strongly recommended to make some scratches in the layer. It will become easier to remove the different pieces done. The removing can be done by two different ways:

a- electrochemical etching

Feed source (*EHQ PS 3003 Power Supply*) is necessary to provide the current and the voltage to the sample. The device used to hold the sample is a simple construction where the cathode is a stainless steel bar and the anode is the sample. The red contact is linked with the sample, and the black contact with the stainless steel bar. Between the anode and the cathode, has to be the electrolyte, in this case three-ethanolamine, which is added with a pipette. One time prepared, the steps are the following:

- Turn the current selector completely to the left (minimum)
- Turn the voltage selector completely to the right (maximum)
- Increase the current until 0.05 and 0.01A. If the current is very high, the attack can be too much hard and the carbon layer breaks.
- The voltage obtained has to be around the value 6.6v (for 0.02A), depends of the current.
- Switch on the feed source (Power on). Since this moment, is possible to see the reaction. The iron is dissolved, and the precipitates stay in the carbon layer. When carbon particles are floating in the solution, means that the etching has being done.



- Time etching is determinate in function of the material. To achieve big depths, are used long times possible.
- Switch off the feed source (Power off).
- With the pipette, is removed the electrolyte within the carbon layers.
- Clean all the components to the next etching.

b- chemical etching

The sample with the carbon layer is submerged in a reactive solution, in this case Nital 4% during a time between 10 minutes and 2 hours. Due to the Nital can dissolve MnS precipitates, should be used the shortest time possible.

CLEAN AND STORAGE

Using a grid and tweezers, the carbon layers (at least three of each sample) are taken out from the solution (three-ethanolamine or Nital) and transported to a methanol solution. They should be inside during 10 minutes approximately. After this, the layers are transported to another solution of methanol, to give a better cleanness.

After few minutes, the samples are submerged in distilled water, and they become flat layers. In this moment, they are picked in a grid, trying to leave them in the middle of the grid.

The grid is dried with high-dry paper and can be stored.

3.3.2. Transmission Electron Microscope observation

The precipitate observations were made by means of different Transmission Electron Microscopes. Main results were reached from 5 full-days measurements at the Centre Pluridisciplinaire de Microscopie électronique et de Microanalyse, in the Faculté des Sciences de Saint Jérôme (Université d'Aix Marseille). The analyzed samples and used microscopes are summarized in Table 9.

Place	Microscope	Techniques	Observed Samples
OCAS	TEM JEOL 2010	-EDX ² diagrams for composition	F00790A and F99406D
MARSEILLE	TEM JEOL 2010F	-EELS ³ diagrams for composition analysis -High resolution micrographs -FTT ⁴ analysis	F00790A F99406D F99406D ⁵ F94266A
	TEM TECNAI	-EDX diagrams for composition analysis -High resolution micrographs -Scanning micrographs	F00712A F00440B Grain oriented ⁶

Table 9: Different techniques applied to precipitates characterization

Artefacts were sometimes found in the observations probably from the sample preparation (diamond particles from the polishing).

In all EDX analysis, copper from the replica holder was detected, and silicon from the carbon evaporator.

In the replica prepared in Marseille, by chemical etching, the precipitates are more dispersed in, and there are less precipitates accumulations.

A short guide of the TEM observation procedures is given for the samples observed at OCAS (Appendix 4).

² Electron Diffraction Spectroscopy

³ Electron Energy Loss Spectra.

⁴ Fourier Function Transform

⁵ Prepared in Marseille

⁶ Prepared in Marseille

3.4. Measurement of magnetic properties and loss separation

These measurements were made at OCAS (Ref. 11). All used equipment was calibrated. The power losses measured corresponds with P15 value. This is the power losses for a frequency of 50 Hz, and an induction of 1.5 Tesla.

The test method is according the IEC norm 60404-3. The samples are inserted inside two coils: the primary coil consists of 700 windings (n_1), the secondary coil of 700 windings (n_2). The proceedings to determine the different magnetic losses are explained following:

3.4.1. Total energy losses (P_{tot})

These losses correspond with the area inside the hysteresis loop. In this curve, it is represented the magnetic induction (B) as a function of the Magnetic field applied (H). The rotation of magnetic domain when H is applied means energy consumption and it corresponds with the hysteresis loss.

The magnetic field H in the material is obtained by controlling the primary winding current (measured by means of a low inductive resistor). In the conversion of the applied current (i) towards the magnetic field (H), the number of windings (n_1) and the magnetic path length (L_g) are used. L_g is a constant obtained in the equipment calibration.

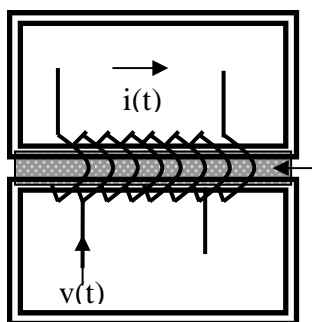


Fig. 5: Schematic draw of the magnetic measurements

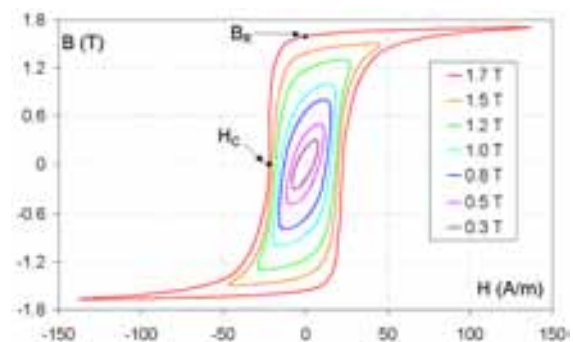


Fig. 6: Schematic hysteresis loop for different frequencies

The integral value of the secondary voltage is related to the induction level B in the material. In the conversion from the analogue integrator signal towards the $B(t)$, the number of windings (n_2), the time constant of the integrator and the active cross sectional area of the material (s) should be taken into account:

$$B = \frac{1}{s \cdot n_2} \int v(t) dt \quad H = \frac{i \cdot n_1}{L_g}$$

Finally, special software draws the hysteresis curve and calculates the internal area of the loops, for a 1.5T value of induction, giving the result of the total power losses in W/Kg, P15.

3.4.2. Quasi-static hysteresis losses (P_{hys})

These losses P_{hys} (W/Kg) were measured by using a quasi-static field excitation. It means that the voltage is applied with a very low frequency (0.5Hz). In this way, the magnetic losses are not frequency dependent.

3.4.3. Classical Foucault losses (P_F)

The classical Eddy current Foucault losses P_F (W/Kg) are computed in function of the thickness, the chemical composition, the electrical conductivity and the density of the samples according with the equations:

$$P_F = \frac{\pi^2}{6} \cdot \frac{1}{\rho} \cdot t^2 \cdot B^2 \cdot f^2 \cdot \frac{1}{d}$$

t = thickness

ρ = resistivity = 55 Ω /cm

B = induction, B = 1.5 T

f = frequency, f = 50 Hz

d = density=cte=7550 Kg/m³

$$\rho = 11.44 + 11.9\% Si + 11.1\% Al + 6.3\% Mn + ..$$

$$d = 7865 - 65(\% Si + 1,7\% Al)$$

3.4.4. Excess losses (P_e)

The excess losses are a function of the induction and the frequency and are computed according to the previous losses showed, through the equation:

$$P_e = P_{tot} - P_{hys} - P_F$$

3.4.5. Magnetic induction (B)

The measurements of magnetic induction were performed in St-Chély factory.

4. RESULTS AND DISCUSSION

4.1. Grain size as a function of annealing parameters. Grain size modelling.

The experimental results show that the highest temperature and the longest time of continuous annealing give the bigger grain size for the observed samples. In addition, the grain size is also bigger for thicker materials, as expected.

4.1.1. Soaking temperature

The behaviour of the grain size as a function of the annealing temperature is plotted in Graph 4. In this case, the maximum grain size is reached for the highest temperature. This behaviour was expected, since the energy applied at higher temperature allows a larger grain growth. The same occurs due to the thickness of the sample. For each thickness, the percent of reduction is different. The influence on the grain size is quite important, having the 0.65mm sample the largest grain size and the 0.35mm the lowest. The number of nucleus is dependent of the reduction percent, because a high applied energy allows more nucleation. Then, an elevated number of nucleus mean that during the growth, they will disturb between them resulting a lower grain size. This effect is noted specially at high annealing temperatures, when the growth is larger. Also the surface of the samples stops the grain growth limiting the biggest grain size. It is due to the boundary movement at the surface means a very high energy condition. A higher thickness permits a bigger grain growth, because otherwise the surface or the material picks the grain boundaries, stopping the growth. The energy of external surfaces may be an important factor in grain growth in thin sheets. (Ref. 12)

4.1.2. Soaking time

The samples were treated at five different annealing speeds. This is equivalent to five different soaking times. In Table 10, the relation between the line speed and the time used is shown.

In Graph 4, the points describes exponential functions, and the grain size is bigger as longer the thermal treatment is. This result was expected, because a longer time at high temperature means longer time for grain growth.

Line speed (m/min)	Soaking time (s)
25	120
30	100
35	80
40	60
50	40

Table 10: Equivalences between line speed and soaking time

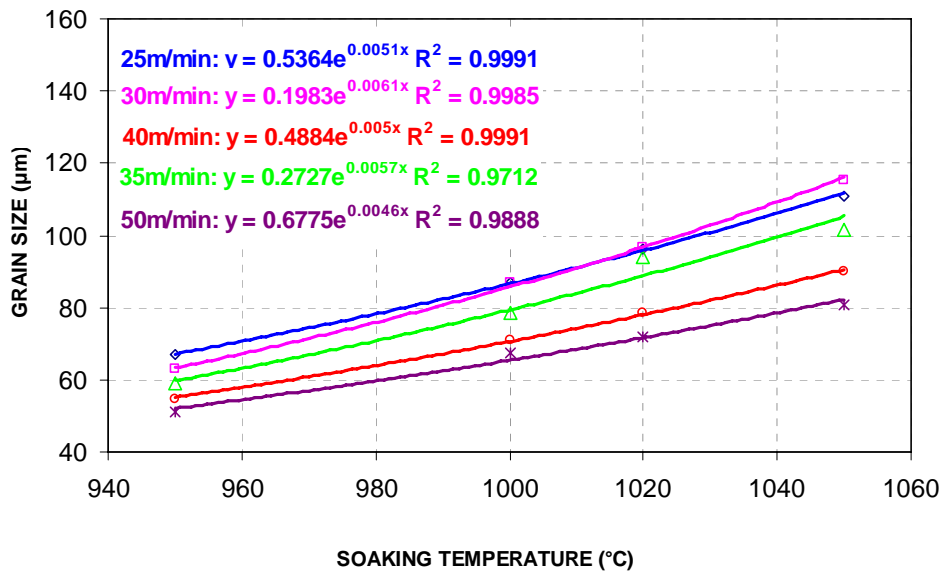
Sample	Thickness ± 0,001mm	Losses ± 0,01 W/Kg				Magnetic induction at 5000 A/m ± 0,01 T	Grain size (µm) ± 11,93	% RA in grain size
		P _{total}	P _{hyst}	P _F	P _e			
F01514 0,35mm	-	-	-	-	0.22	1.66	66,85	12.77
	0,346	2,23	1,75	0.27	0.31	1.65	62,83	9.73
	0,339	2,53	1,97	0.25	0.20	1.67	58,97	6.99
	0,342	2,35	1,88	0.26	0.15	1.66	54,83	8.22
	0,343	2,30	1,89	0.26	0.21	1.66	51,27	7.59
	0,346	2,05	1,57	0.27	0.22	1.66	87,13	11.71
	0,350	2,06	1,57	0.27	0.20	1.66	86,92	9.80
	0,353	2,11	1,64	0.28	0.26	1.65	78,51	10.52

	0,352	2,21	1,68	0.28	0.24	1.66	71,11	5.95
	0,350	2,21	1,70	0.27	0.24	1.64	67,24	18.15
	0,348	2,02	1,51	0.27	0.24	1.65	96,35	22.01
	0,338	2,04	1,54	0.25	0.25	1.65	96,67	16.80
	0,345	2,12	1,60	0.26	0.23	1.66	94,23	11.14
	0,351	2,12	1,61	0.28	0.24	1.66	78,31	17.51
	0,342	2,09	1,59	0.26	0.30	1.64	71,84	8.20
	0,350	2,06	1,49	0.27	0.28	1.65	110,93	15.53
	0,346	2,06	1,51	0.27	0.29	1.64	115,30	23.21
	0,346	2,09	1,54	0.27	0.21	1.68	101,56	13.79
	0,349	2,02	1,54	0.27	0.23	1.65	90,04	12.63
	0,356	2,11	1,59	0.28	0.26	1.67	80,89	15.41
F01494	0,475	2,33	1,57	0.50	0.13	1.67	73,99	6.52
0,50mm	0,479	2,19	1,55	0.51	0.21	1.67	72,66	8.45
	0,477	2,34	1,62	0.51	0.24	1.67	65,95	10.32
	0,471	2,41	1,68	0.49	0.24	1.67	64,18	8.52
	0,473	2,48	1,74	0.50	0.38	1.67	54,26	15.52
	0,474	2,36	1,48	0.50	0.28	1.67	96,28	23.56
	0,497	2,29	1,46	0.55	0.25	1.67	90,00	20.16
	0,498	2,34	1,53	0.55	0.22	1.67	86,56	10.59
	0,497	2,27	1,50	0.55	0.27	1.68	74,59	3.70
	0,472	2,31	1,54	0.50	0.28	1.67	70,30	7.81
	0,482	2,22	1,42	0.52	0.27	1.67	96,24	19.60
	0,478	2,21	1,44	0.51	0.27	1.67	101,32	14.18
	0,461	2,22	1,48	0.47	0.22	1.67	98,22	11.64
	0,461	2,20	1,51	0.47	0.26	1.67	86,97	7.24
	0,473	2,25	1,49	0.50	0.28	1.67	89,05	12.20
	0,498	2,26	1,43	0.55	0.33	1.67	117,28	10.40
	0,497	2,27	1,39	0.55	0.32	1.66	123,81	10.57
	0,481	2,22	1,39	0.51	0.29	1.67	114,09	18.04
0,496	2,24	1,41	0.55	0.26	1.67	108,13	10.42	

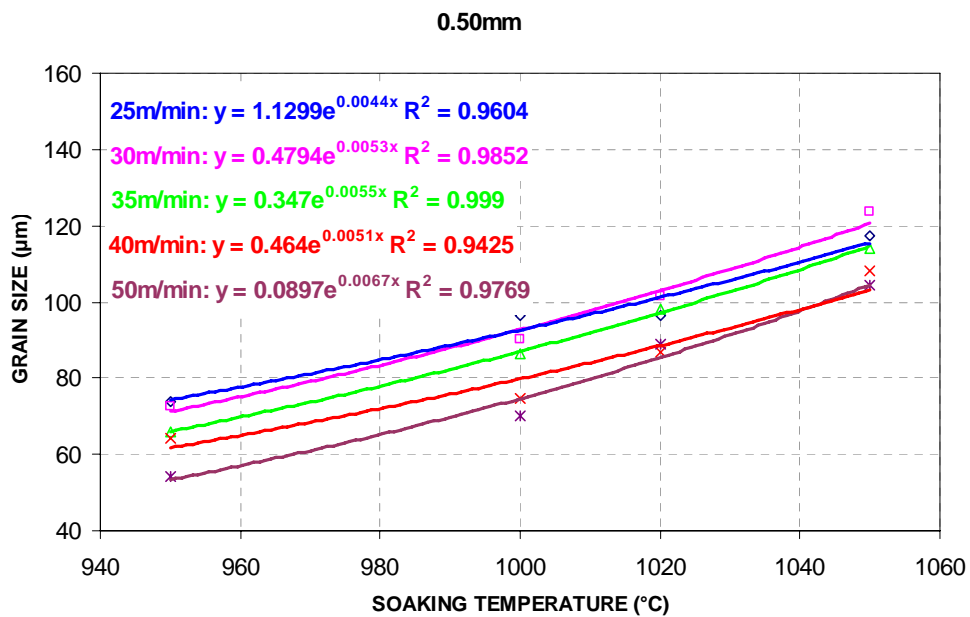
	0,495	2,24	1,43	0.55	0.29	1.63	104,52	12.00
F98843 0,65mm	0,641	3,05	1,84	0.92	0.26	1.63	70,70	5.05
	0,643	2,92	1,75	0.92	0.27	1.63	71,10	20.66
	0,634	3,03	1,86	0.90	0.22	1.64	70,24	8.38
	0,642	3,14	2,00	0.92	0.23	1.64	56,52	12.80
	0,646	3,30	2,15	0.93	0.40	1.63	45,65	12.64
	0,642	2,86	1,54	0.92	0.30	1.63	97,99	16.11
	0,639	2,73	1,51	0.91	0.43	1.62	99,76	11.27
	0,640	2,97	1,63	0.91	0.31	1.64	90,89	9.39
	0,643	2,91	1,68	0.92	0.40	1.63	76,54	11.53
	0,633	3,06	1,77	0.89	0.43	1.62	76,70	11.24
	0,639	2,80	1,46	0.91	0.43	1.62	114,75	9.43
	0,633	2,82	1,50	0.89	0.35	1.62	108,14	8.82
	0,640	2,81	1,54	0.91	0.35	1.63	103,44	8.84
	0,644	2,87	1,58	0.93	0.39	1.63	93,87	19.94
	0,646	2,92	1,59	0.94	0.33	1.62	88,09	11.87
	0,641	2,68	1,43	0.92	0.51	1.62	128,48	5.64
	0,636	2,80	1,39	0.90	0.48	1.62	121,25	7.13
	0,642	2,84	1,44	0.92	0.38	1.62	126,15	2.39
	0,640	2,80	1,50	0.91	0.34	1.63	104,97	2.76
	0,641	2,76	1,50	0.92	0.22	1.66	109,45	8.93

Table 11: Results of losses, magnetic induction and grain size

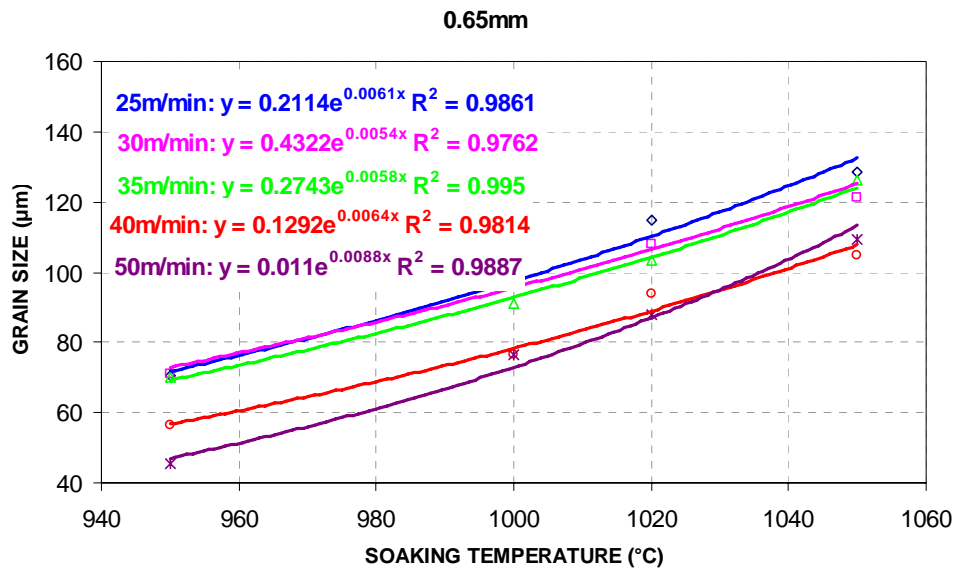
a)



b)



c)



Graph 4: Grain size vs annealing temperature for different annealing speeds:

a) 0.35mm, b) 0.50mm and c) 0.65mm

4.1.3. Grain size modelling

All the parameters already described can be used to build a grain size model. The model gives the kinetics of grain growth during recrystallization of ferrite. The grain size after recrystallization is function of the reduction percent in the cold rolling (thickness) and the annealing parameters (temperature and annealing time)

$$D = \frac{K_{rec}}{\% red} + K_0 \cdot t^{0.25} \cdot \exp\left(\frac{-E_A}{RT}\right)$$

$$D_{rec} = \frac{K_{rec}}{\% red}$$

$$\% red = \frac{th_0 - th_1}{th_0}$$

E_A = activation energy of grain growth (J/mol·K)

R = Boltzmann constant = 8.314 (J/mol·K)

D_{rec} = grain size before of second recrystallization (µm)

th_0 = initial thickness (mm)

th_1 = thickness before cold rolling

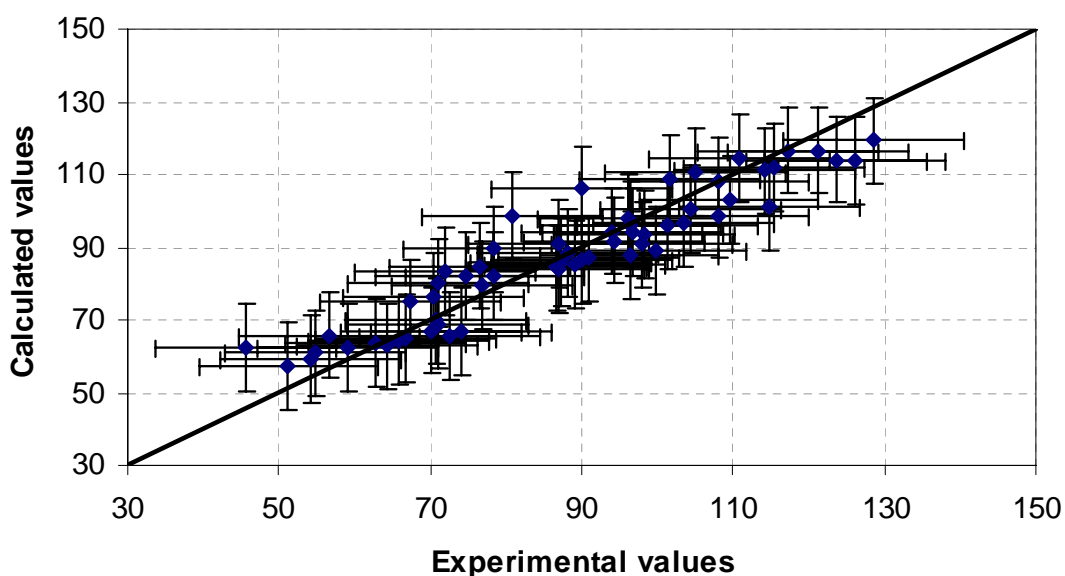
t = time (s)

T = temperature (°K)

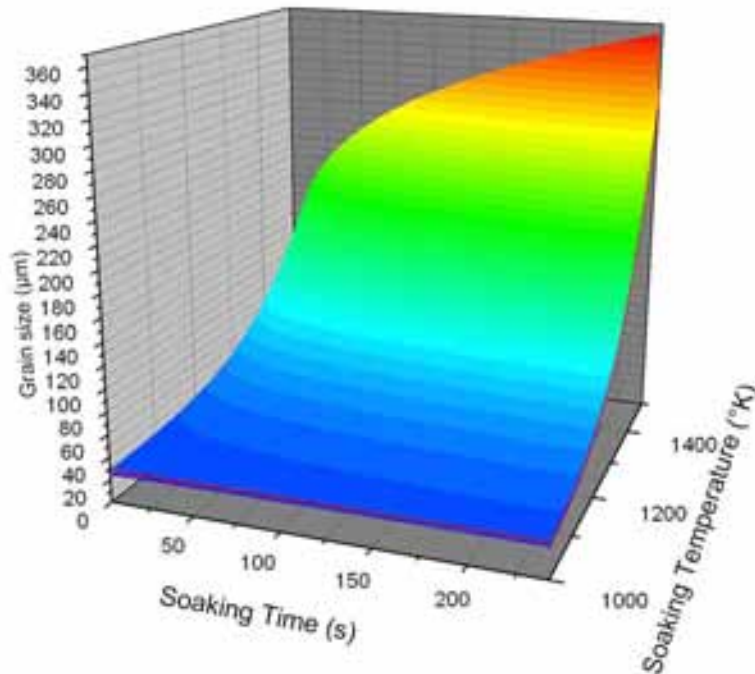
Using the experimental values with calculus software (excel), the three constants of the of grain growth formula were determined. The modelling gives the following equation, where the activation energy of grain growth is 104kJ/mol·K:

$$D = \frac{18.5}{\%red} + 355 \times 10^3 \cdot t^{0.25} \cdot \exp\left(\frac{-104 \times 10^3}{RT}\right)$$

A complete and exact modelling of grain growth phenomena is complicated by a number of different factors (Ref. 13). The development of this semi-empirical approach is based on the experimental observations. To determine the precision of the modelling, the experimental and calculated values of the grain size were compared. The dots in the graphic should lie close to the black line in order to have an exact modelling. The errors in the grain size values are also plotted, and it can be seen that the modelling can be valid in this grain size range.



Graph 5: Accuracy of the grain size modelling. Calculated values vs Experimental values



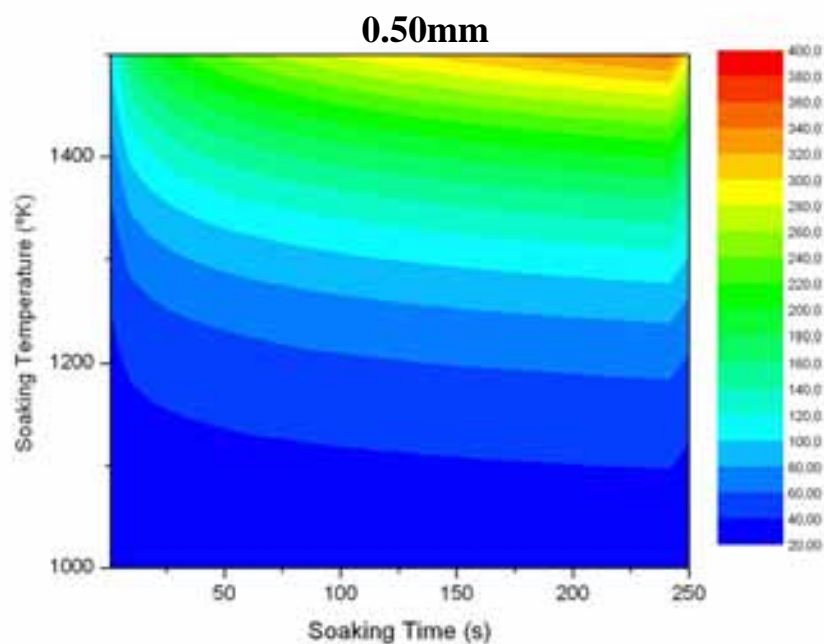
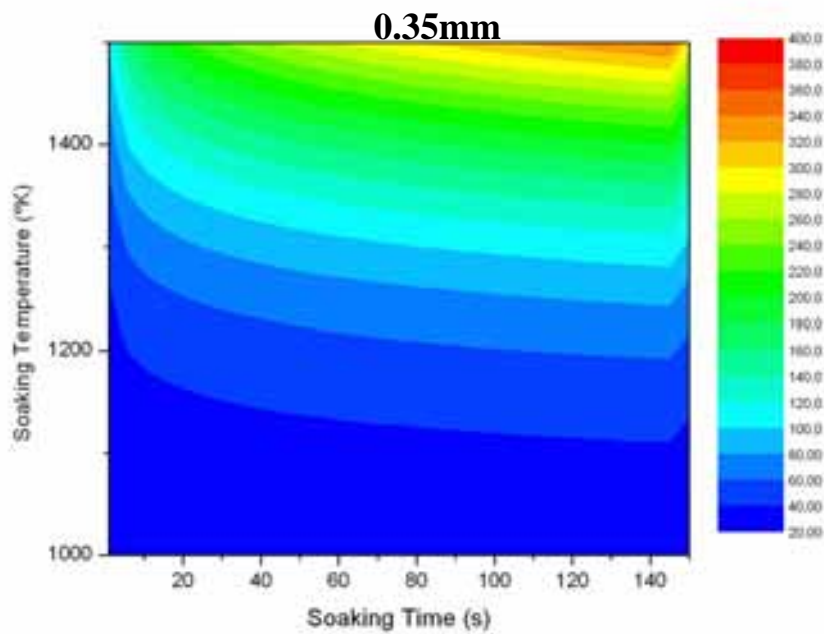
Graph 6: 3D representation of the grain size modelling

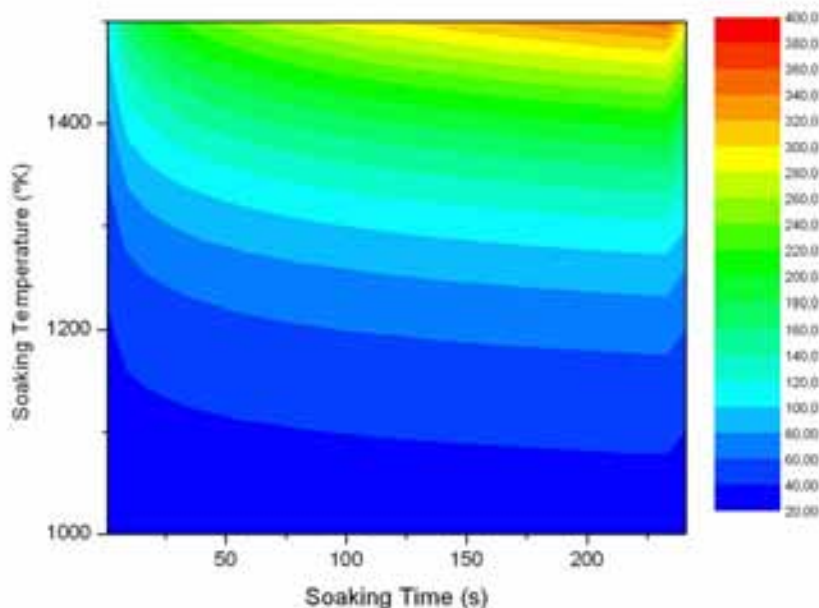
Thickness (mm)	Reduction in cold roll (%)	Recrystallized grain size (µm)
0.35	82.5%	22.42
0.50	75%	24.66
0.65	67.5%	27.41
Modelling equation		
$D = \frac{K_{rec}}{\%red} + K_0 \cdot t^{0.25} \cdot \exp\left(\frac{-E_A}{RT}\right)$		$K_{rec} = 18.5$
		$K_0 = 355 \times 10^3$
		$E_A = 104 \times 10^3 \text{ J / molK}$

Table 12: Parameters in the grain size modelling equation

Statistical analysis was made in order to determine the accuracy of the model. The results provide a regression coefficient $R^2=0.87$, and the standard error in the grain size values is $\pm 7.05\mu\text{m}$.

The model was represented by different graphs: Graph 6 and Graph 7. The influence of the annealing parameters on grain size can be noticed.





Graph 7: 2D representation of the modelling for each thickness.

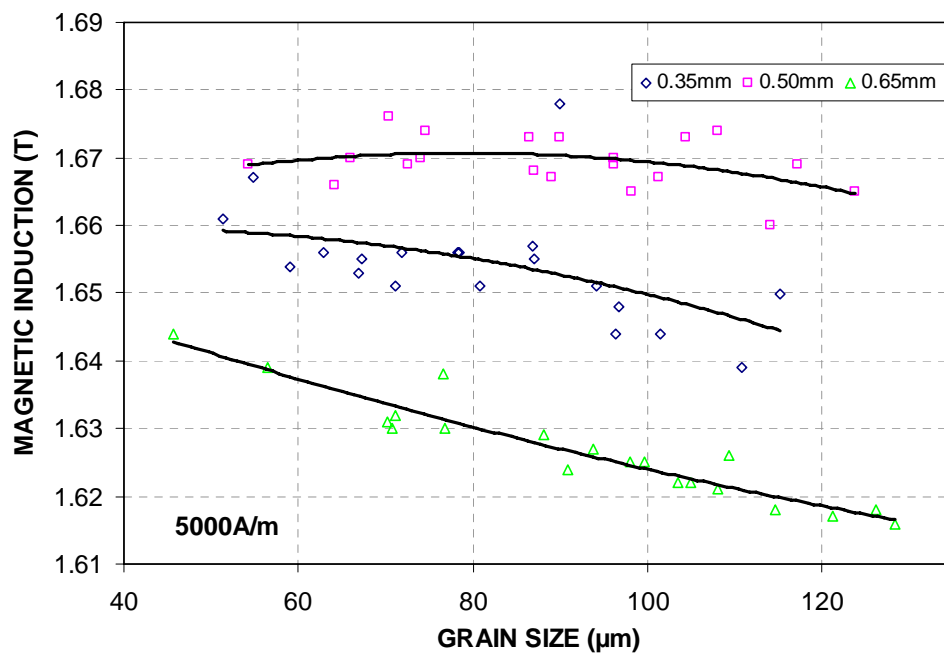
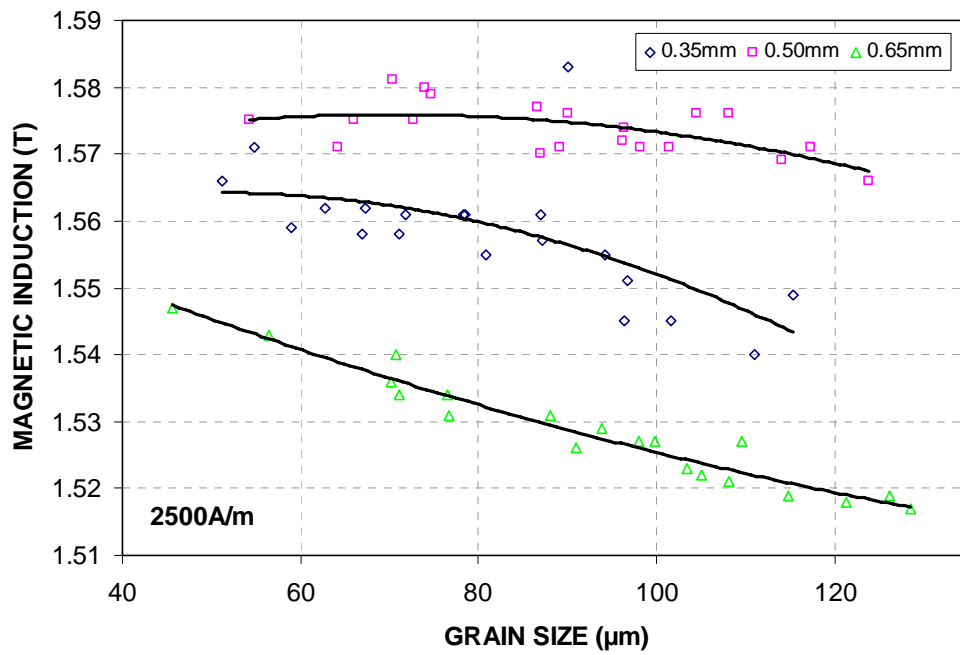
The grain size is represented by colour gradient in μm

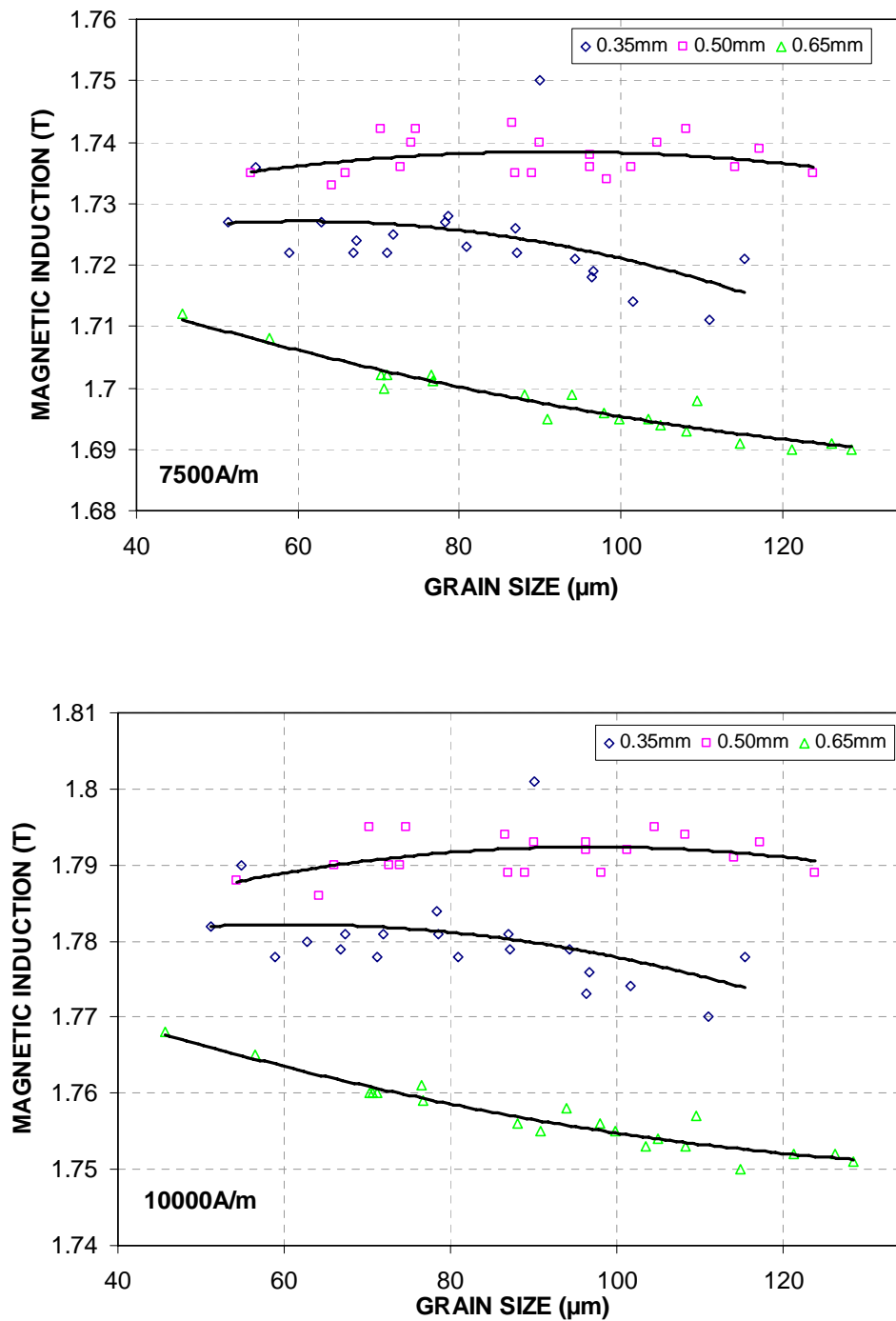
It should be noted that exists a limit grain size (See 4.5.1.2. Limit grain size).

4.2. Effect of grain size on magnetic induction

Graph 8 shows the tendency of the magnetic induction when the grain size changes. The different curves have different behaviour. This behaviour is due to the texture of the samples. When the cold rolling actuates over the samples, it introduces internal tensions and it produces a higher texture and better magnetic properties. In addition, it is shown that the thick sample (0.50mm) has higher induction, because the thickness also influences in the grain orientation. A higher thickness allows higher texturization of the sample.

It is also seen that the magnetic induction values are not depending strongly on the grain size. It means that is possible to adjust an optimum grain size for the annealing parameters optimization, without a significant modification of the induction magnetization.





Graph 8: Magnetic Induction for different values of applied magnetic field: a) 2500A/m, b) 5000A/m, c) 7500A/m, d) 10000A/m

4.3. Foucault losses, Hysteresis losses and Excess losses in function of grain size

The separation of total magnetic losses in its hysteresis, classical (Foucault) and anomalous or excess losses components can bring important clues to the development of electrical steels processing (Ref. 14). The total power losses were separated to determine the influence of each kind of them.

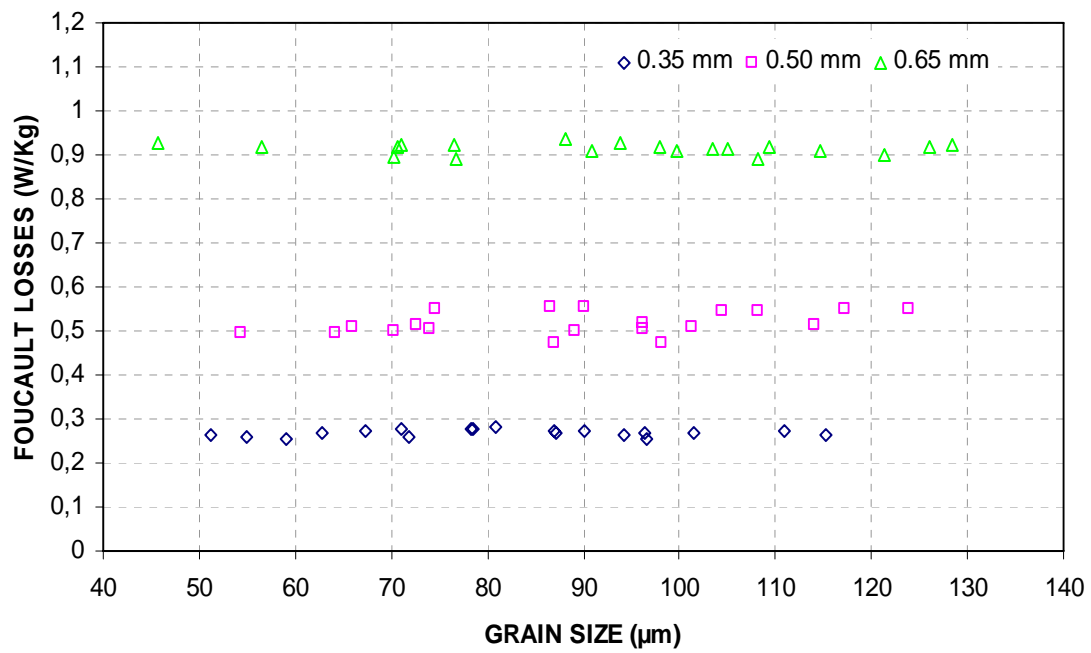
Hysteresis loss and total core loss decrease with increasing grain size. Both the increasing annealing time and temperature are beneficial to the core loss (Ref. 15). Foucault losses are not depending of the grain size, and excess losses increases with increasing grain size.

For each different thickness, it is possible to determine the optimum grain size to obtain the lowest power loss.

The thickness of the steel influences both the eddy current losses (Foucault losses and Excess losses) and the hysteresis losses. The Foucault losses and Excess losses also depend on the frequency and thus the optimum thickness with respect to low loss varies with the frequency and the polarization (Ref. 16).

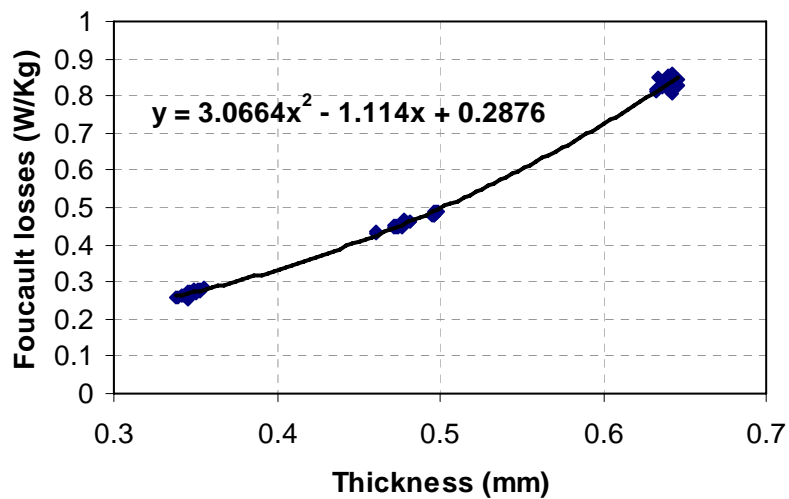
4.3.1. Foucault losses

The grain size does not have influence in the Foucault losses. These losses mainly are dependent of the frequency, the thickness and the magnetic induction. It is shown in Graph 9 that the Foucault losses are almost constant in the range of studied grain size, for each thickness.



Graph 9: Foucault losses as a function of Grain size.

The values of Foucault losses were plotted as a function of the measured samples thickness. A quadratic equation has been done in order to calculate it.



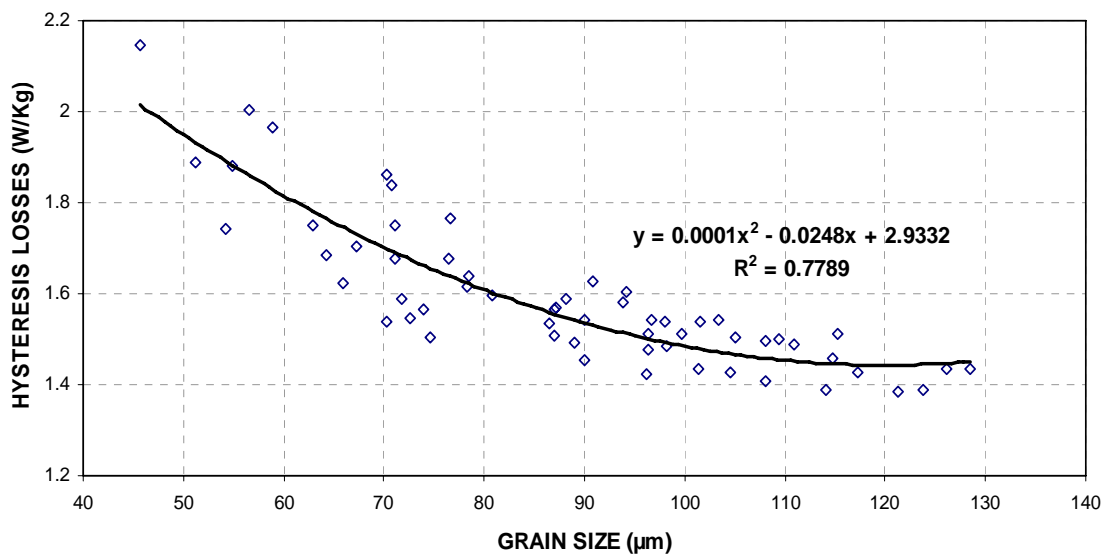
Graph 10: Foucault losses vs Thickness

SAMPLE AND THICKNESS	FOUCAULT LOSSES	
	Measures Average	$y = 3.0664x^2 - 1.114x + 0.2876$
F01514, 0,35mm	0,2698	0,2733
F01494, 0,50mm	0,4797	0,4972
F98893, 0,65 mm	0,8325	0,8590

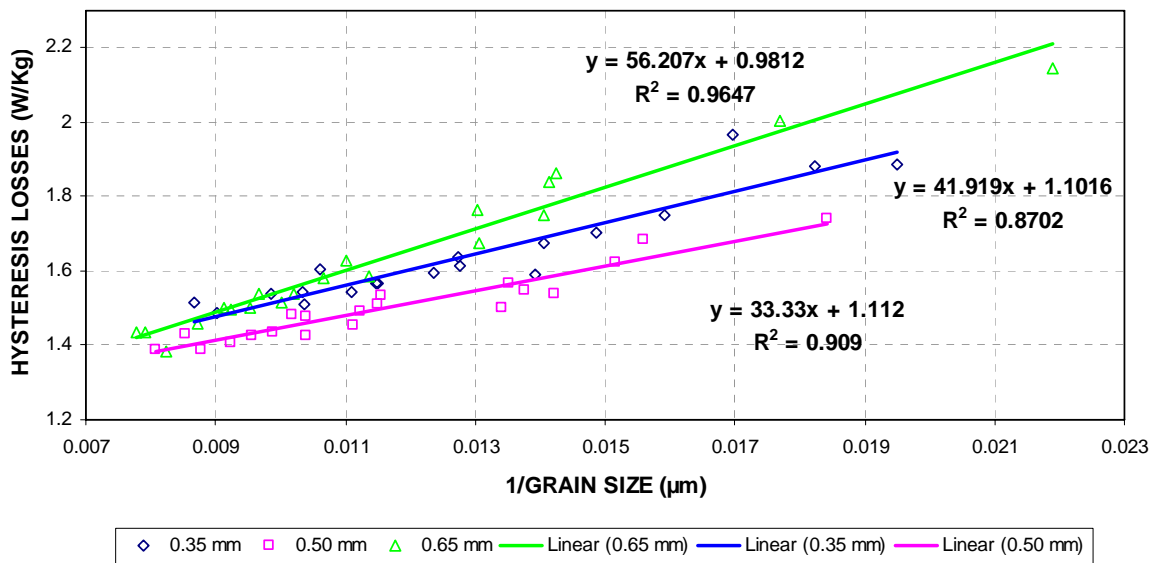
Table 13: Foucault losses

4.3.2. Hysteresis losses

The evolution of hysteresis losses with the grain size is shown in Graph 10. In general, the hysteresis loss decreases in order the grain size increases. It was obtained a quadratic equation to describe the behavior of hysteresis losses as a function of grain size.



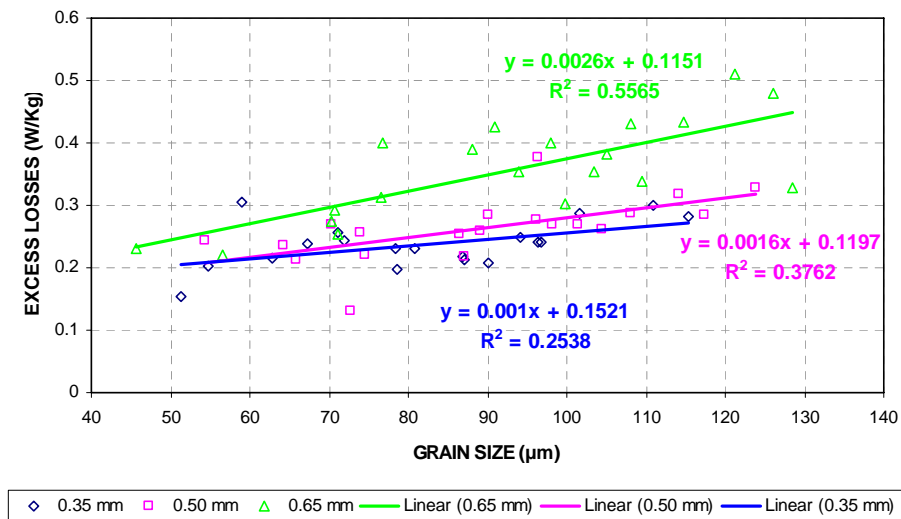
The different results can be separated to determine a descriptive linear equation for each thickness, if it is done as a function of the inverse of the grain size. The accuracy of these equations is better than in quadratics equations.



Graph 11: Hysteresis losses vs Grain size

4.3.3. Excess losses

The excess losses depend on the frequency, but also on the grain size as is shown in the Graph 12. For larger grain sizes, the anomalous or excess loss generally increases.



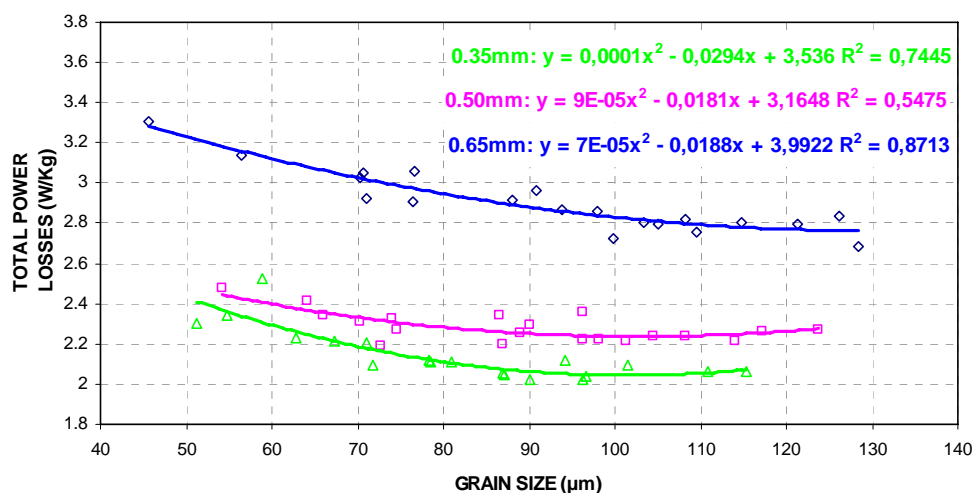
Graph 12: Excesses losses vs Grain size

The graph in this case indicates that the thickness has also an influence on the excess loss, i.e. that a higher thickness leads to a higher excesses loss.

It is possible to determine a linear relation for each thickness, but the value of the regression coefficient is quite low for all of them.

4.3.4. Total power losses

If all the components of the power loss are plotted in a graphic, Graph 13 the relation between total losses and grain size is obtained. In these graphics, the largest variation is found in the hysteresis loss.



Graph 13: Total losses vs Grain size

It should be noted that the error in the obtained equations might to deteriorate the accuracy in posteriors calculus.

The function obtained describes a curve with a minimum, different for each thickness. As the grain size increases, hysteresis losses decrease, but the excess losses increases. Therefore, there is an optimal grain size, between 100 and 150 micron, where the power loss reaches a minimum. (Ref. 1)

Sample	Hysteresis losses	Foucault losses	Excess losses
F01514	76,36%	12,53%	11,11%
F01494	65,79%	22,70%	11,51%
F98843	56,07%	31,58%	12,35%

Table 14: Average percent of losses separation for each thickness

4.4. Optimum annealing parameters

4.4.1. Effect of grain size on total power losses

For a given silicon content, core loss value in the steel initially decreases with an increase in the grain size. After attaining an optimum grain size, core loss value starts increasing with a further increase in grain size. It is due to the fact that the size of magnetic domains present in the steel is directly linked with the grain size. An increase in grain size results in corresponding increase in the size of magnetic domains and hence, there is lesser number of domain walls to move during magnetization, which results in lowering of core loss. However, when magnetic domain size becomes very large, the domain walls have to move faster to cover the same distance during magnetization which results in enhancing the core loss value of the steel, which contains ferrite grains coarser than an optimum grain size. (Ref. 17)

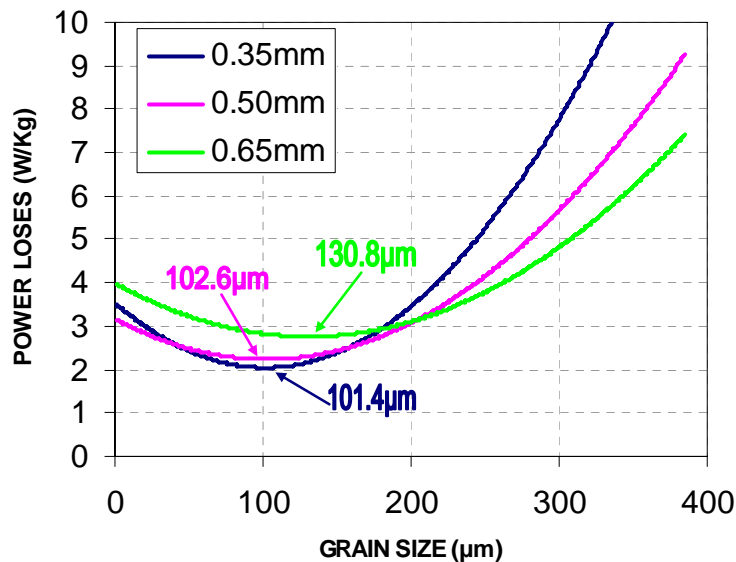
For the determination of the optimum grain size, the experimental equations obtained for total power losses as a function of grain size, have been minimized. To do it, the derivate of the total power loses must be equaled to zero, corresponding with the inflection point of the curves. The results are shown in Table 15, and the functions are plotted in Graph 14.

SAMPLE	DERIVATE	OPTIMUM GRAIN SIZE ⁷
0.35mm	$d(0.000145x^2 - 0.0294x + 3.536) = 0.00029x - 0.0294 = 0$	$x = \frac{0.0294}{0.00029} = 101.4\mu m$
0.50mm	$d(0.000088x^2 - 0.0181x + 3.1648) = 0.000176x - 0.0181 = 0$	$x = \frac{0.0181}{0.000176} = 102.6\mu m$
0.65mm	$d(0.000072x^2 - 0.0188x + 3.9922) = 0.000144x - 0.0188 = 0$	$x = \frac{0.0188}{0.000144} = 130.8\mu m$

Table 15: Optimum grain size for different thicknesses

4.4.2. Optimum annealing parameters

The variation of grain size for each thickness is directly linked to the different parameters used in the experimental processing. The variation of the power loss with the grain size has been described. Consequently, it is possible to determine the optimum processing parameters to minimize the loss for each thickness.



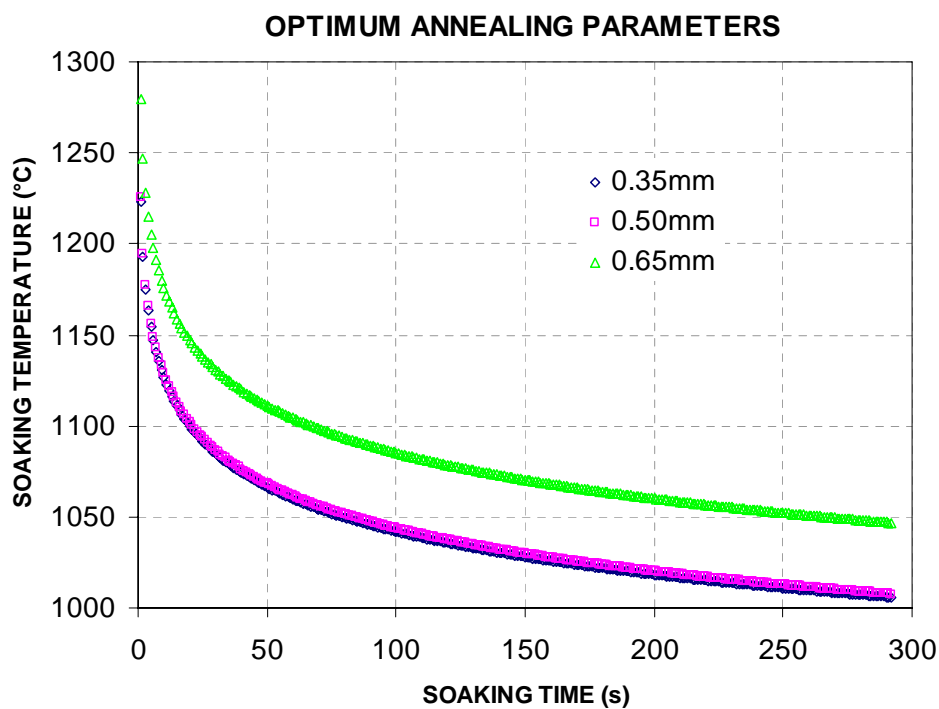
Graph 14: Optimum grain size in terms of total power losses for each thickness

⁷ Statistical analysis can be made in future works.

Using the grain size modelling, a curve of optimum annealing parameters is obtained, as it is shown in Graph 15. This graph was plotted using the modeling equation in terms of temperature as a function of grain size and time⁸:

$$D = \frac{K_{rec}}{\%red} + K_0 \cdot t^{0.25} \cdot \exp\left(\frac{-E_A}{RT}\right) \Rightarrow$$

$$T = \frac{\frac{-E_A}{R}}{\ln\left(\frac{D - K_{rec}}{K_0}\right) - 0.25\ln(t)} = \frac{\frac{-104 \times 10^3}{8.314}}{\ln\left(\frac{D - 18.5}{355 \times 10^3}\right) - 0.25\ln(t)}$$

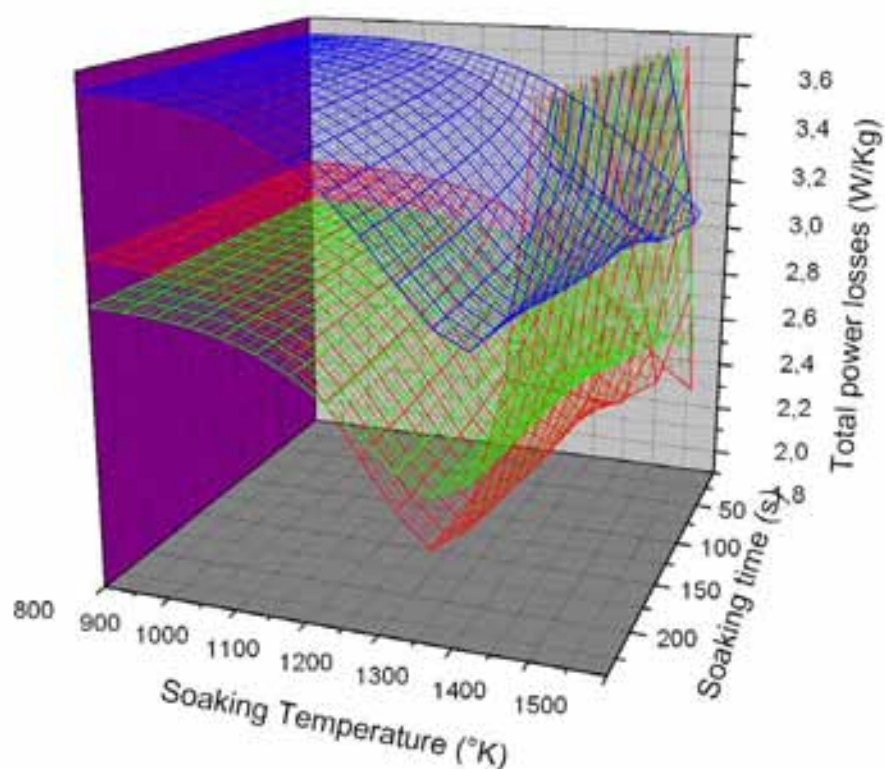


Graph 15: Annealing parameters to obtain optimum grain size for different thickness

⁸ Statistical analysis can be made in future works.

4.4.3. Total power losses as a function of annealing parameters

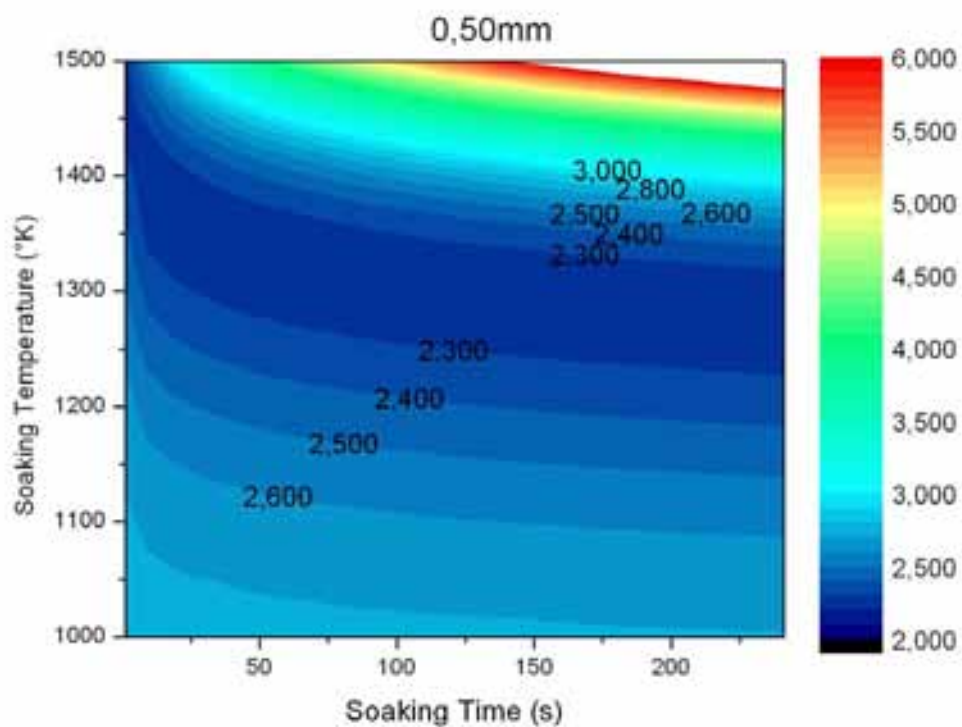
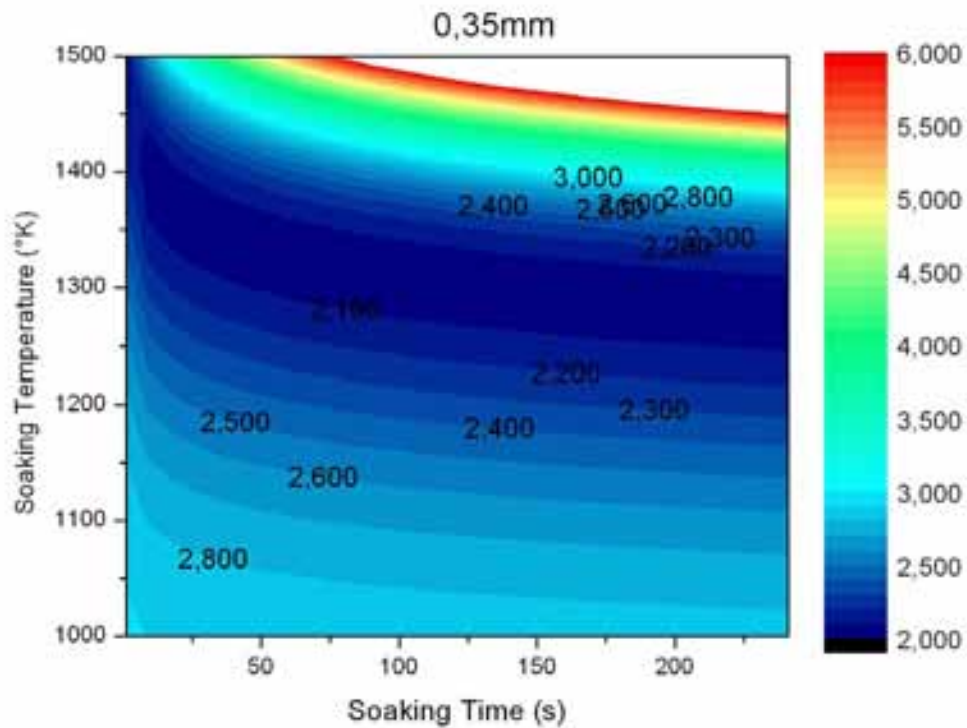
Using the grain size modelling and the relation between grain size and total power losses, the relation between annealing parameters and total power losses was determined (Graph 16). It should be noted that the errors in the previous equations might to deteriorate the accuracy of the results.

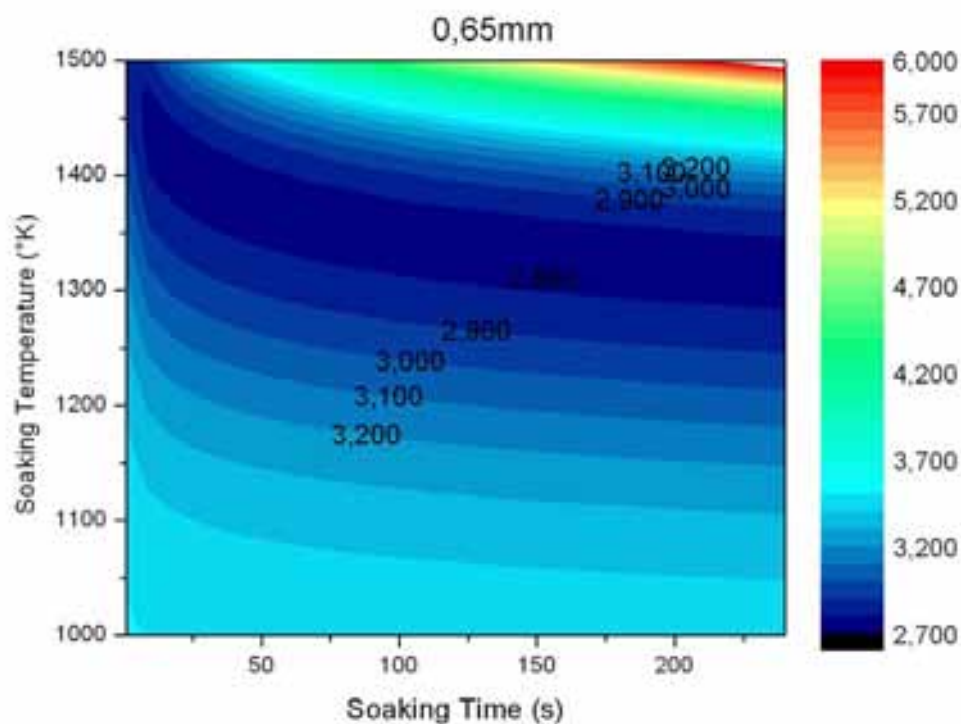


Graph 16: 3D representation of total power losses as a function of the annealing parameters. The red surface corresponds with 0.35 samples, green with 0.50 and blue with 0.65mm thickness

The different heat treatments have an effect on the grain size and precipitates as a result of the different recovery, recrystallization and grain growth phenomena. This characteristic has effects in power losses as was showed. In the other hand, when the magnetic domains growth over an optimum value, the domain walls should move faster to arrive to the same magnetization. This produces an increase of the hysteresis losses (Ref. 18). Then it is possible to

see a minimum in the power losses, which corresponds with the optimum annealing parameters, in Graph 17.





Graph 17: 2D representation of total power losses as a function of the annealing parameters for 0.35, 0.50 and 0.65mm thickness

4.5. The role of precipitates on grain size and power losses

The indirect effect of precipitates on magnetic properties is that they can limit the grain growth during the final annealing and the direct effect is pinning of domain wall movements with a resulting increase of hysteresis loss. (Ref. 19)

During grain growth, if precipitates of the appropriate size, number, distribution, etc. are present, it is possible that they can inhibit the growth of the whole set of grains, resulting in an intermediate or finished product with a small grain size. The growing boundary is pinned by the array of inclusions, which produce a restraining stress on the grain boundary and thus inhibit its growth. (Ref. 23)

During domain walls movement, the inclusions smaller than domain walls thickness reduces domain wall energy, and the inclusions larger than domain walls thickness reduces magnetostatic energy of the system (Ref. 20). In all cases the hysteresis loss is increased.

In the processing of electrical steels the final product must have a coarse grain size, and an appropriate (generally low) amount of precipitates helps to achieve this goal.

4.5.1. Effect of precipitates on grain size

4.5.1.1. Grain growth

Grain growth occurs to reduce the total grain boundary energy. Fine second phase particles have long been known to limit grain growth by pinning the grain boundaries. Movement of the grain boundary requires pulling away from the pinning effects of these particles. Coarsening is a much slower process than precipitate growth, as is reasonable in that growth of one grain only occurs by cannibalizing other grains. It is also seen that the key material variables are solubility and diffusion coefficient. (Ref. 12)

Normal grain growth in metals and alloys is a diffusion controlled process driven by the reduction in the grain boundary energy. Physically, it occurs by growth of the larger grains at the expense of the smaller ones which tends to shrink.

There are different possible situations:

- Grain growth in the absence of pinning precipitates.
- Grain growth in the presence of stable precipitates.
- Grain growth in the presence of growing precipitates.
- Grain growth in the presence of dissolving precipitates.

In the dissolved state, impurity and alloying elements will retard grain growth through elastic attraction of the atoms towards the open structure of the grain boundary. The boundary must then either drag the impurity atoms along (so that its speed is limited by the diffusion rate of these atoms) or break away if the impurity concentration is sufficiently small or the driving pressure or temperature is high enough.

When dispersed particles have some solubility in the matrix in which they are contained, there is a tendency for the smaller particles to dissolve and for the material in them to precipitate on larger particles. The driving force is provided by the consequent reduction in the total interfacial energy and ultimately, only a single large particle would exist within the system.

There is an associated reduction in the grain boundary mobility in the presence of impurity elements in solid solution. The grain boundary pinning effect of the precipitates is determined by the relative rates of particle coarsening and grain growth in the material (Ref. 22).

The depinning is a thermally activated process. In grain oriented electrical steels, the mechanism for starting the secondary recrystallization process (also called abnormal grain growth⁹) usually is associated with the presence of second-phase particles inhibiting the growth of matrix grains. Thermal depinning favors abnormal versus normal growth, and in this way it can start the secondary recrystallization process. (Ref. 23)

⁹ That is, of the fine crystal grains produced through the normal recrystallization, grains of a particular orientation grow abnormally on the whole (Ref. 21).

4.5.1.2. Limit grain size

The grain size growth is affected by the grain surface energy by unit volume. As grain size increases, the growth speed decreases until it is zero, arriving to a limit grain size (Ref. 18). Grain growth will stop when the free energy to pull the boundary away from the particles equals the free energy gained through decrease in grain boundary energy (Ref. 12). If grain growth occurs in the presence of stable precipitates, the limiting grain size becomes constant and independent of the thermal cycle. (Ref. 22)

4.5.1.3. Cooling rate

During the annealing process, less recovery takes place during fast heating than during slow heating so more stored energy is preserved in the specimen heated by fast heating before recrystallization commences. Higher stored energy increases the nucleation rate faster than the growth rate. as a result, the annealing by fast heating leads to a smaller grain size than that by slow heating (Ref. 24). If the precipitation occurs during cooling after annealing, the cooling rate should have an influence on the precipitates (Ref. 19).

4.5.1.4. Precipitate size

The precipitates too fine inhibit the grain growth very tightly (Ref. 25). The pinning force of a particle, F , decreases with increase in its size:

$$F = 6f\gamma / \pi r$$

where f is the volume fraction of particles, γ is the grain boundary energy and r is the particle radius. If the size of a particle exceeds a critical size, the pinning effect of the particle disappears and grain coarsening occurs with lowering of energy associated with grain boundary and particle interaction. The critical size of particles depends upon a number of factors and is described as follows:

$$r_c = \frac{6R_0 f}{\pi} \left(\frac{3}{2} - \frac{2}{Z} \right)^{-1}$$

r_c is the radius of critical size of particles, f is the volume fraction of particles, R_0 is the matrix grain radius and Z is the ratio of growing grains and matrix grains. Such coarser particles lost their capability to pin down grain coarsening. (Ref. 17)

The final grain size is proportional to the diameter of inclusions in hot bands (Ref. 26). It is reported that fine precipitates inhibited normal grain growth (Ref. 27). Fine MnS and or AlN particles (~10nm) serve to selectively pin the grain boundaries until they are coarsened or removed during the final anneal (Ref. 12).

Lower slab reheat temperature results in less dissolved precipitates containing impurities (MnS and AlN) and, therefore, less precipitates will form during the hot rolling which. It means a more favorable size distribution of the small precipitates deteriorating the magnetic properties of the steel. (Ref. 3)

4.5.1.5. Precipitate shape and orientation

The effect of the shape of the precipitates seems to be an important factor. If there are needle-shaped precipitates, the pinning action would be different if the boundary meets it frontally or laterally. Interaction of a growing boundary with a cubic-shaped precipitate, the enhancement of the drag is greater than in the ellipsoidal case and even more pronounced if the precipitate is coherent with the matrix.

The boundary has a surface tension (or energy per unit area), denoted by γ , and the motion of the deformed boundary is restrained by a force sometimes called Zener's force, F .

$$F = 2\pi r\gamma \sin \theta \cos \theta$$

Where r is the radius of the precipitate, and θ is the contact angle between precipitate and grain boundary, assuming that the precipitate is spherical and incoherent with the matrix grains (Ref. 23). It is noted that the orientation and the shape of the precipitates respect to the grain boundary is an important factor in grain growth.

4.5.2. Effect of precipitates on power losses

Grain boundaries and inclusions inhibit the rotation of magnetic vectors by a mechanism known as domain boundary pinning (Ref. 4).

The thickness domain wall is a balance between exchange energy and anisotropy energy. Exchange energy is a force that binds the atomic moments parallel one another.

Anisotropy energy is the force that in the case of Fe, makes the atomic magnetic moments align spontaneously in the $\langle 100 \rangle$ directions.

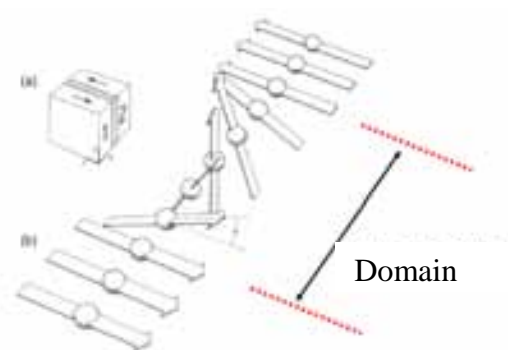


Fig. 7: Wide of domain walls

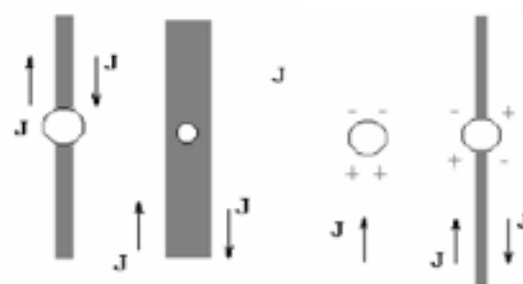


Fig. 8: Effect of precipitates in domain wall properties

Inclusions smaller than domain walls thickness reduce domain wall energy (Fig. 8).

Inclusions larger than domain walls thickness reduce magnetostatic energy of the system (Ref. 20).

Most of the microstructure-magnetic properties relations are mechanisms based on coercivity H_c . The microstructure is considered a source of pinning centers and H_c is the “force” you have to apply to get the domain wall to overcome the pinning.

Domain walls are pinned by defects. When the magnetic field is increasing, the magnetic lines start to bend.

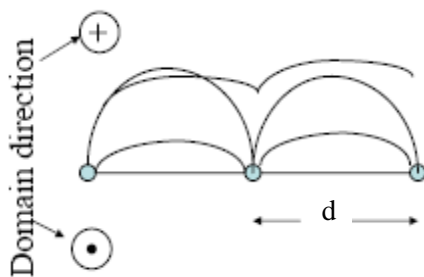


Fig. 9: Domain walls pinning

At a critical field, a domain wall leaves pinning center. This critical field depend on the distance d between centers and γ , the domain wall energy (Ref. 20).

$$H_{critical} = \frac{3\gamma}{J_s \cdot d}$$

It is counted that the maximum permeability region of the magnetization curve separates the area of domain wall movement and the domain rotation as the predominant mechanisms of magnetization change. The growth of a second phase or the decrease in grain size shows changes in the domain wall movement region (coercitive force), and in the domain annihilation region (lower branch of second quadrant), which little change in the domain nucleation region (upper branch) (Ref. 14).

4.5.3. Effect of steel composition

In the following table is showed the different effects produced by the components of the steel.

Element	Properties
Si	Less than 2.5% → iron loss is aggravated.
	More than 4.0% → steel becomes brittle, making it to be impossible to subject the steel to cold rolling.
C	Less than 0.01% → loss strain energy for cold rolling
	More than 0.10% → problem during the decarburization, as well as degrading the magnetic properties.
Mn	More than 0.15% → it becomes difficult to dissolve completely into a solid solution in the reheating furnace during hot rolling.
P	More than 0.04% → it becomes difficult to carry out cold rolling.
S	Less than 0.005% → problem in the formation of MnS for inhibiting the growth of the primary recrystallization grains in grain oriented electrical steels.
	More than 0.04% → it becomes difficult to desulpherize in the final annealing process, aggravating iron loss.
Al	Less than 0.01% → problems in the formation of AlN for inhibiting the growth of the primary recrystallization grains.
	More than 0.05% → precipitation of AlN becomes excessive, while its performance as the inhibitor for the growth of the primary recrystallization grains is rather weakened.
N	The range of N should be in consideration of the content of AlN.
Sn ^{*10}	More than 0.04% → the cold rollability is deteriorated, as well as causing insufficient decarburization.
Cr*	More than 0.12% → can be resulted insufficient decarburization.
Ni*	More than 0.12% → the effect is not increased at all.
Mo*	Shows the effect of preventing cracks hot rolling

Table 16: Effects of the steel composition

¹⁰ *Sn, Cr, Ni and Mo have a relatively low solubility in steel, and they are segregated around the precipitates, so that the fine precipitates used as the inhibitors for the growth of the primary recrystallization grains should be protected, and that the secondary recrystallization should be stabilized. This effect is reinforced as more kinds of elements among Sn, Cr, Ni and Mo are added, because the more complicated protecting films are formed around the precipitates. Therefore, adding these elements together give stronger effects compared with the case of adding a single element.

However, if the addition of the Sn, Cr, Ni and Mo is excessive, there will occur cracks during hot rolling (Ref. 21)

Silicon: can vary from almost zero to some 3.5%.

Aluminium and manganese: these could be present at up to some 1% each.
These elements raise resistivity.

Phosphorus: the level of phosphorus is important. In the range 0.03-0.08% shows that purposeful additions were made. It is used to raise hardness for easier stamping.

Carbon: carbon as low as 0.003% could have been produced at steelmaking, but levels below 0.003% probably came by a later wet hydrogen anneal of thin sheet.

Sulphur: low levels of sulphur (less than 0.008%) could suggest a desulphurization stage at steelmaking.

Nitrogen: a low nitrogen level (less than 0.006%) suggests extra care being taken to avoid nitrogen pick up. Higher levels could suggest a form of grain oriented steel in which aluminum nitride is used for grain growth control.

Titanium: the presence of titanium above 0.005% suggests the use of iron making ores higher in titanium than is best for good magnetic quality. This element is not normally controllable after smelting. It has been used as a stabilizing agent to prevent the precipitation of carbon. Titanium becomes an undesirable element, forming titanium oxide inclusions which can damage magnetic permeability. (Ref. 28)

The impurity elements in steel can form various kinds of precipitates and these precipitates can inhibit the grain growth. (Ref. 15)

4.5.3.1. Manganese sulfides

The grain boundaries can be pinned by a MnS precipitates (Ref. 23). The size of manganese sulfide inclusions plays an important role during the final annealing. Manganese sulfide inclusions would prevent the movement of grain boundary and slow down the grain growth at the grain growth stage during final annealing. The size of manganese sulfide inclusion increased with increasing hot band annealing temperature. Therefore, final grain size of low carbon electrical steels increased with increasing hot band annealing temperature. In this reference, the effect of manganese sulfide inclusion size is more significant than hot band grain size. These indicate that the effects of grain size and manganese sulfide inclusion size on the hysteresis loss are more significant than that of texture. (Ref. 26)

4.5.3.2. Carbide and Nitrides

The steel is ferritic at all stages in the processing. In fact the carbon content has to be kept low to prevent the formation of austenite during the processing cycle (Ref. 12).

After final annealing, carbon and nitrogen tend to form carbide and nitride. With the above premise, the effects of carbide, nitride and oxide on the hysteresis loss of low-carbon electrical steels are almost the same. (Ref. 26)

Titanium can form nitride and carbide precipitates (Ref. 25). Magnetic ageing due to too high carbon content in the steel leads to precipitation of carbides at exposure to elevated temperature (Ref. 17), but the TiC can dissolve at 800°C approximately (Ref. 25).

The theory predicts, in Ref. 12 that the presence of nitrogen in the TiC precipitates would reduce the coarsening rate by an order of magnitude, as compared to the coarsening of pure TiC.

Presence of nitrogen is undesirable because nitrogen both as interstitial and nitride particle obstructs the movement of magnetic domain walls. (Ref. 29)

4.5.3.3. Aluminium nitrides

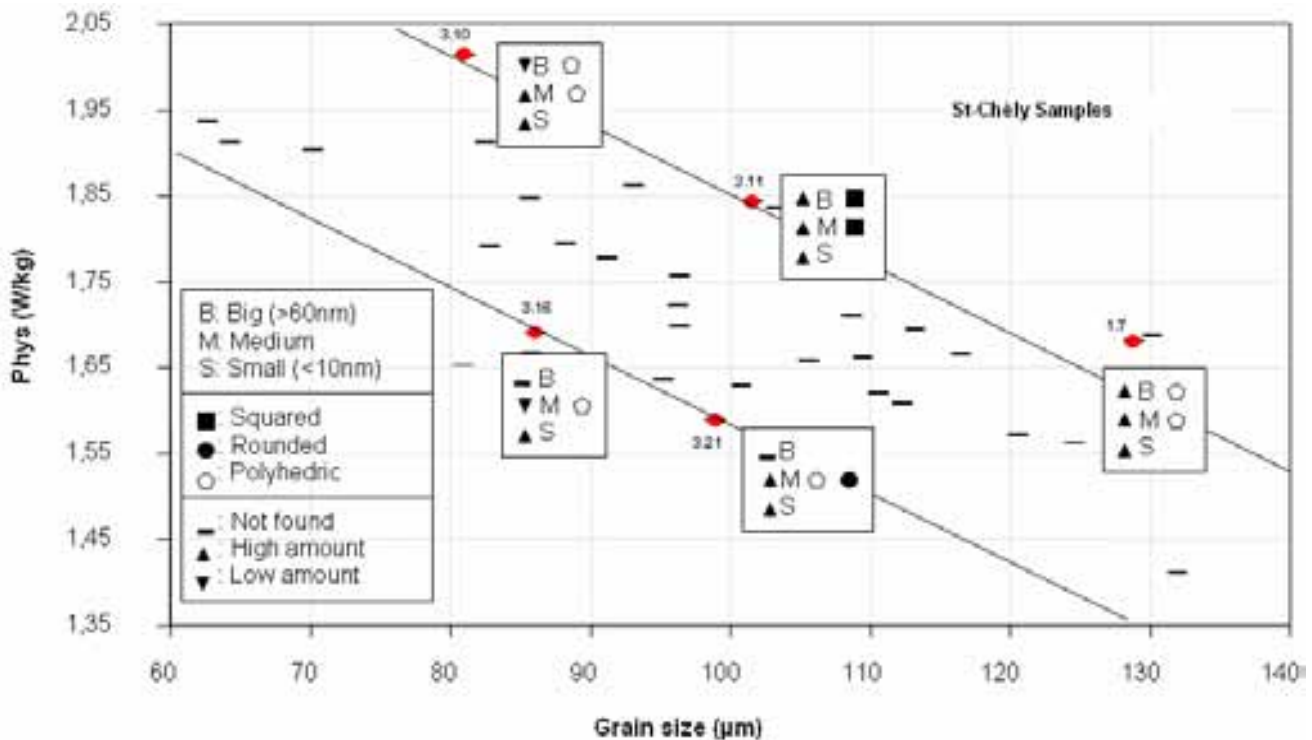
Aluminium is added to the non-oriented electrical steels to form AlN by combining with the nitrogen available in the liquid steel and consequently, to minimize the detrimental effect of free nitrogen on the magnetic properties of the steel. Aluminium addition lowers core loss value by increasing electrical resistivity from the steel and, under specific processing conditions, by developing favourable texture for magnetization. (Ref. 17)

The addition of Al affects the grain growth. Aluminium can form nitride precipitates, and titanium can form nitride and carbide precipitates. Aluminium coarsens nitride precipitates and accelerates grain growth. The size of titanium precipitates are quite different when the amount of aluminium changes. The precipitates are smaller as more aluminium is content in the material (Ref. 25).

Presences of coarser AlN particles facilitate the grain growth because these particles were ineffective in pinning the movement of grain boundaries during annealing (Ref. 17).

4.5.4. Precipitates observations by TEM

For the same grain size, the differences founded in hysteresis losses can be explained with a precipitates study. The precipitates characteristics are close linked with the steel composition.



Graph 18: Results of Precipitates Characterization

Samples 3.10 and 3.11 have high amount of titanium and carbon. Consequently, the losses are higher than samples 3.16 and 3.21, with the same grain size. There were found approximately de same amount of small precipitates, but the number of big and medium squared precipitates are higher in samples with higher hysteresis losses. Titanium and carbon tend to form small precipitates and if the amount of these elements is high, they can form big and medium squared precipitates which ones worse the hysteresis losses.

Samples 3.16 and 1.7 have similar hysteresis losses, and different grain size. In this case is more important the precipitates characterization than the grain size. Sample 1.7 has higher amount of medium and big precipitates. These kinds of precipitates increase the hysteresis losses.

Ti-precipitates are mostly found, especially Ti (C,N) and not so many $Ti_4C_2S_2$. No trace of AlN is present in the materials and very few of MnS. Work is now being performed to discern clearly between TiN and TiC.

All the studied samples have a high amount of small precipitates. Consequently, it can be concluded that the small precipitates have not a strong effect in the magnetic properties, and high amounts of big and medium size precipitates make the effect to raise the magnetic losses due to the pinning of the domain walls effect.

Sample	Precipitates	Placement	Predominant Shape	Amount		
				Small <10nm	Medium (10-60) nm	Big >60nm
F00790A (3.11)	Ti(C,N)	Grain boundaries	square	High	High	High
F99406D (3.21)	Ti(C,N), Ti(C,S), Zr(C,N)	Grain boundaries	rounded and polyhedric	High	High	Low
F00712A (3.10)	TiC, Ti(C,S),	All	polyhedric	High	High	Medium
F00440B (3.16)	Ti(C,N)	All	polyhedric	High	Medium	Low
F94266A (1.7)	Ti(C,N), Zr(C,N)	All	polyhedric	High	High	High

Table 17: Precipitates Characterization

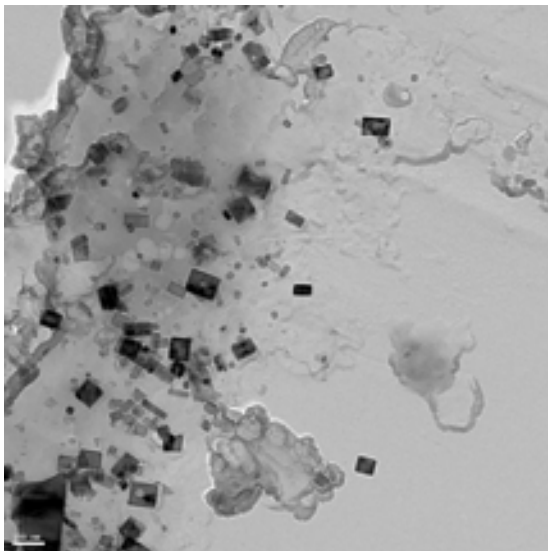
Sample F00790A (3.11)

The material contains a significant amount of precipitates of all sizes between 5 and 100 nanometres, especially in the grain boundaries (it can be due to the sample preparation, cleaning after etching).

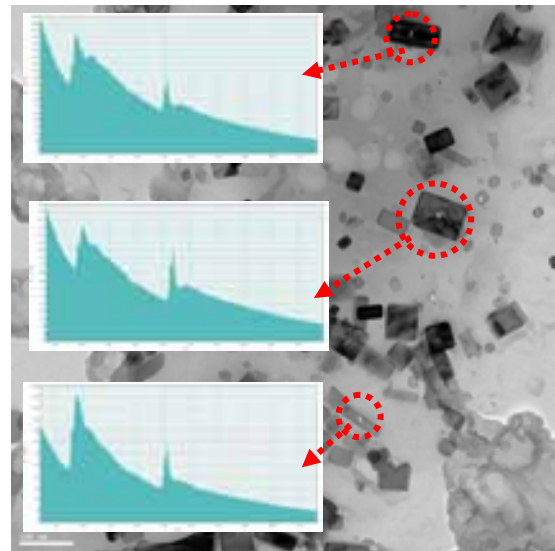
Generally the shapes founded are squared

Amount of titanium carbides, nitrides or carbonitrides.

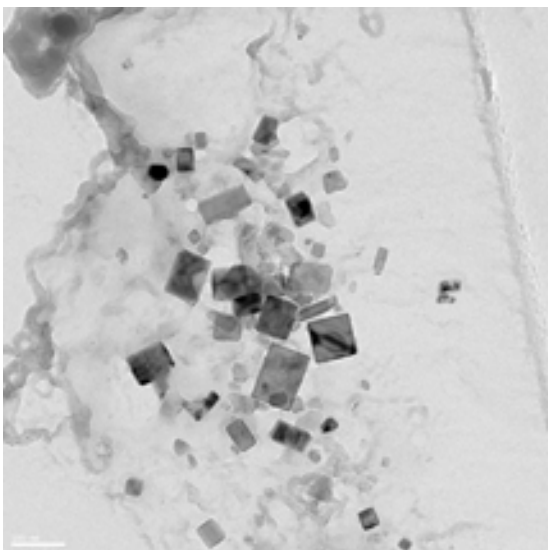
Zirconium was not found.



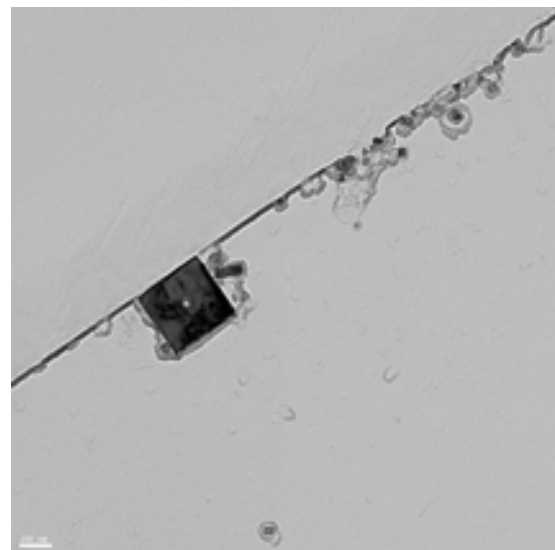
3.11 – Scale: 100nm



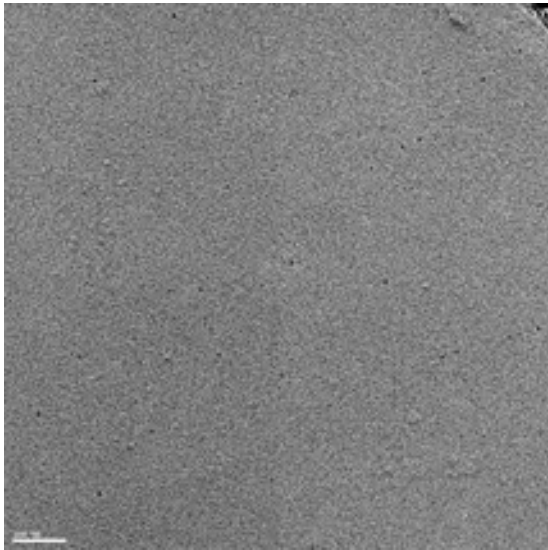
3.11 – Scale: 100nm



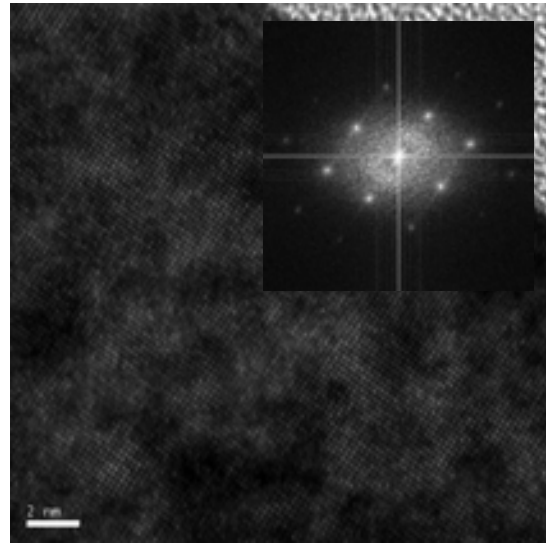
3.11 – Scale: 100nm



3.11 – Scale: 100nm



3.11 – Scale: 100nm



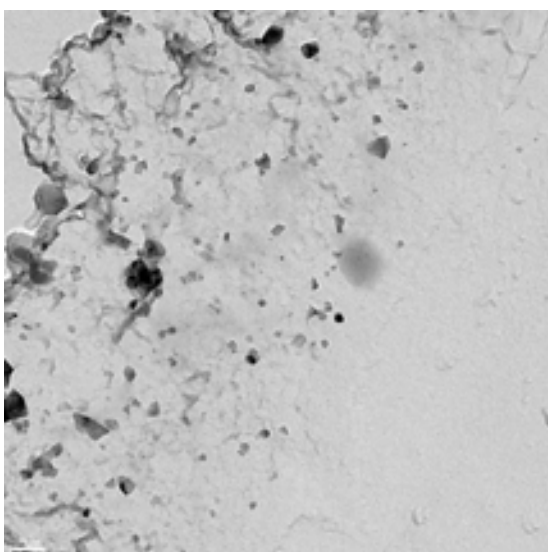
3.11 – Scale: 2nm

Sample F99406D (3.21)

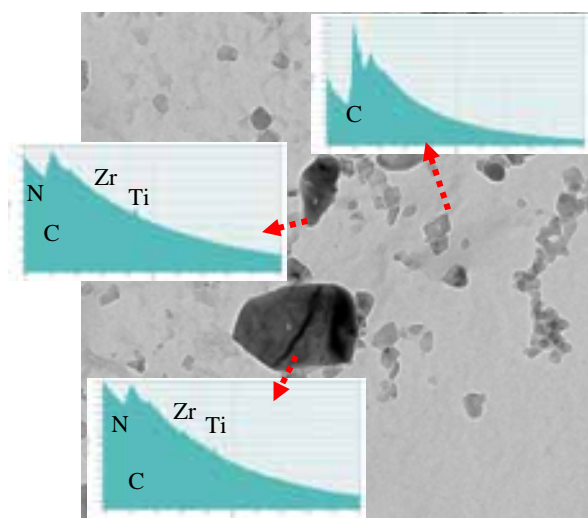
Medium size precipitates, between 30 and 60 nanometers, in the grain boundaries are found in majority.

The shape varies, between rounded sulfides and faceted zirconium nitrides.

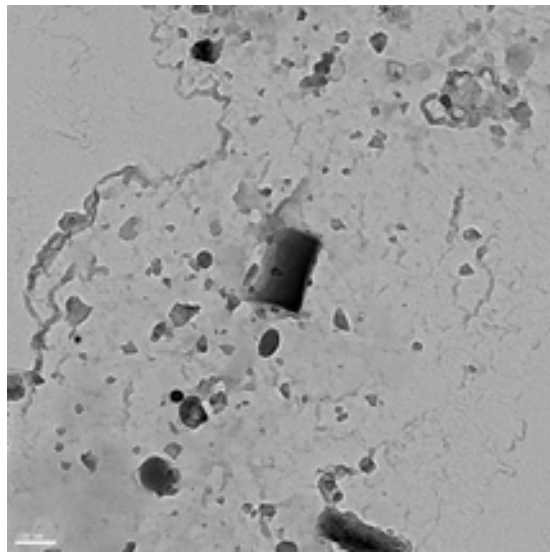
Not many squared titanium nitrates. The rest of the titanium that is not a nitride could form medium size carbosulfides, with rounded shape.



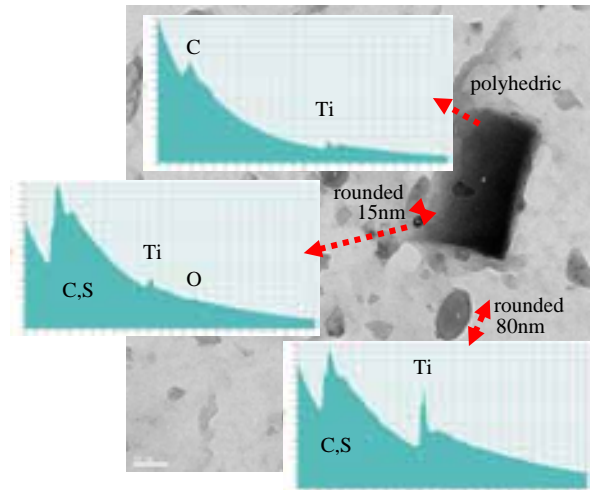
3.21 – Scale: 100nm



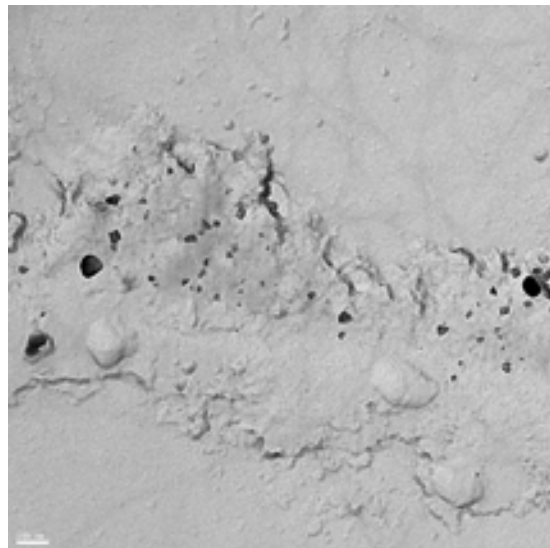
3.21 – Scale: 50nm



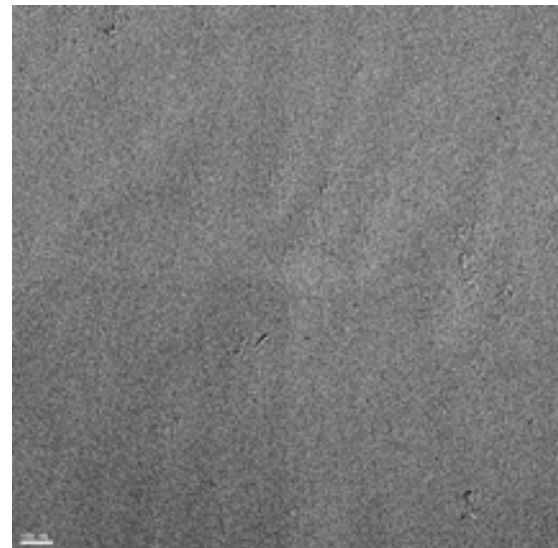
3.21 – Scale: 100nm



3.21 – Scale: 50nm



3.21 – Scale: 100nm

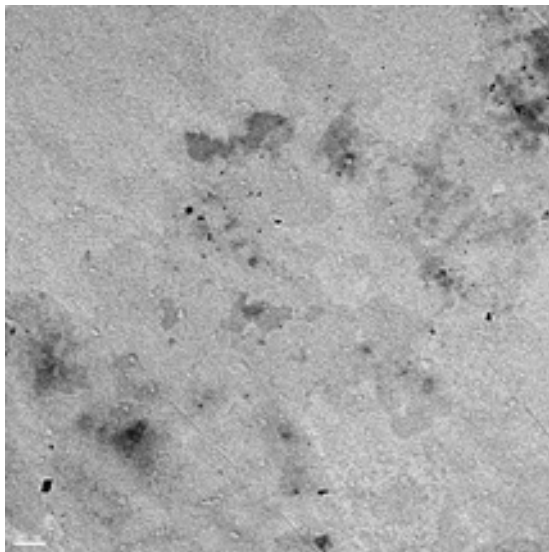


3.21 – Scale: 100nm

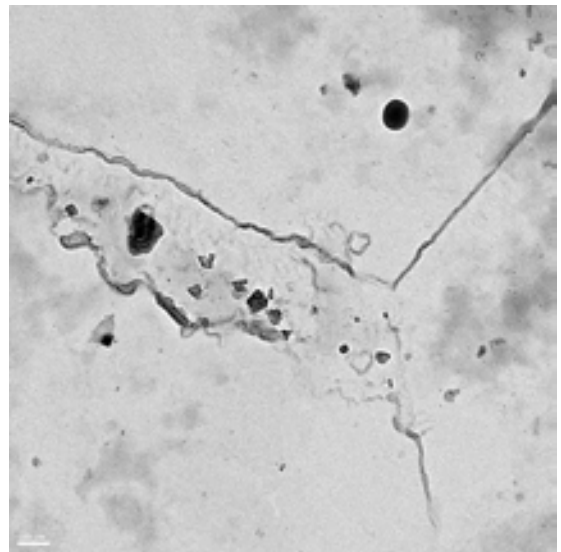
If it is compared samples 3.11 and 3.21, due to the high amount of Ti, the sample 3.11 shows quite squared precipitates of TiN. The sample 3.21 has low Ti, and maybe for this reason, it is possible to see more rounded carbosulfides. In addition, it is possible that the nitrogen had higher affinity for the zirconium. In this case, all the nitrogen forms polyhedral ZnN and it is not possible to create squared TiN. In the other hand the number of small precipitates is similar for both samples. For the same grain size, the losses in sample 3.11 are bigger than in sample 3.21, maybe due to the presence of big and medium squared precipitates.

Sample F00712A (3.10)

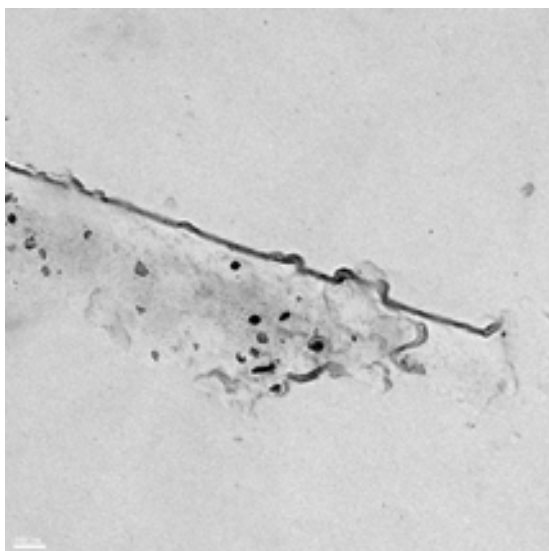
In this sample also is founded a quite amount of small precipitates, smaller than 10 nanometers, in grain boundaries and inside them. It shows high amount of medium polyhedric precipitates. There were found rounded titanium sulfates and polyhedric titanium carbides.



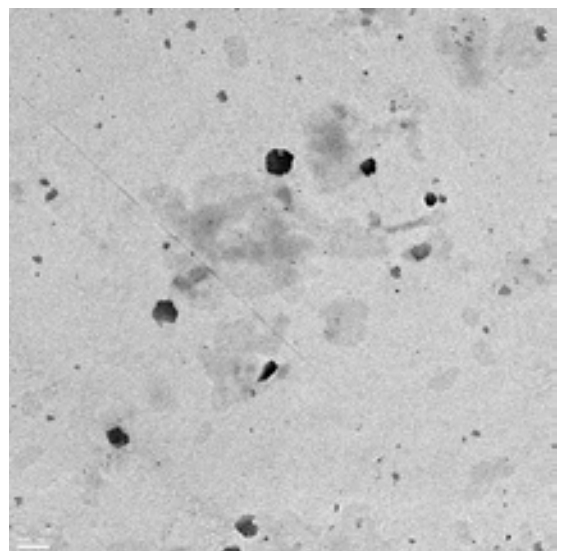
3.10 – Scale: 100nm



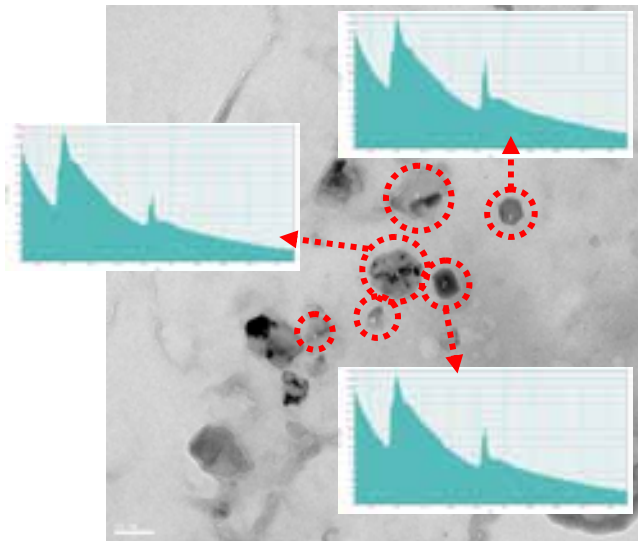
3.10 – Scale: 100nm



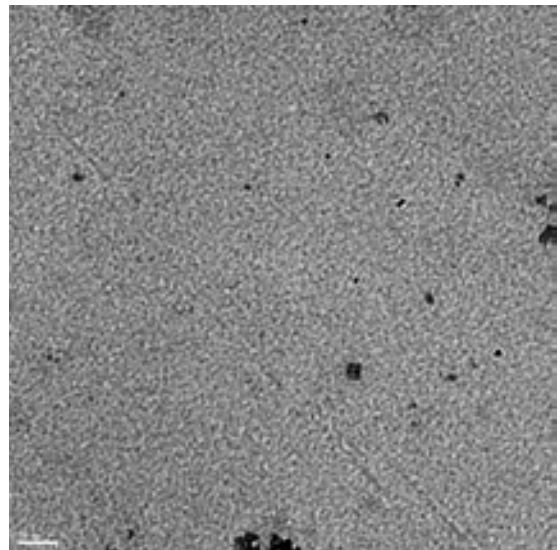
3.10 – Scale: 100nm



3.10 – Scale: 100nm



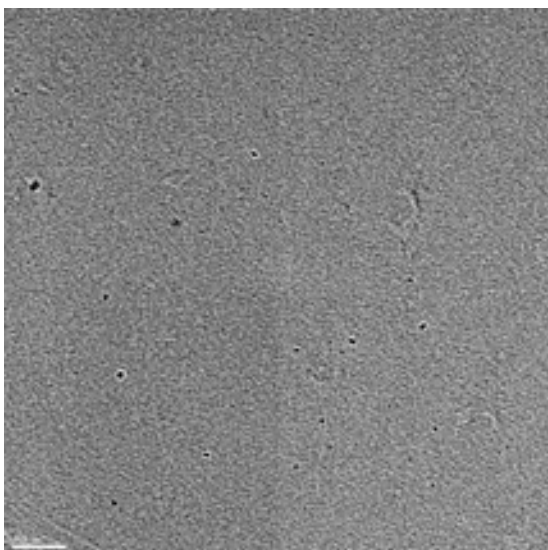
3.10 – Scale: 50nm



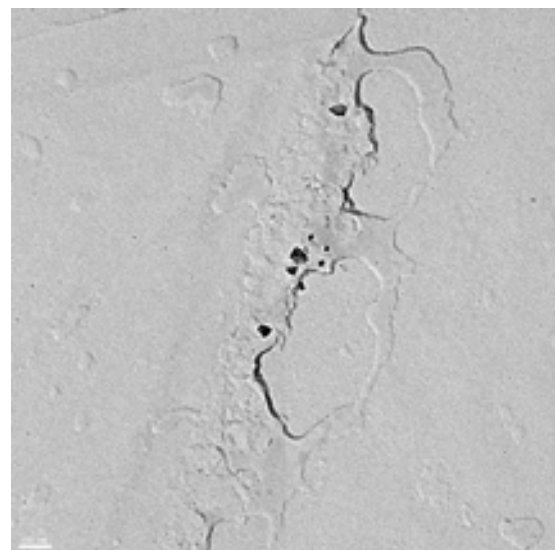
3.10 – Scale: 50nm

Sample F00440B (3.16)

The sample shows mainly small polyhedral precipitates of less than 10 nanometers, in the entire sample. Especially there are not big precipitates, only a small quantity of medium polyhedral precipitates.



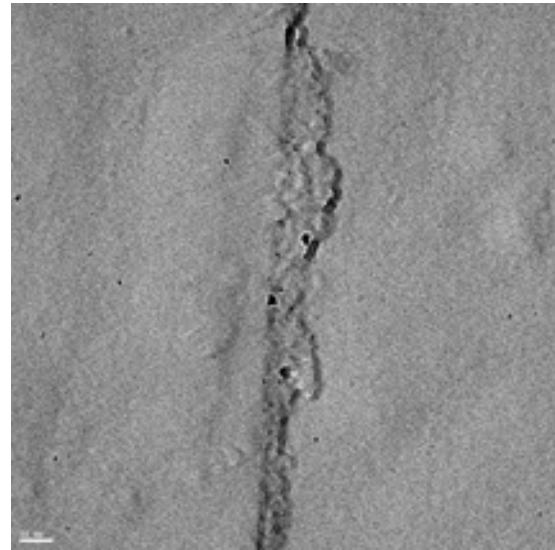
3.16 – Scale: 100nm



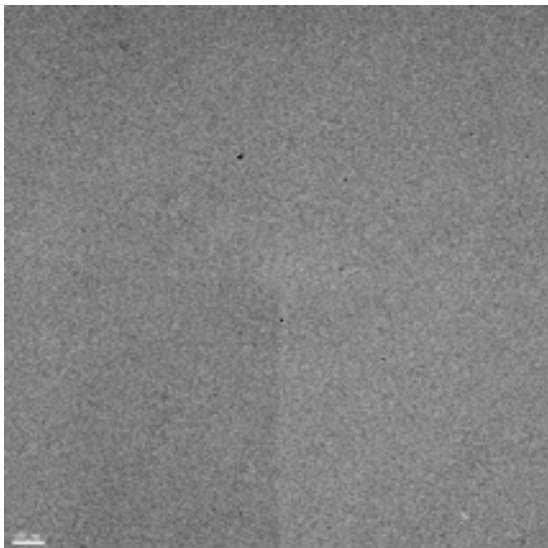
3.16 – Scale: 100nm



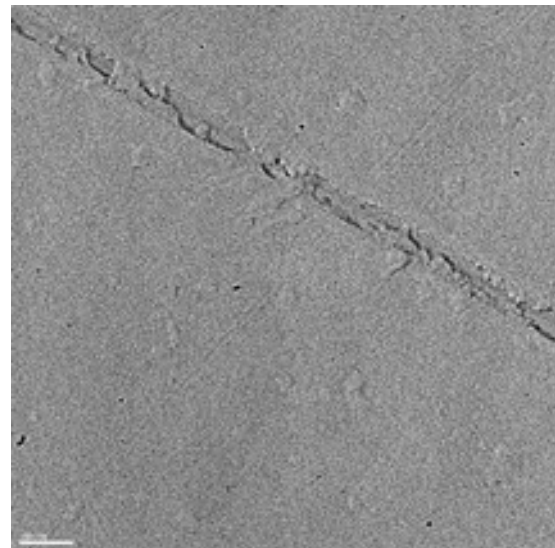
3.16 – Scale: 100nm



3.16 – Scale: 50nm



3.16 – Scale: 100nm



3.16 – Scale: 100nm

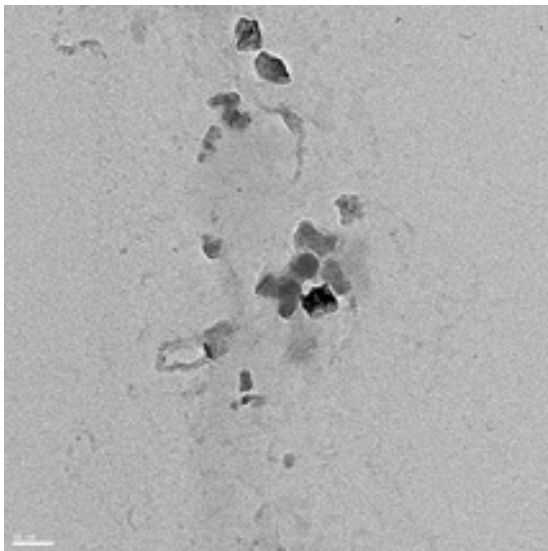
If it is compared samples 3.10 and 3.16, it is noted that the amount of small precipitates are quite similar. The first sample contains high carbon, and it is probable that it was precipitate both in small and in medium polyhedric TiC. The hysteresis losses in 3.10 sample is hence higher than sample 3.16, maybe due to the effect of medium size precipitates (10-60nm).

Sample F94266A (1.7)

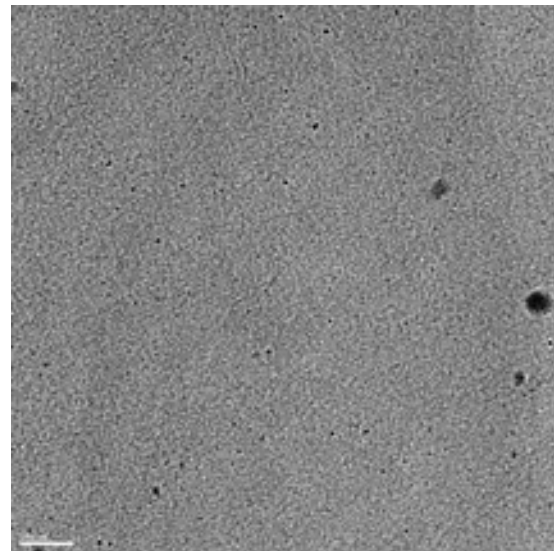
There were found a lot of small precipitates, smaller than 10 nanometers, in the grain boundaries and within the grains. Especially there are not a lot of big precipitates.

The predominant shape is polyhedral, from zirconium carbides. Not many squared titanium nitrates.

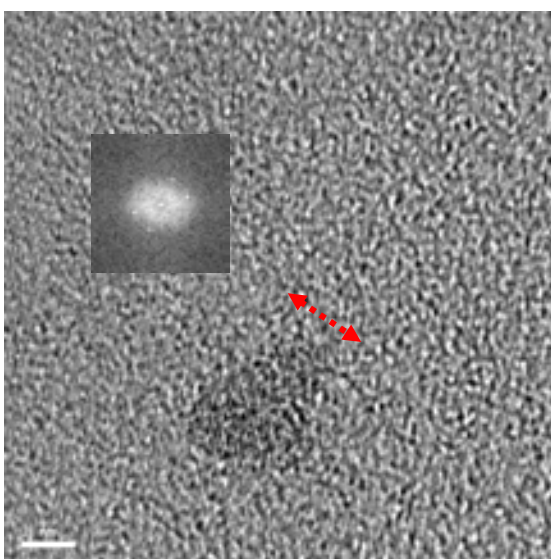
This sample contains high amount of carbon and nitrogen, and in this way is possible to form high quantity of small squared titanium carbides and nitrides.



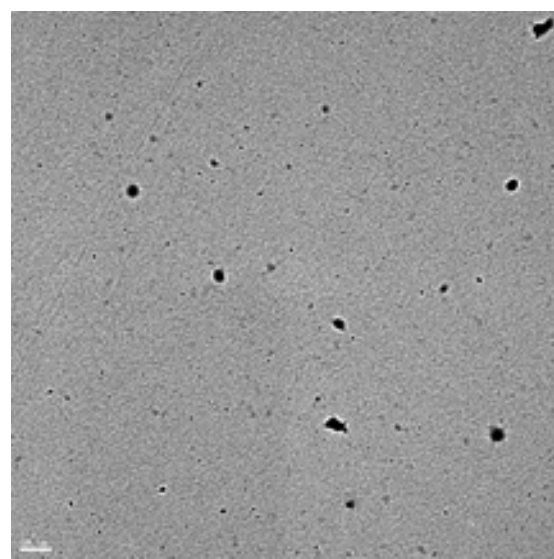
1.7 – Scale: 50nm



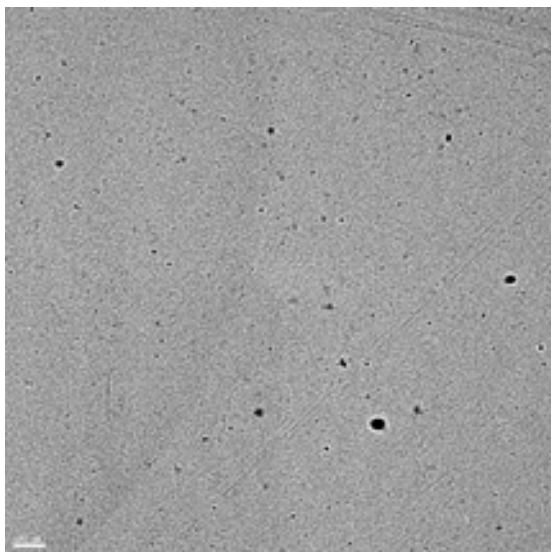
1.7 – Scale: 100nm



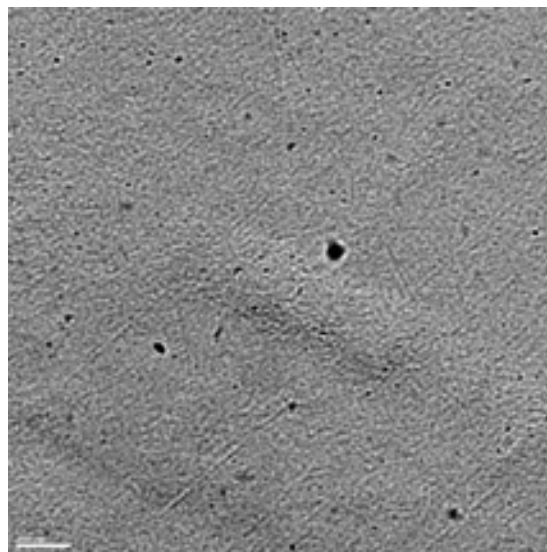
1.7 – Scale: 2nm



1.7 – Scale: 100nm



1.7 – Scale: 100nm



1.7 – Scale: 100nm

If it is compared samples 1.7 and 3.16, it is showed that the sample 1.7 with smaller grain size has similar power losses (it should be better), due to the not desirable effect of big and medium size precipitates.

5. SUMMARY AND CONCLUSIONS

Taking M32 (3.25%Si+0.9%Al) as the basis chemical composition and three different thicknesses (0.35, 0.5 and 0.65mm), different annealing conditions (temperature and time) have been applied in the laboratory simulator at St.Chély. In total, 60 samples have been characterized in terms of grain size and magnetic properties. The aim was to link annealing parameters, grain size and energy loss.

In addition, M250-50 samples having different magnetic behaviour (high and low losses) but the same grain size and texture, have been analyzed in terms of TEM observations of their precipitates. Ti-precipitates are mostly found, especially Ti (C,N) and not so many $Ti_4C_2S_2$. No trace of AlN is present in the materials and very few of MnS. Work is now being performed to discern clearly between TiN and TiC. However first results have reveal that a high amount of medium and big precipitates (>10 nm) worsen the magnetic properties of the material. The small precipitates (<10nm) do not have a strong influence on the magnetic properties. The presence of precipitates can have a great influence on the power losses and further work is clearly necessary.

The main conclusions are:

- The experimental results show that the highest temperature and the longest time during continuous annealing give the biggest grain size for the observed samples. Moreover the grain size is bigger for the thickest sample, as it was expected.

- A grain size modelling was built using the experimental values to give the kinetics of grain growth during recrystallization of ferrite. The equation is done as function of three factors: the thickness reduction percent in cold rolling, the annealing temperature and the annealing time. Once compared the experimental and calculated values, the model accuracy is very good.

- The values of magnetic induction are not strongly dependent of the samples grain size. This means that it is possible to adjust an optimum grain size to minimize the power losses, without a significant modification on the induction magnetization.

- The total magnetic losses for each thickness is the addition of three different losses that have different behaviour when the grain size changes: Foucault losses (constant with grain size); Hysteresis losses (decreasing when increasing the grain size) and Excess losses (increasing when increasing the grain size). The total balance of the magnetic losses gives a minimum value that corresponds with the optimum grain size.

- It is possible to determinate the optimum processing parameters to achieve the lowest total power losses for each thickness, by means of the grain size modelling and the relation between grain size and losses. The accuracy of the optimum processing parameters equation is lower than in the grain size modelling.

- The precipitates analysis in this study confirms that a high amount of medium and big precipitates (>10 nm) worsen the magnetic properties of the material. The small precipitates (<10nm) do not have strong influence in the magnetic properties. The presence of precipitates can influence the power losses more than the grain size.

6. BIBLIOGRAPHIC REFERENCES

Ref. 1: Cardoso, R.F.A.; Brandão, L.P.M.; Cunha, M.A. Influence of grain size and Al and Mn additions on the magnetic properties of non-oriented electrical steels with 3%Si. Cardoso, R.F.A.; Brandão, L.P.M.; Cunha, M.A.

Ref. 2 REVISTA PESQUISA FAPESP - Tecnologia- Innovaciones de acero 01.2004 - Edição 95

Ref. 3 Magnus Lindenmo. Journal of Magnetism and Magnetic Materials. Lean non-oriented electrical steel grades.

Ref. 4: Yan Hu, Valerie Randle, Terry Irons. Material Science and Engineering A 392 (2005) 282-291: Role of silicon content and final annealing temperature on microtexture and microstructure development in non-oriented silicon steel.

Ref. 5 M. De Wulf - 2. International Workshop Magnetism and Metallurgy, WMM 06, Freiberg, Germany - June 2000. Development of non oriented electrical steels at the ARCELOR group. Advances on experimental techniques, new material qualities and modelling tools. -

Ref. 6: Internal jobs: 40601 (Loss separation measurement on 60 samples), 38867 (Microscopic characterization and grain size in longitudinal and transverse direction; N-determination) and 41648 (Determination of Zr-content)

Ref. 7 ASTM E 112-96: Standard Test Methods for Determining Average Grain Size

Ref. 8 R. Spolenak. Praktische Metallographie, 2000. The Preparation of TEM-Specimens Using Focused Ion Beam (FIB) Systems.

Ref. 9 TEM Sample Preparation and FIB-Induced Damage, MRS Bulletin, 2007

Ref. 10 KC Thompson-Russell and JW Edington, 1977: Electron Microscope Specimen Preparation Techniques in Materials Science.

Ref. 11: Internal jobs: 41405 and 40103

Ref. 12 Precipitate Coarsening and Grain Growth in Steels.

Ref. 13 Y. Sidor, F. Kovac, V. Petrychka. Metallurgija 44 (2005) 3, 169-174. Secondary Recrystallization in Non-oriented Electrical Steels.

Ref. 14 F.J.G. Landgraf, M. Emura, J.C. Teixeira, M.F. de Campos. Journal of Magnetic Materials 215-216 (2000) 97-99. Effect of grain size, deformation, aging and anisotropy on hysteresis loss of electrical steels.

Ref. 15 Hou, C-K. China Steel Technical Report, No 5, pp 18-24, 1991: Isothermal Annealing of 0.5% Si Electrical Steel

Ref. 16 A. Broddefalk and Bruks AB. Dependence of the Power Loss of a Non-oriented S-steel on Frequency and Gauge.

Ref. 17: Atul Saxena and Sajal Kanti Chaudhuri. ISIJ International, Vol 44 (2004), no 7, pp 1273-1275: Correlating the Aluminum Content with Ferrite Grain Size and Core Loss in Non-oriented Electrical Steel.

Ref. 18: Carlos Alberto Cattaneo. Evolución del tamaño de grano en aceros eléctricos de bajo contenido en carbono. Facultad de Ciencias Exactas y Tecnologías. Universidad Nacional de Santiago del Estero.

Ref. 19: Keith Jenkins, Magnus Lindenmo. Journal of Magnetism and Magnetic Materials, 00 (2004) 000-000: Precipitates in Electrical Steels.

Ref. 20 Fernando J.G Landgraf. Short Course on Interactions Between Domain Walls and Microstructural Features

Ref. 21 Kim, Jong K. (Phang, KR), Lee, Sung J. (Phang, KR), Yoon, Young J. (Phang, KR). Process for manufacturing high magnetic flux density grain oriented electrical steel sheet having superior magnetic properties. United States Patent 5453136.

Ref. 22 I. Andersen and Ø. Grong. Acta Metall. Mater. Vol. 43, No7, pp 2673-2688, 1995. Analytical Modelling of Grain Growth in Metals and Alloys in the presence of Growing and Dissolving Precipitates-I.

Ref. 23 C.H. Wörner and P.M. Hazzledine. Grain Growth Stagnation by Inclusions or Pores.

Ref. 24 Jong-Tae Park, Jerzy A. Szpunar and Sang-Yung Cha. ISIJ International, Vol 43 (2003), No 10, pp 1611-1614: Effect of Heating Rate on the Development of Annealing Texture in Non-oriented Electrical Steels.

Ref. 25 ARITA Y. and USHIGAMI Y. Materials Science Forum 2007, vol. 539-43 (5), pp. 4428-4433. Effect of aluminum and titanium content on grain growth, texture and magnetic properties in 3% Si non-oriented electrical steel

Ref. 26 Chun-Kan HOU. ISIJ International, Vol 36 (1996), No 5, pp 563-571: Effect of Hot Band Annealing Temperature on the Magnetic Properties of Low-carbon Electrical Steels.

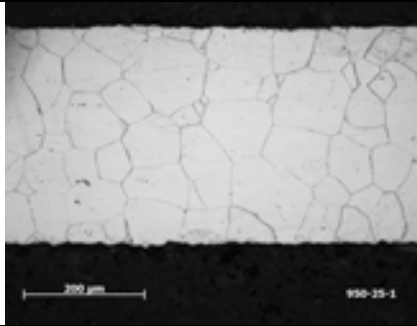
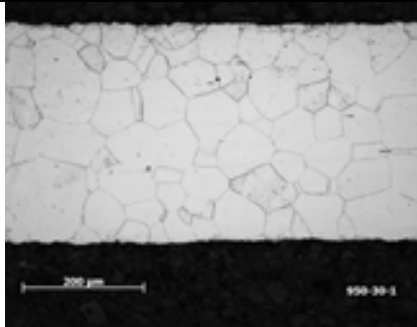
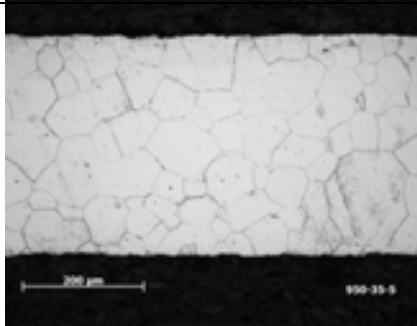
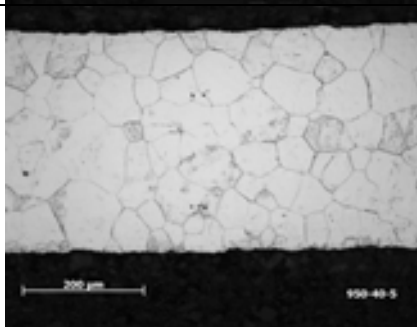
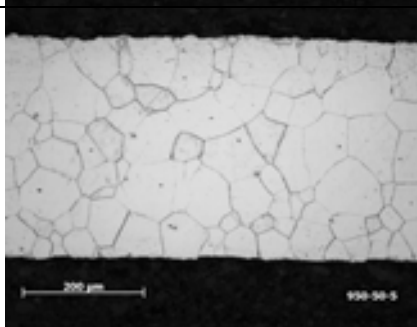
Ref. 27 Y. Arita and Y. Ushigami. Materials Science Forum Vols 539-543 (2007) pp 4428-4433: Effect of Aluminum and Titanium Content on Grain Growth, Texture and Magnetic Properties in 3%Si Non-Oriented Electrical Steel.

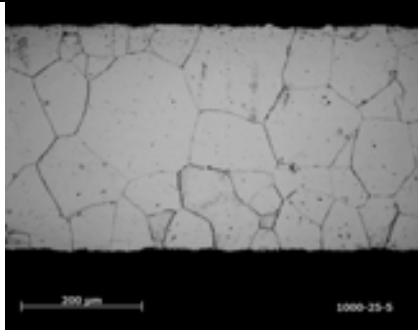
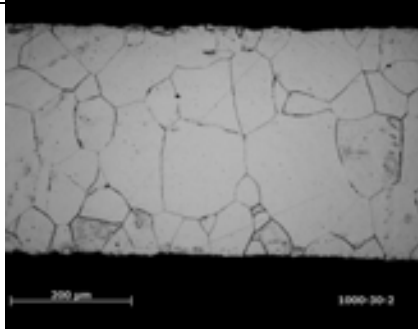
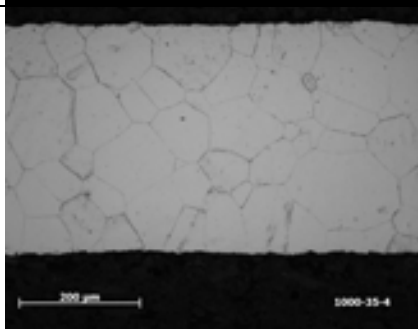
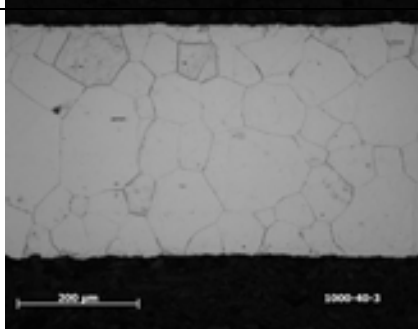
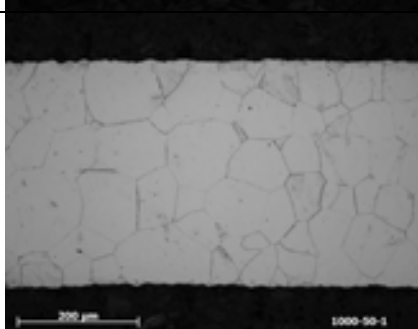
Ref. 28 Philip Beckley. Electrical Steels, 2000.

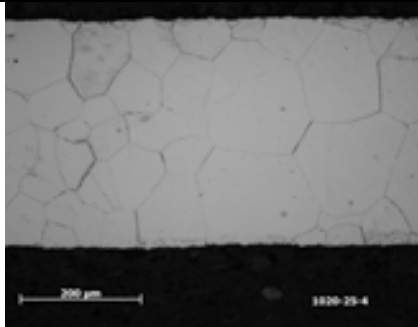
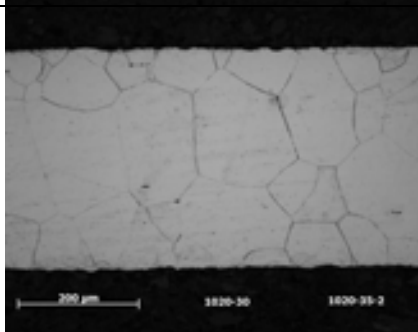
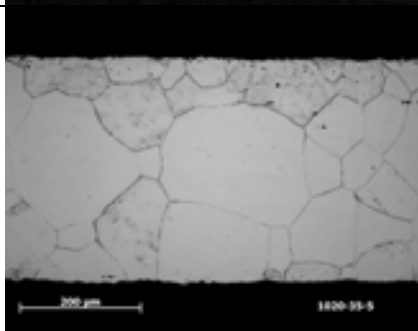
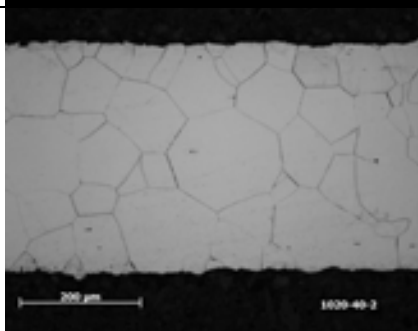
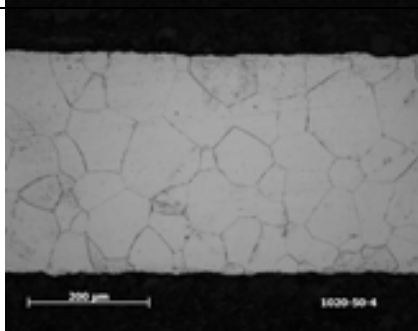
Ref. 29 Atul SAXENA, Ashit SENGUPTA and Sajal Kanti CHAUDHURI. ISIJ International Vol. 45 (2005) , No. 2 pp.299-301. Effect of Absorbed Nitrogen on the Microstructure and Core Loss Property of Non-oriented Electrical Steel.

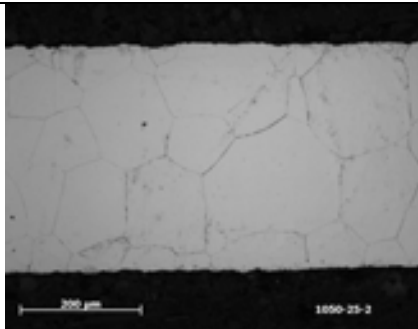
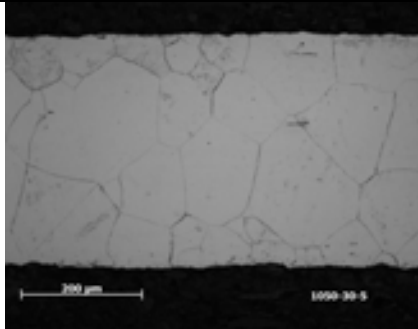
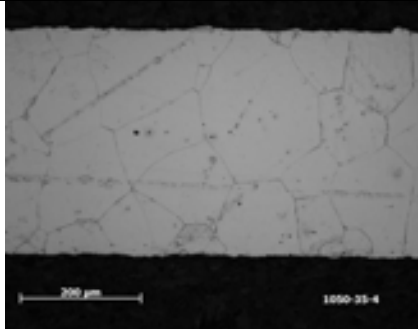
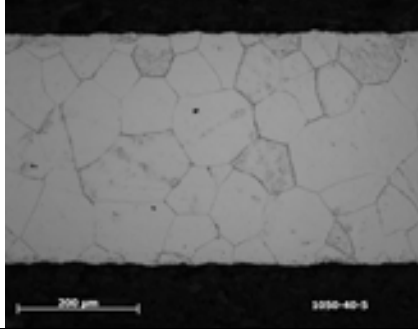
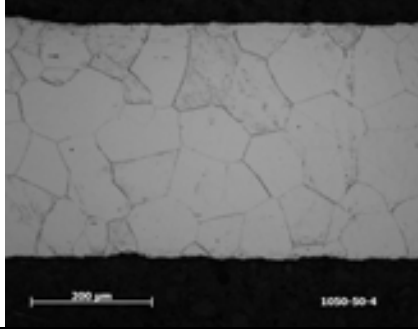
APPENDICE

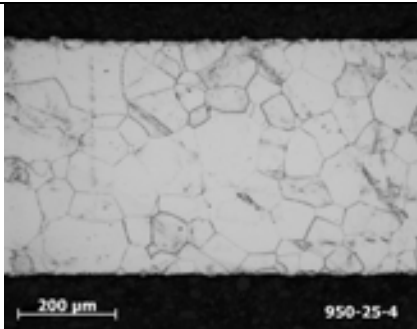
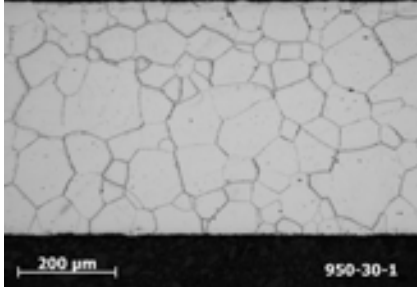
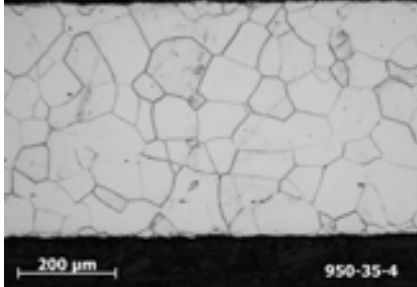
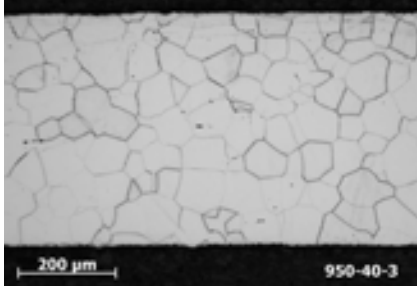
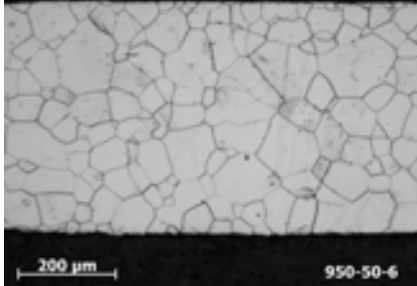
Appendix 1: Results of Grain Size

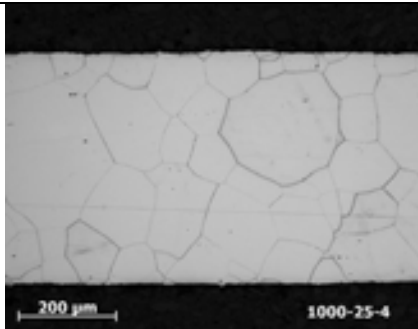
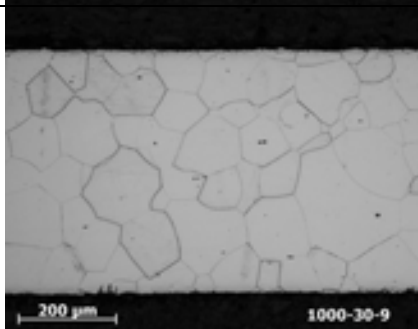
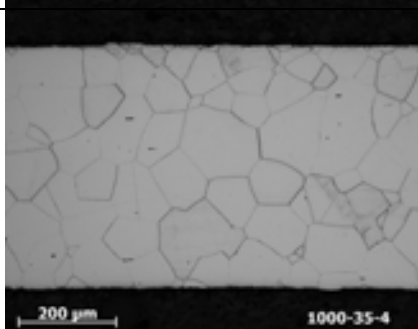
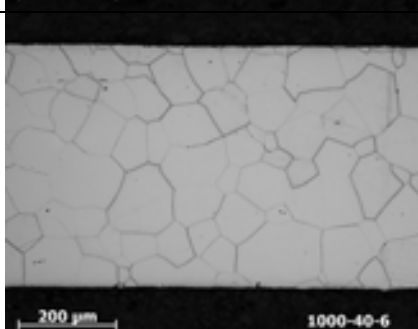
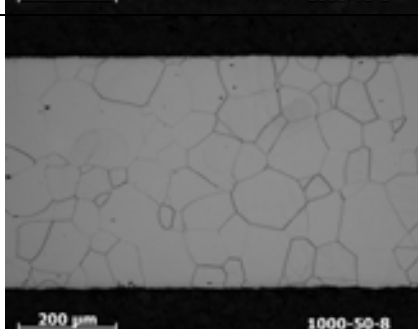
sample	Annealing temperature (°C)	Line speed	Representative micrographs	Nominal diameter (µm/int) (±10,62)	ASTM number (±0,40)	Mean diameter (µm) (±11,93)
F01514	950	25		59,53	4,85	66,85
F01514	950	30		55,94	5,03	62,83
F01514	950	35		52,50	5,22	58,97
F01514	950	40		48,82	5,43	54,83
F01514	950	50		45,64	5,62	51,27

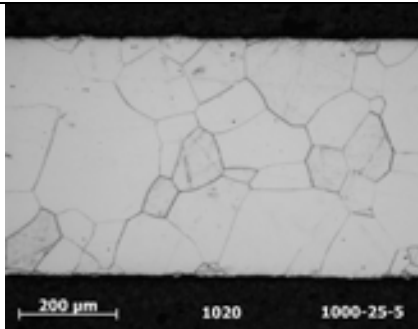
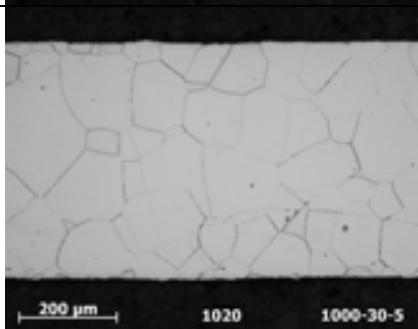
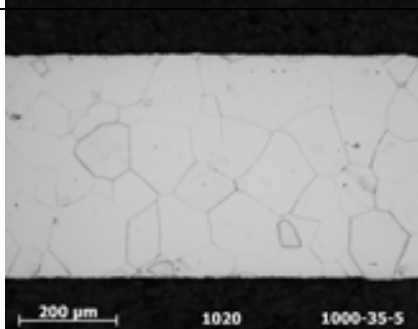
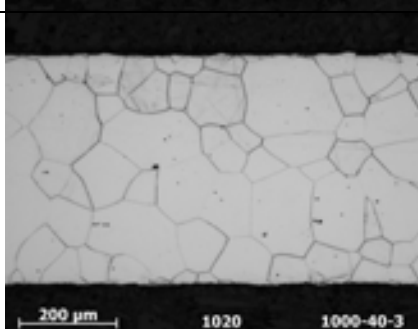
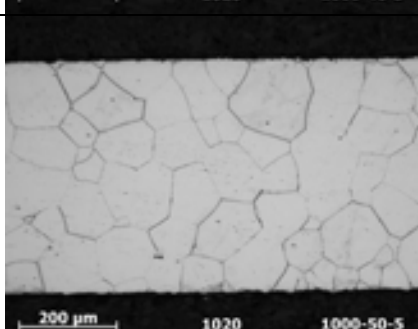
sample	Annealing temperature (°C)	Line speed	Representative micrographs	Nominal diameter (μm/int) (±10,62)	ASTM number (±0,40)	Mean diameter (μm) (±11,93)
F01514	1000	25		77,61	4,09	87,13
F01514	1000	30		77,40	4,10	86,92
F01514	1000	35		69,91	4,39	78,51
F01514	1000	40		63,31	4,67	71,11
F01514	1000	50		59,87	4,84	67,24

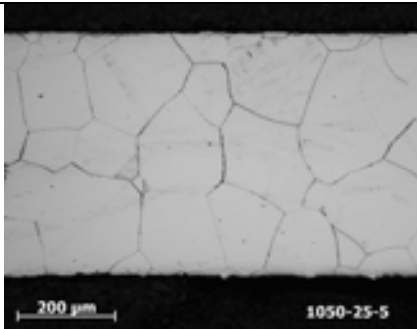
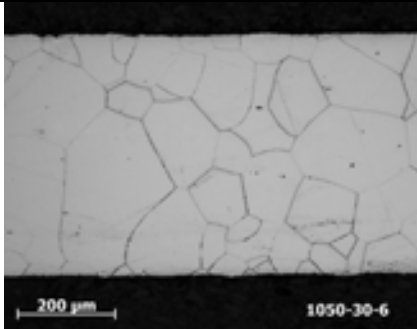
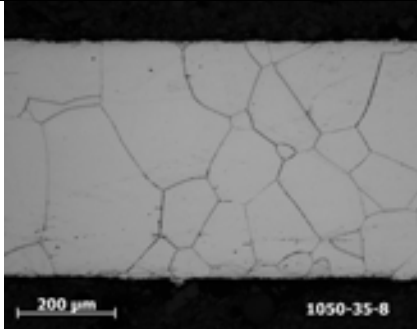
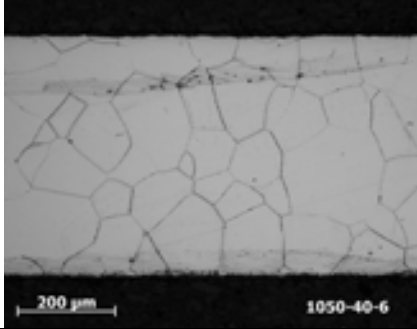
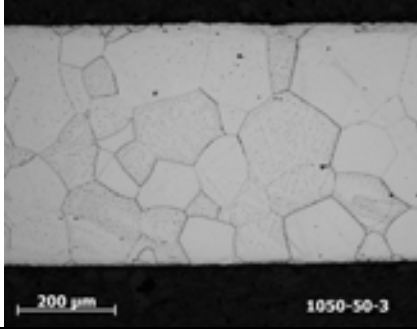
sample	Annealing temperature (°C)	Line speed	Representative micrographs	Nominal diameter (μm/int) (±10,62)	ASTM number (±0,40)	Mean diameter (μm) (±11,93)
F01514	1020	25		85,82	3,80	96,35
F01514	1020	30		86,09	3,79	96,67
F01514	1020	35		83,93	3,86	94,23
F01514	1020	40		69,74	4,40	78,31
F01514	1020	50		63,97	4,65	71,84

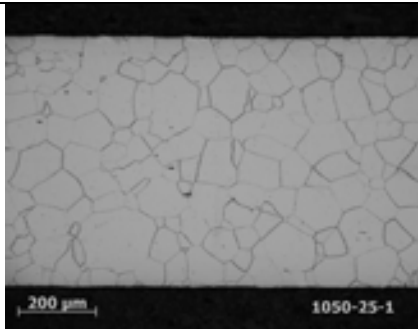
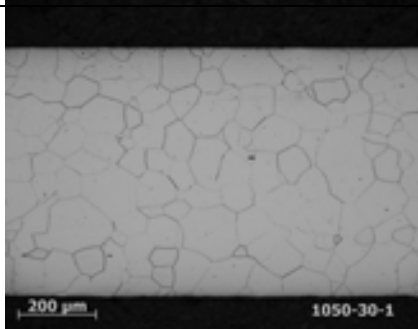
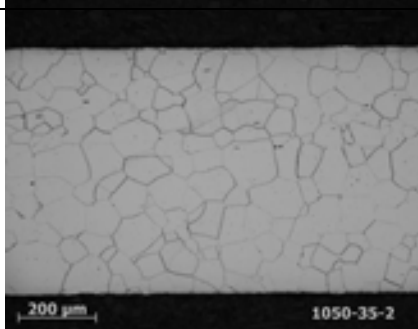
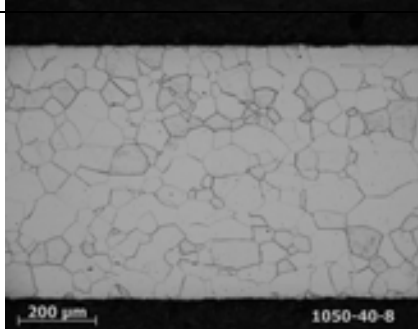
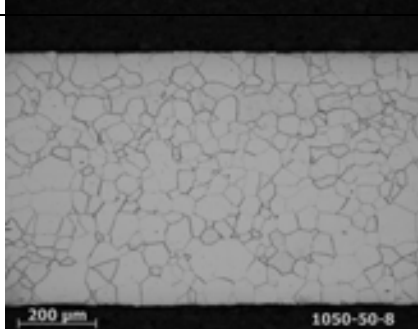
sample	Annealing temperature (°C)	Line speed	Representative micrographs	Nominal diameter (μm/int) (±10,62)	ASTM number (±0,40)	Mean diameter (μm) (±11,93)
F01514	1050	25		98,79	3,39	110,93
F01514	1050	30		102,67	3,28	115,30
F01514	1050	35		90,45	3,65	101,56
F01514	1050	40		80,18	3,99	90,04
F01514	1050	50		72,03	4,30	80,89

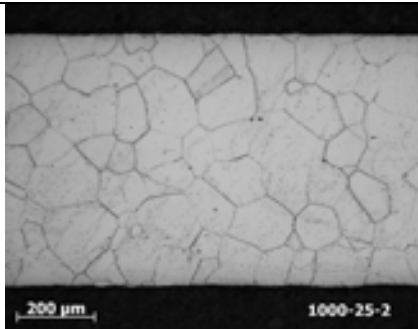
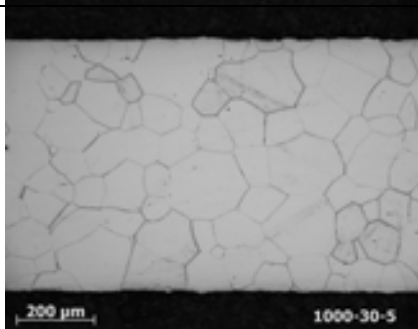
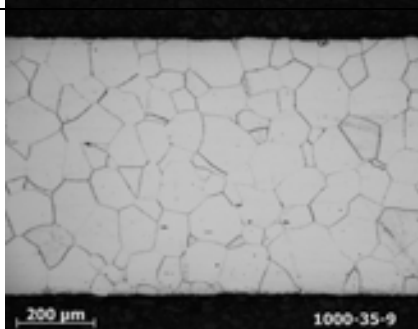
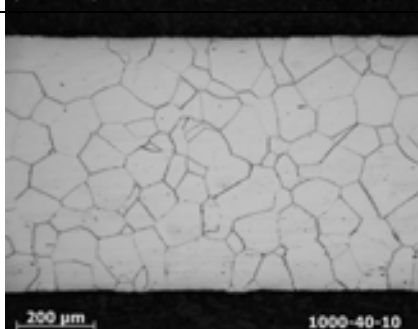
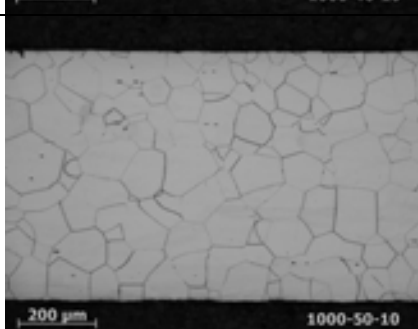
sample	Annealing temperature (°C)	Line speed	Representative micrographs	Nominal diameter (µm/int) (±10,62)	ASTM number (±0,40)	Mean diameter (µm) (±11,93)
F01494	950	25		65,88	4,56	73,99
F01494	950	30		64,70	4,61	72,66
F01494	950	35		58,73	4,89	65,95
F01494	950	40		57,15	4,97	64,18
F01494	950	50		48,32	5,46	54,26

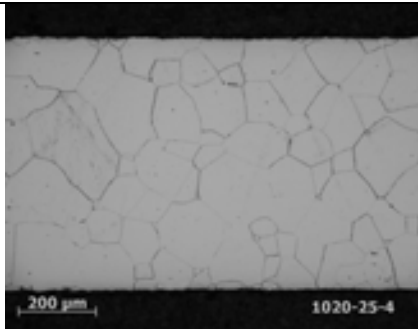
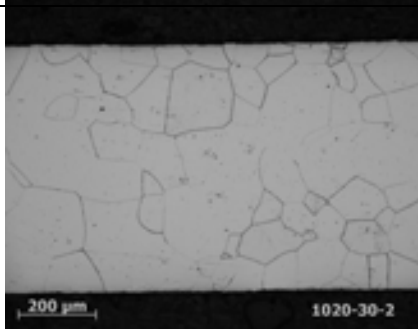
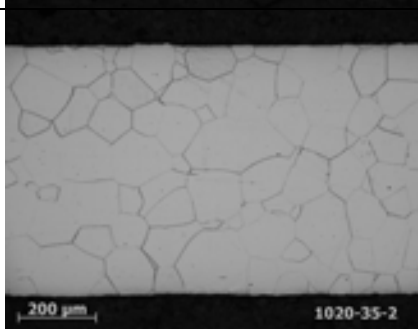
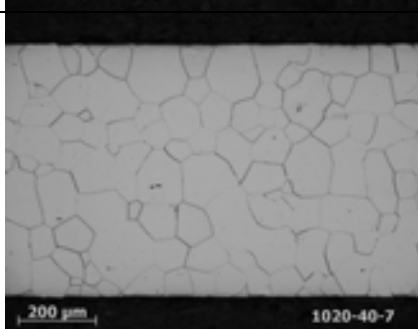
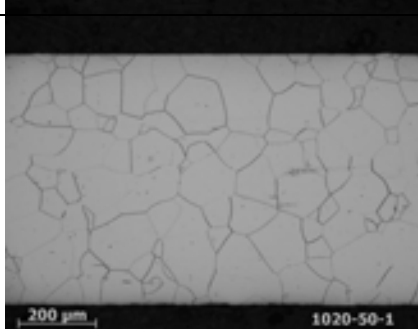
sample	Annealing temperature (°C)	Line speed	Representative micrographs	Nominal diameter (µm/int) (±10,62)	ASTM number (±0,40)	Mean diameter (µm) (±11,93)
F01494	1000	25		85,73	3,80	96,28
F01494	1000	30		80,14	3,99	90,00
F01494	1000	35		77,09	4,11	86,56
F01494	1000	40		66,42	4,54	74,59
F01494	1000	50		62,59	4,71	70,30

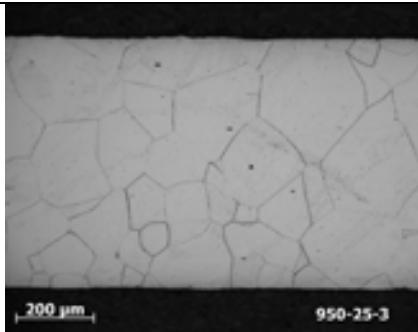
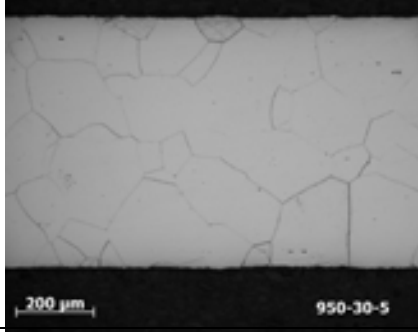
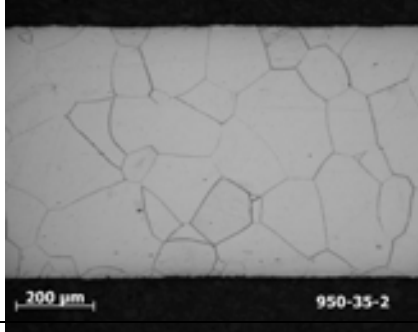
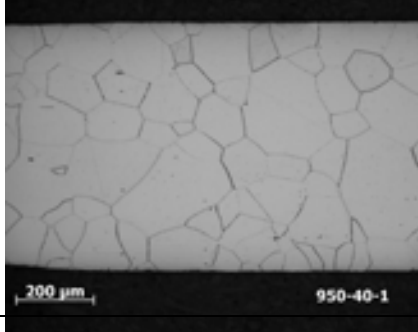
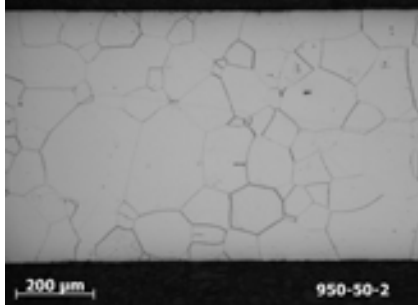
sample	Annealing temperature (°C)	Line speed	Representative micrographs	Nominal diameter (µm/int) (±10,62)	ASTM number (±0,40)	Mean diameter (µm) (±11,93)
F01494	1020	25		85,70	3,80	96,24
F01494	1020	30		90,22	3,65	101,32
F01494	1020	35		87,49	3,74	98,22
F01494	1020	40		77,46	4,09	86,97
F01494	1020	50		79,30	4,03	89,05

sample	Annealing temperature (°C)	Line speed	Representative micrographs	Nominal diameter (μm/int) (±10,62)	ASTM number (±0,40)	Mean diameter (μm) (±11,93)
F01494	1050	25		104,46	3,23	117,28
F01494	1050	30		110,28	3,07	123,81
F01494	1050	35		101,62	3,31	114,09
F01494	1050	40		96,30	3,46	108,13
F01494	1050	50		93,09	3,56	104,52

sample	Annealing temperature (°C)	Line speed	Representative micrographs	Nominal diameter (μm/int) (±10,62)	ASTM number (±0,40)	Mean diameter (μm) (±11,93)
F98843	950	25		62,96	4,69	70,70
F98843	950	30		63,31	4,68	71,10
F98843	950	35		62,55	4,71	70,24
F98843	950	40		50,32	5,34	56,52
F98843	950	50		40,64	5,95	45,65

sample	Annealing temperature (°C)	Line speed	Representative micrographs	Nominal diameter (μm/int) (±10,62)	ASTM number (±0,40)	Mean diameter (μm) (±11,93)
F98843	1000	25		87,29	3,75	97,99
F98843	1000	30		88,84	3,70	99,76
F98843	1000	35		80,93	3,97	90,89
F98843	1000	40		68,16	4,46	76,54
F98843	1000	50		68,30	4,46	76,70

sample	Annealing temperature (°C)	Line speed	Representative micrographs	Nominal diameter (μm/int) (±10,62)	ASTM number (±0,40)	Mean diameter (μm) (±11,93)
F98843	1020	25		102,21	3,29	114,75
F98843	1020	30		96,31	3,46	108,14
F98843	1020	35		92,13	3,59	103,44
F98843	1020	40		83,58	3,87	93,87
F98843	1020	50		78,45	4,06	88,09

sample	Annealing temperature (°C)	Line speed	Representative micrographs	Nominal diameter (μm/int) (±10,62)	ASTM number (±0,40)	Mean diameter (μm) (±11,93)
F98843	1050	25		114,44	2,97	128,48
F98843	1050	30		108,02	3,13	121,25
F98843	1050	35		112,36	3,02	126,15
F98843	1050	40		93,50	3,55	104,97
F98843	1050	50		97,48	3,43	109,45

Appendix 2: Correlations ASTM Number for uniform, randomly oriented and equiaxed grains

E 112

TABLE 4 Grain Size Relationships Computed for Uniform, Randomly Oriented, Equiaxed Grains

Grain Size No. G	\bar{N}_A Grains/Unit Area		\bar{A} Average Grain Area		\bar{D} Average Diameter		\bar{T} Mean Intercept		\bar{N}_L No./mm
	No./in. ² at 100X	No./mm ² at 1X	mm ²	μm ²	mm	μm	mm	μm	
00	0.25	3.88	0.2581	258064	0.5080	508.0	0.4825	482.5	2.21
0	0.50	7.75	0.1290	129032	0.3592	359.2	0.3200	320.0	3.12
0.5	0.71	10.95	0.0912	91239	0.3021	302.1	0.2691	269.1	3.72
1.0	1.00	15.50	0.0645	64518	0.2540	254.0	0.2263	226.3	4.42
1.5	1.41	21.92	0.0456	45620	0.2136	213.6	0.1903	190.3	5.26
2.0	2.00	31.00	0.0323	32258	0.1796	179.6	0.1600	160.0	6.25
2.5	2.83	43.84	0.0228	22810	0.1510	151.0	0.1345	134.5	7.43
3.0	4.00	62.00	0.0161	16129	0.1270	127.0	0.1131	113.1	8.84
3.5	5.66	87.68	0.0114	11405	0.1068	106.8	0.0951	95.1	10.51
4.0	8.00	124.00	0.00806	8065	0.0898	89.8	0.0800	80.0	12.50
4.5	11.31	175.36	0.00570	5703	0.0755	75.5	0.0673	67.3	14.87
5.0	16.00	248.00	0.00403	4032	0.0635	63.5	0.0566	56.6	17.68
5.5	22.63	350.73	0.00285	2851	0.0534	53.4	0.0476	47.6	21.02
6.0	32.00	496.00	0.00202	2016	0.0449	44.9	0.0400	40.0	25.00
6.5	45.25	701.45	0.00143	1426	0.0378	37.8	0.0336	33.6	29.73
7.0	64.00	992.00	0.00101	1008	0.0318	31.8	0.0283	28.3	35.36
7.5	90.51	1402.9	0.00071	713	0.0267	26.7	0.0238	23.8	42.04
8.0	128.00	1984.0	0.00050	504	0.0225	22.5	0.0200	20.0	50.00
8.5	181.02	2805.8	0.00036	358	0.0189	18.9	0.0168	16.8	59.46
9.0	256.00	3968.0	0.00025	252	0.0159	15.9	0.0141	14.1	70.71
9.5	362.04	5611.6	0.00018	178	0.0133	13.3	0.0119	11.9	84.09
10.0	512.00	7936.0	0.00013	126	0.0112	11.2	0.0100	10.0	100.00
10.5	724.08	11223.2	0.000089	89.1	0.0094	9.4	0.0084	8.4	118.9
11.0	1024.00	15872.0	0.000063	63.0	0.0079	7.9	0.0071	7.1	141.4
11.5	1448.15	22446.4	0.000045	44.6	0.0067	6.7	0.0060	5.9	168.2
12.0	2048.00	31744.1	0.000032	31.5	0.0056	5.6	0.0050	5.0	200.0
12.5	2896.31	44892.9	0.000022	22.3	0.0047	4.7	0.0042	4.2	237.8
13.0	4096.00	63488.1	0.000016	15.8	0.0040	4.0	0.0035	3.5	282.8
13.5	5792.62	89785.8	0.000011	11.1	0.0033	3.3	0.0030	3.0	336.4
14.0	8192.00	126976.3	0.000008	7.9	0.0028	2.8	0.0025	2.5	400.0

Table 1: Correlations ASTM number for uniform, randomly oriented and equiaxed grains

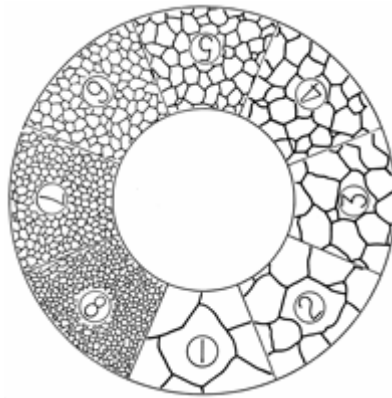


Fig. 1: Graphic representation of ASTM number

Appendix 3: Statistical results for grain size

Instrumental error: the error in the rule estimated is 0.5mm.

Propagated error calculus:

$$F = F(x, y, z, \dots) \Rightarrow \Delta F = \sqrt{\left(\frac{\partial F}{\partial x} \cdot \Delta x\right)^2 + \left(\frac{\partial F}{\partial y} \cdot \Delta y\right)^2 + \left(\frac{\partial F}{\partial z} \cdot \Delta z\right)^2 + \dots}$$

Linear length: $L = H + V + D1 + D2$ (mm)	$\Delta H = \Delta V = \Delta D1 = \Delta D2 = 0.5mm$ $\Delta L = \sqrt{\Delta H^2 + \Delta V^2 + \Delta D1^2 + \Delta D2^2} = \sqrt{4 \cdot 0.5^2} = \pm 1mm$
Mean linear length: $\bar{L} = \frac{\sum X_i}{n} = \frac{\sum L_i}{5}$ (mm)	$\Delta L = 1mm$ $\Delta \bar{L} = \sqrt{5 \cdot \left(\frac{1}{5} \cdot \Delta L\right)^2} = \sqrt{5 \cdot \left(\frac{1}{5}\right)^2} = \pm 0,45mm$
Intersections number: $I = IH + IV + ID1 + ID2$	$\Delta I = 0$
Number of intercepts per unit length: $N_L = \frac{I}{L}$ (int/mm)	$\Delta L = 0,45mm, \Delta I = 0$ $\Delta N_L = \sqrt{\left(\frac{-I}{L^2} \cdot \Delta L\right)^2}$ Variable
Mean number of intercepts per unit length: $\bar{N}_L = \frac{\sum X_i}{n} = \frac{\sum N_{Li}}{5}$ (int/mm)	$\Delta \bar{N}_L = \sqrt{5 \cdot \left(\frac{1}{5} \cdot \Delta N_L\right)^2}$ Variable
Nominal diameter: $D_n = \frac{\bar{L}}{I}$ ($\mu\text{m/int}$)	$\Delta \bar{L} = \pm 0,45mm, \Delta I = 0$ $\Delta D_n = \frac{1}{I} \cdot \Delta L = \frac{0,45}{I}$ (mm) Variable
ASTM number grain size: $G = -3,2877 + 6.643856 \log_{10}(\bar{N}_L)$	$\Delta G = \frac{6,643856}{N_L \cdot \ln 10} \cdot \Delta \bar{N}_L$ Variable
Mean diameter: $D_M = 359,08 \cdot \exp(-0.3464G)$	$\Delta D_M = 359,08 \cdot (-0,3464) \cdot e^{-0,3454 \cdot G} \cdot \Delta G$ Variable

Table 1: Statistical calculus equations of grain size

Sample	N_L (Int/mm)	Number of intercepts per unit length ($\pm\Delta N_L$)	Nominal diameter ($\pm\Delta D_n$) μm	ASTM grain size ($\pm\Delta G$)	Mean diameter ($\pm\Delta D_M$) μm	Standard deviation on N_L	% Relative accuracy
F01514-950-25	16,79882526	2,8861418	10,227273	0,4957278	11,50247897	1,728634461	12,77
F01514-950-30	17,87571867	3,0856168	9,6566524	0,4980682	10,86284535	1,401150298	9,73
F01514-950-35	19,04571385	3,2781305	9,0361446	0,4966029	10,16771378	1,072230652	6,99
F01514-950-40	20,48290767	3,522049	8,3955224	0,4961649	9,448276511	1,356320395	8,22
F01514-950-50	21,90714318	3,7628926	7,8397213	0,4955823	8,825651781	1,339864842	7,59
F01514-1000-25	12,88808724	2,2105847	13,313609	0,4950009	14,95738458	1,21574916	11,71
F01514-1000-30	12,91887171	2,209388	13,235294	0,4934093	14,87388257	1,020013203	9,80
F01514-1000-35	14,30251989	2,4490469	11,968085	0,4939869	13,45531318	1,212509645	10,52
F01514-1000-40	15,79326511	2,6985162	10,817308	0,492977	12,16441409	0,75651355	5,95
F01514-1000-50	16,70195612	2,8662847	10,273973	0,4951461	11,5553911	2,442240951	18,15
F01514-1020-25	11,65346328	1,9966117	14,705882	0,494421	16,51703815	2,065665953	22,01
F01514-1020-30	11,61542771	2,010355	14,900662	0,4993944	16,73763125	1,571989747	16,80
F01514-1020-35	11,91605861	2,0477395	14,423077	0,4958734	16,20172386	1,069619556	11,14
F01514-1020-40	14,33978586	2,447726	11,904762	0,4925454	13,38130282	2,022195649	17,51
F01514-1020-50	15,63259825	2,6952041	11,029412	0,497481	12,4012894	1,032220143	8,20
F01514-1050-25	10,12170328	1,733585	16,917293	0,4941315	18,99644763	1,26583714	15,53
F01514-1050-30	9,737299163	1,6674362	17,578125	0,4939869	19,73801782	1,820602322	23,21
F01514-1050-35	11,05517801	1,8966555	15,517241	0,4950009	17,42822761	1,228424206	13,79
F01514-1050-40	12,4711755	2,1339039	13,719512	0,4936979	15,41500781	1,268639565	12,63
F01514-1050-50	13,88313093	2,3700205	12,295082	0,4925454	13,81993954	1,722925307	15,41
		MAX	17,59	0,50	19,74		
		MIN	7,84	0,49	8,83		
		AVERAGE	12,39	0,50	13,92	1,437	12,88

F01494-950-25	15,17774854	2,0570006	8,9285714	0,3910324	10,03883949	0,79762996	6,52
F01494-950-30	15,45587621	2,091431	8,7548638	0,390437	9,843785789	1,05203677	8,45
F01494-950-35	17,02826149	2,313155	7,9787234	0,3919887	8,97326069	1,415637523	10,32
F01494-950-40	17,49889429	2,3758702	7,7586207	0,3917492	8,727393215	1,200883588	8,52
F01494-950-50	20,69887562	2,8100809	6,5597668	0,3917492	7,382354535	2,587068238	15,52
F01494-1000-25	11,66202253	1,5860246	11,658031	0,3923486	13,09753616	2,213141495	23,56
F01494-1000-30	12,47588536	1,6762238	10,76555	0,3876043	12,09783538	2,026350212	20,16
F01494-1000-35	12,97241114	1,7368356	10,321101	0,3863197	11,59775349	1,106876922	10,59
F01494-1000-40	15,05493808	2,0156853	8,8932806	0,3863197	9,998483393	0,44897771	3,70
F01494-1000-50	15,97524785	2,1670793	8,490566	0,3913905	9,54807777	1,004990863	7,81
F01494-1020-25	11,66716487	1,5710567	11,538462	0,3884851	12,96286819	1,842288559	19,60
F01494-1020-30	11,08203348	1,494109	12,162162	0,3889565	13,66149153	1,266148754	14,18

F01494-1020-35	11,43202578	1,5635394	11,968085	0,3947038	13,44033914	1,072145339	11,64
F01494-1020-40	12,91112227	1,7606007	10,56338	0,3934925	11,8689735	0,75302279	7,24
F01494-1020-50	12,61006299	1,711742	10,76555	0,3916894	12,09568998	1,239228746	12,20
F01494-1050-25	9,573489311	1,2807787	13,975155	0,386029	15,68741424	0,801624389	10,40
F01494-1050-30	9,067688929	1,2172313	14,802632	0,3873116	16,61445123	0,77167357	10,57
F01494-1050-35	9,840619114	1,3285345	13,719512	0,3895474	15,40210185	1,429985466	18,04
F01494-1050-40	10,38318189	1,3942517	12,931034	0,3874287	14,52052102	0,871798414	10,42
F01494-1050-50	10,74217031	1,4423294	12,5	0,3874287	14,03687775	1,038120658	12,00
		MAX	14,80	0,40	16,61		
		MIN	6,56	0,39	7,38		
		AVERAGE	10,75	0,39	12,08	1,25	12,07
F98843-950-25	15,88391637	1,674469	6,6371681	0,3041827	7,463143308	0,355289821	5,05
F98843-950-30	15,79429235	1,6705661	6,6964286	0,3051813	7,529989807	1,540621923	20,66
F98843-950-35	15,988206	1,6966038	6,6371681	0,3061866	7,463472053	0,600464569	8,38
F98843-950-40	19,87244728	2,0955677	5,3066038	0,3042732	5,971536047	1,103027983	12,80
F98843-950-50	24,60746108	2,5947477	4,2857143	0,3042732	4,825966388	1,044629032	12,64
F98843-1000-25	11,45894301	1,2004153	9,1463415	0,3023389	10,27105467	1,486974824	16,11
F98843-1000-30	11,255661	1,1830022	9,3360996	0,3032355	10,48692981	1,02172107	11,27
F98843-1000-35	12,35416851	1,2961946	8,490566	0,3026969	9,540484905	0,934177339	9,39
F98843-1000-40	14,67211821	1,5422535	7,1656051	0,3033254	8,054608537	1,362477701	11,53
F98843-1000-50	14,64037359	1,545699	7,2115385	0,3046358	8,10688511	1,325446201	11,24
F98843-1020-25	9,784647878	1,030502	10,76555	0,3039115	12,08469308	0,74289819	9,43
F98843-1020-30	10,38306219	1,1026912	10,227273	0,306416	11,48436076	0,737650929	8,82
F98843-1020-35	10,85428559	1,1425478	9,6982759	0,3037309	10,8911508	0,772846489	8,84
F98843-1020-40	11,96205651	1,258125	8,7890625	0,3034155	9,875532496	1,921083892	19,94
F98843-1020-50	12,74752342	1,3392868	8,2417582	0,3031456	9,260777723	1,218336847	11,87
F98843-1050-25	8,738496306	0,9236746	12,096774	0,3049993	13,57468916	0,721016311	5,64
F98843-1050-30	9,25958339	0,9788844	11,42132	0,3050903	12,81709879	0,906686749	7,13
F98843-1050-35	8,899857191	0,9379348	11,842105	0,3040922	13,28975309	0,307911382	2,39
F98843-1050-40	10,69613691	1,1288765	9,8684211	0,3045451	11,08125929	0,441617483	2,76
F98843-1050-50	10,25855513	1,0810933	10,273973	0,3040922	11,53512464	1,770414937	8,93
		MAX	12,10	0,31	13,57		
		MIN	4,29	0,30	4,83		
		AVERAGE	8,71	0,30	9,78	1,02	10,24

Table 2: Statistical results of grain size

Appendix 4: Marseille TEM Images

MUESTRA 1

IMÁGENES DE TEM

MUESTRA 1

JEOL JEM 2010F
Field Emission Electron Microscope

IMÁGENES
DE TEM

Precipitados de todos los tamaños, sobre todo en las fronteras de grano. La forma predominante es cuadrada o rectangular.

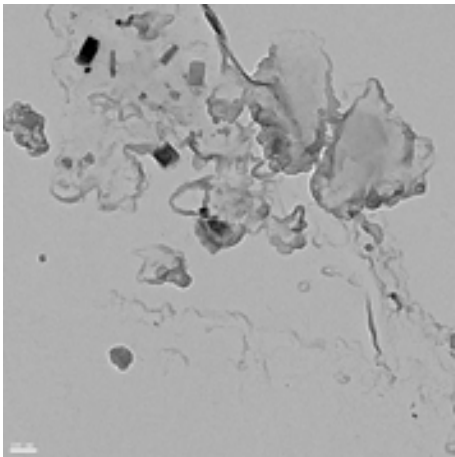
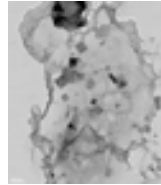
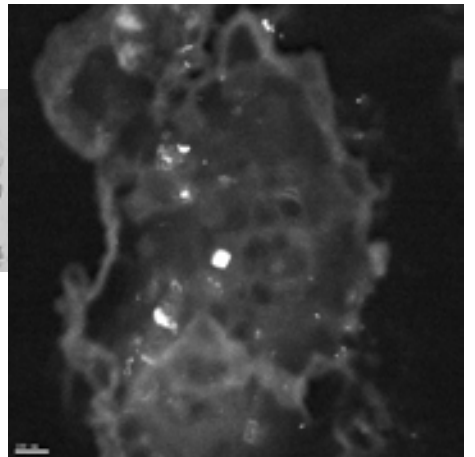


foto1
100nm

IMÁGENES
DE TEM



dark field
foto2
100nm



IMÁGENES
DE TEM

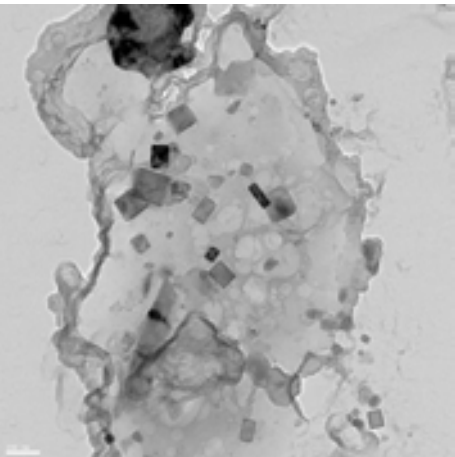
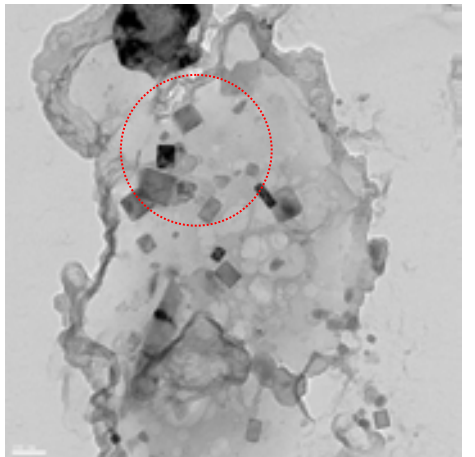


foto2
100nm

IMÁGENES
DE TEM



100nm

IMÁGENES DE TEM

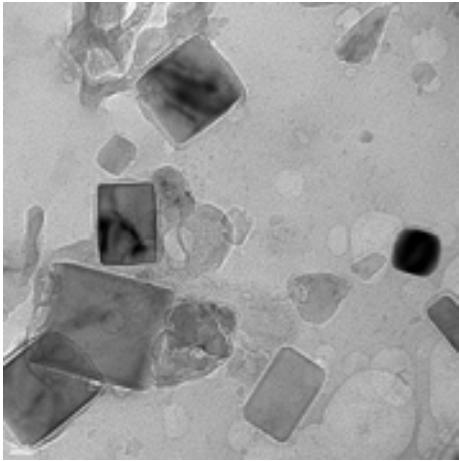
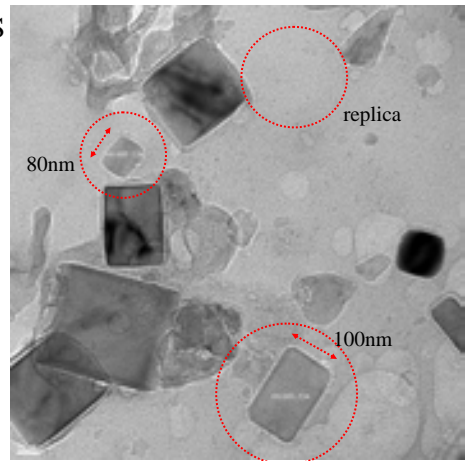


foto3
20nm

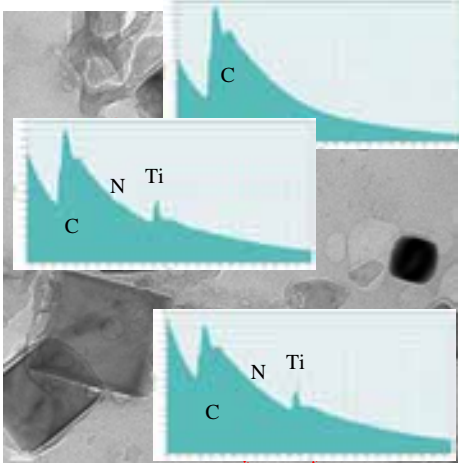
IMÁGENES DE TEM



EELS

foto3
20nm

IMÁGENES DE TEM



EELS

Gran cantidad de nitratos de titanio. También pueden ser carbonitratos.

foto3
20nm

IMÁGENES DE TEM

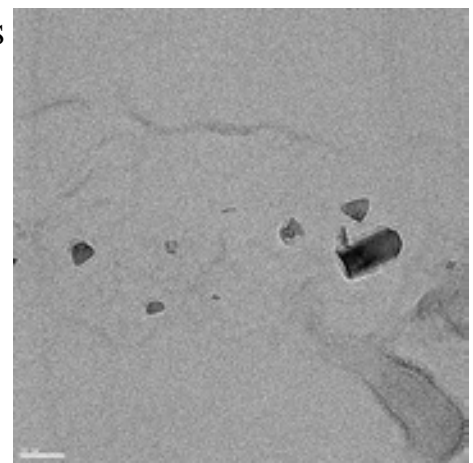


foto4
50nm

IMÁGENES DE TEM

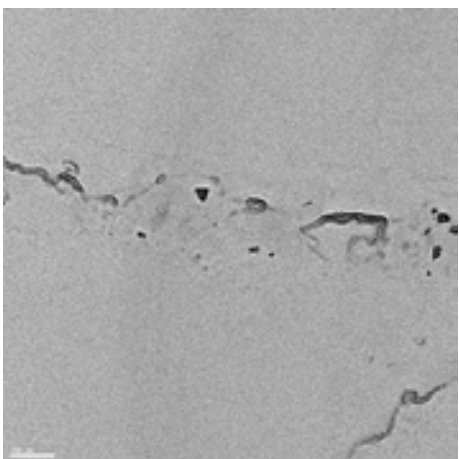


foto5
100nm

IMÁGENES DE TEM

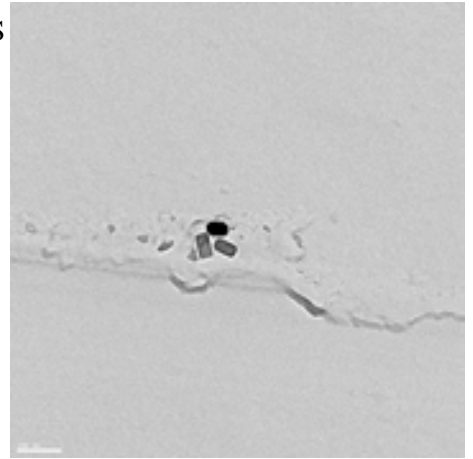


foto6
100nm

IMÁGENES DE TEM

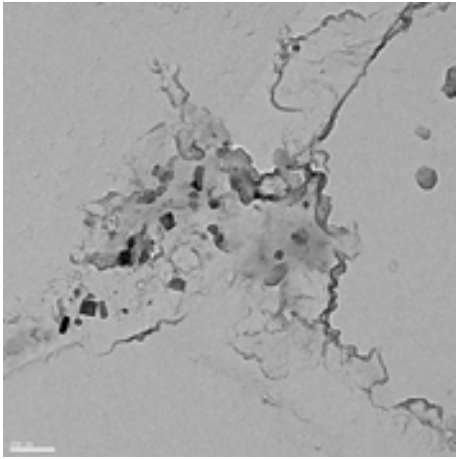


foto7
200nm

IMÁGENES DE TEM

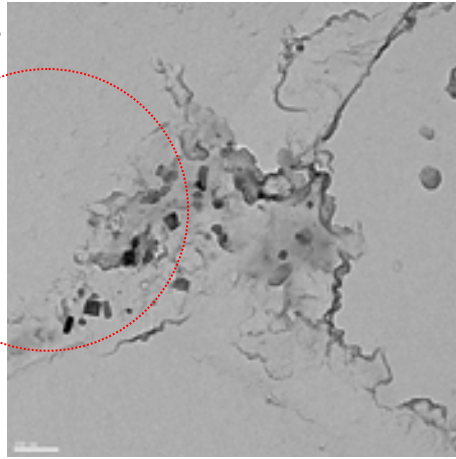


foto7
200nm

IMÁGENES DE TEM

No se encuentran precipitados en el interior de los granos.

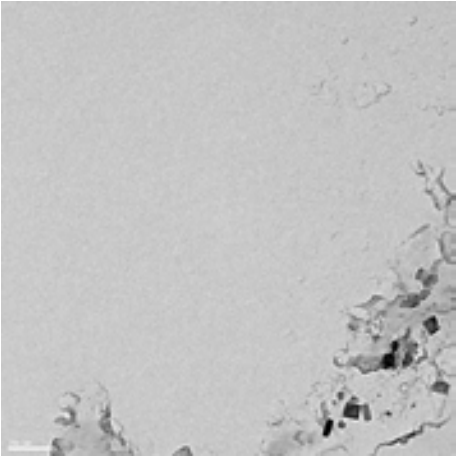


foto8
200nm

IMÁGENES DE TEM

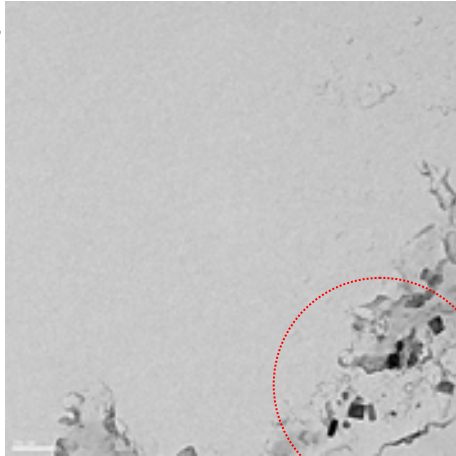


foto8
200nm

IMÁGENES DE TEM

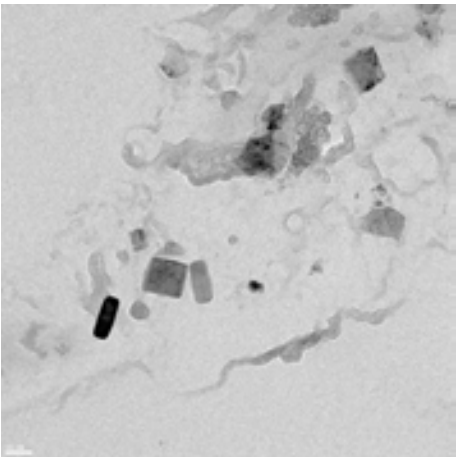


foto9
50nm

IMÁGENES DE TEM

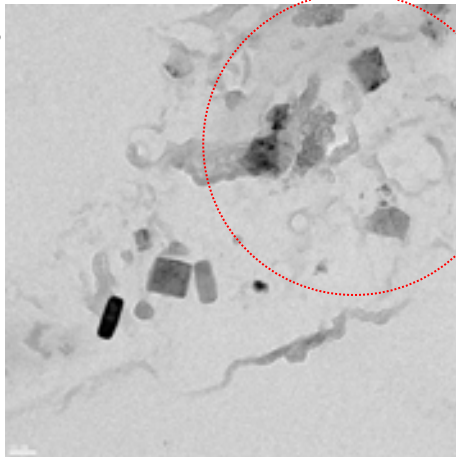


foto9
50nm

IMÁGENES
DE TEM

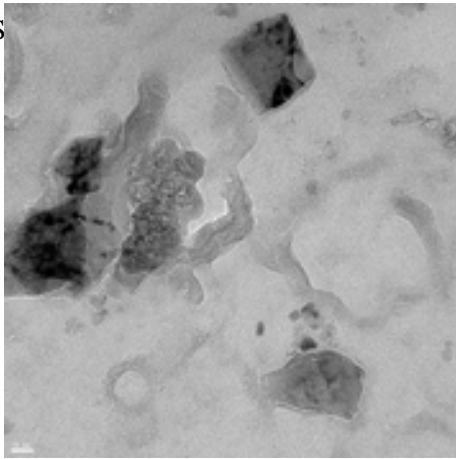


foto10
20nm

IMÁGENES
DE TEM

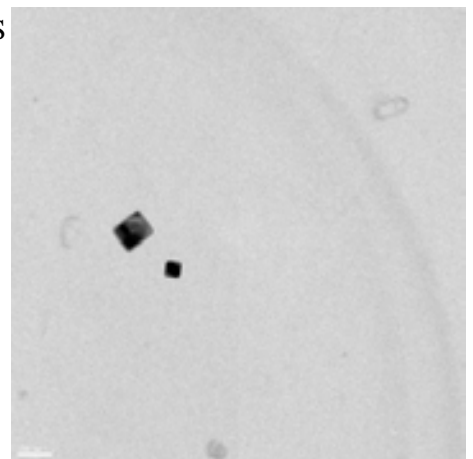


foto11
100nm

IMÁGENES
DE TEM

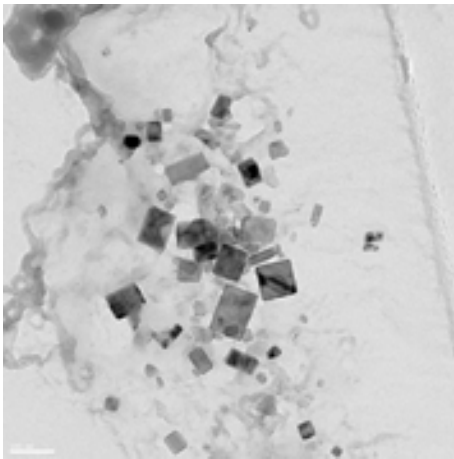


foto12
100nm

IMÁGENES
DE TEM

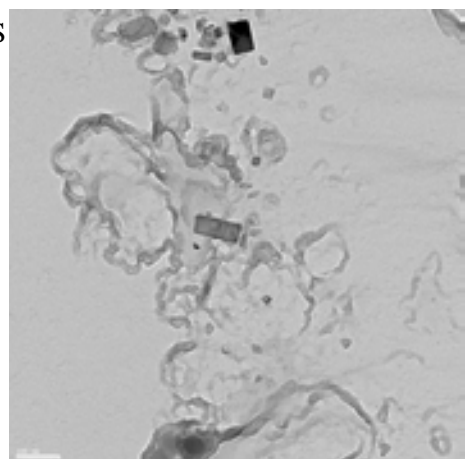


foto13
100nm

IMÁGENES
DE TEM

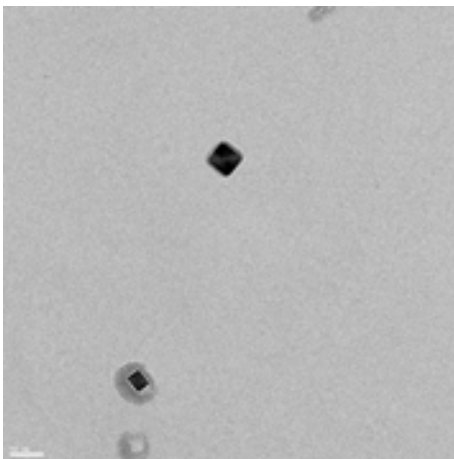


foto14
50nm

IMÁGENES
DE TEM

Precipitados de
pequeño tamaño.

Dark field

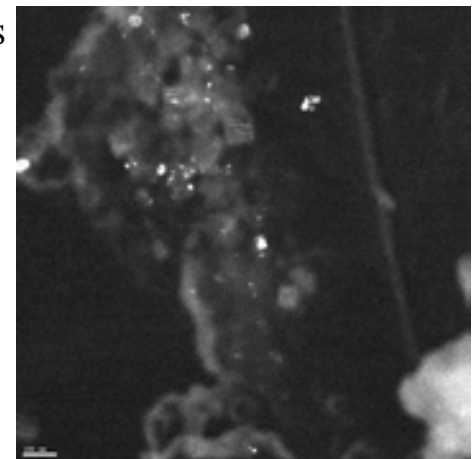


foto15
100nm

IMÁGENES
DE TEM

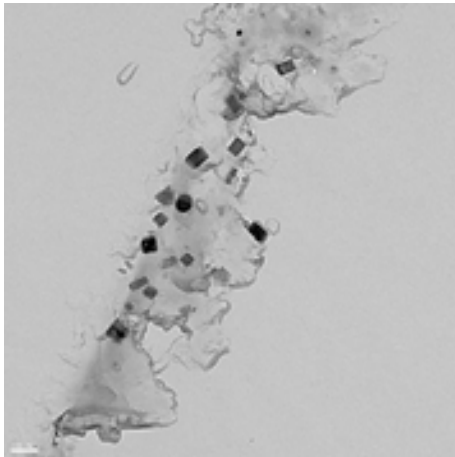


foto16
100nm

IMÁGENES
DE TEM

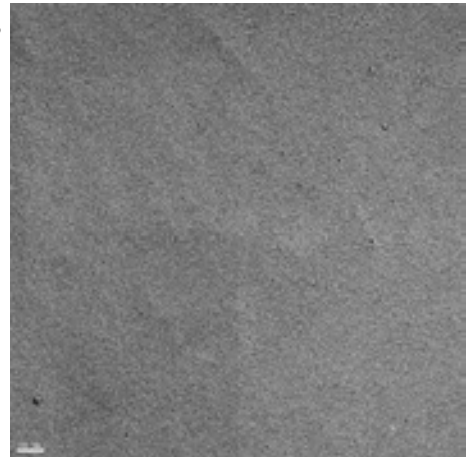


foto17
100nm

IMÁGENES
DE TEM

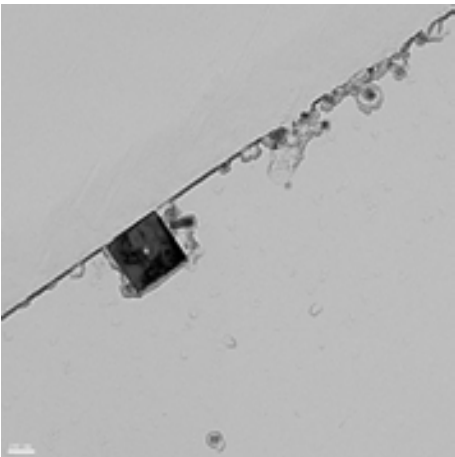


foto18
100nm

IMÁGENES
DE TEM

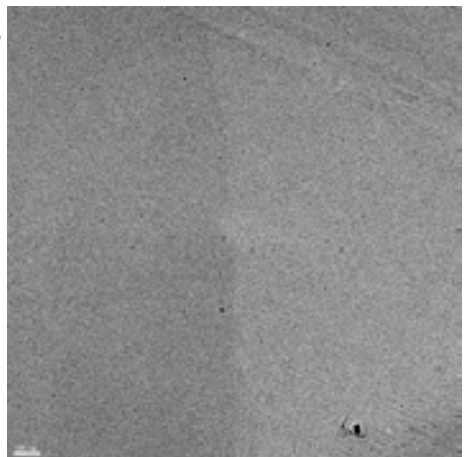


foto19
100nm

IMÁGENES
DE TEM

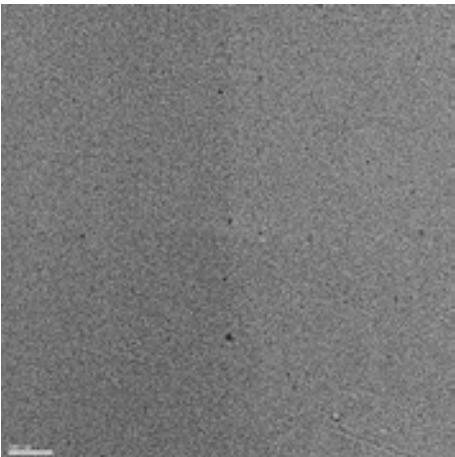


foto20
100nm

IMÁGENES
DE TEM

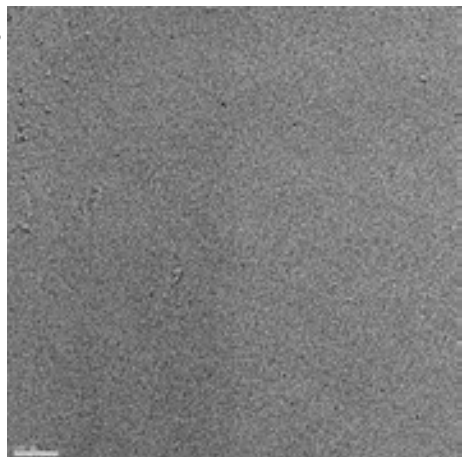


foto21
100nm

IMÁGENES DE TEM

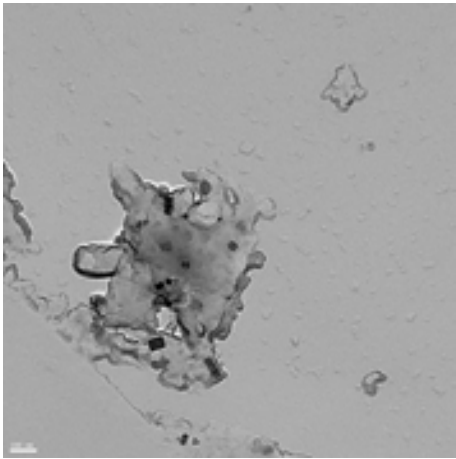


foto22
100nm

IMÁGENES DE TEM

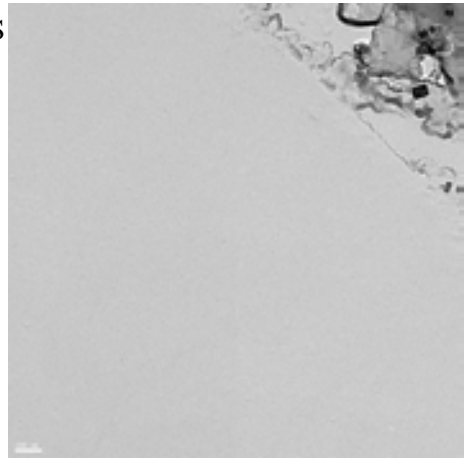


foto23
100nm

IMÁGENES DE TEM

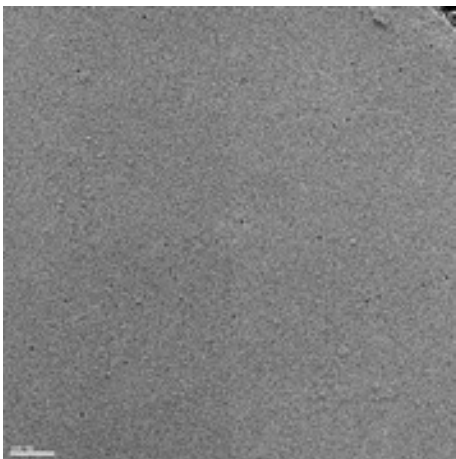
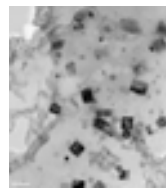


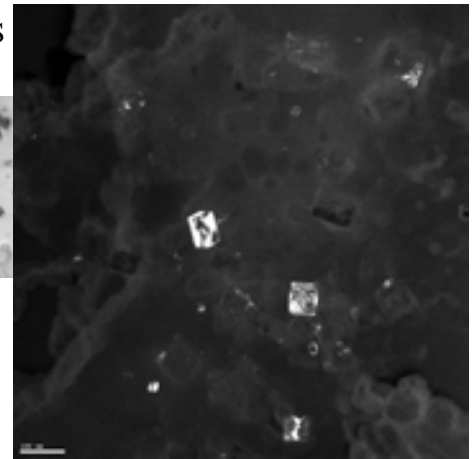
foto24
100nm

IMÁGENES DE TEM



dark field

foto26
100nm



IMÁGENES DE TEM

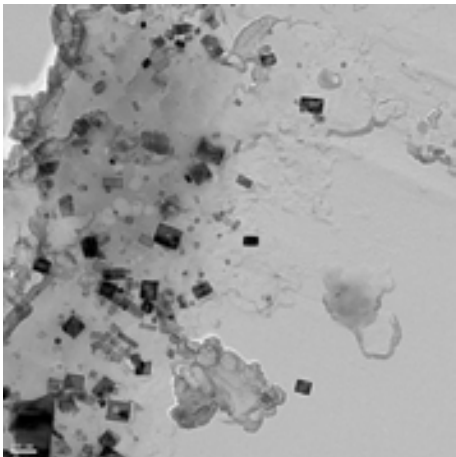


foto25
100nm

IMÁGENES DE TEM

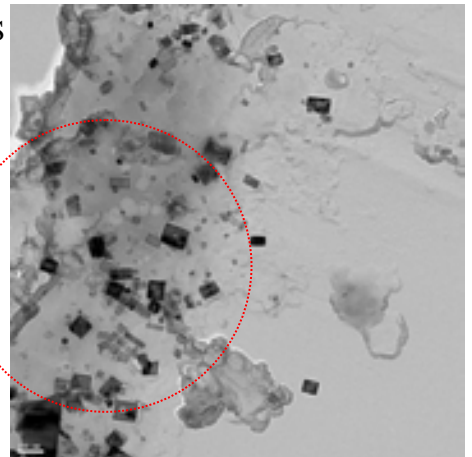


foto25
100nm

IMÁGENES DE TEM

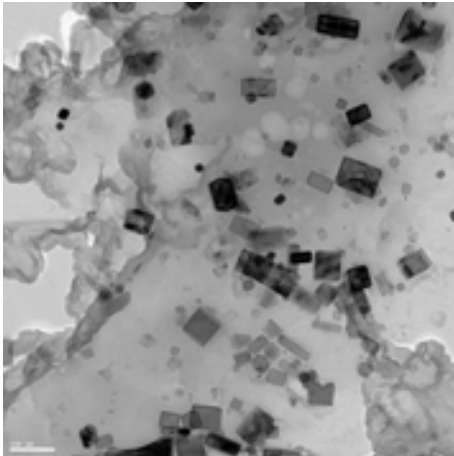
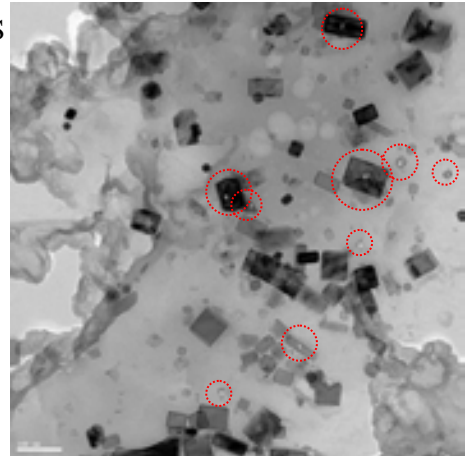


foto26
100nm

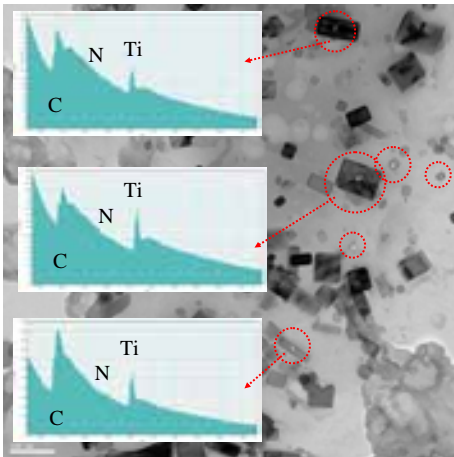
IMÁGENES DE TEM



EELS

foto26
100nm

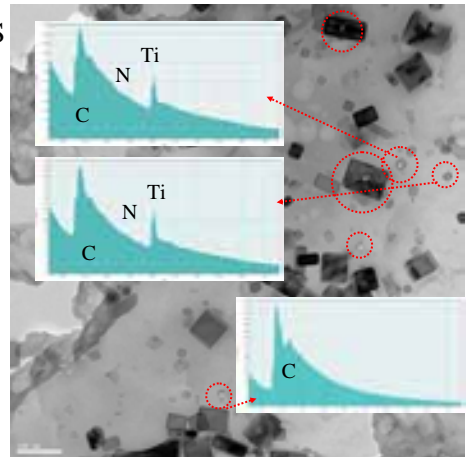
IMÁGENES DE TEM



EELS

foto26
100nm

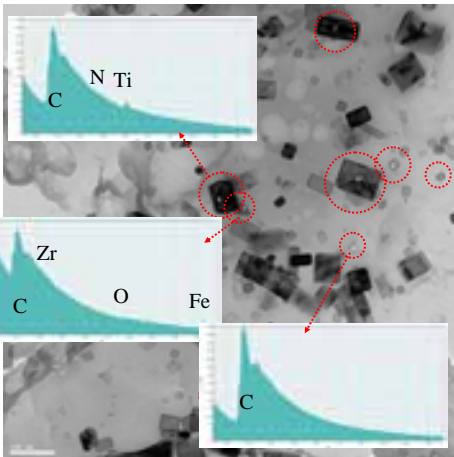
IMÁGENES DE TEM



EELS

foto26
100nm

IMÁGENES DE TEM



EELS

foto26
100nm

IMÁGENES DE TEM

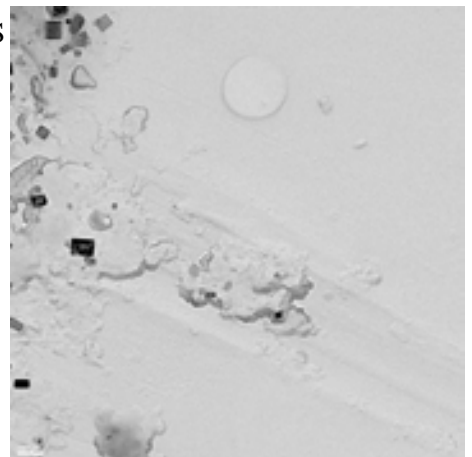


foto27
100nm

IMÁGENES
DE TEM

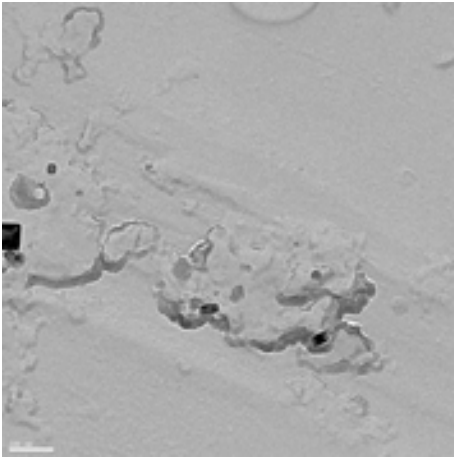


foto28
100nm

IMÁGENES
DE TEM

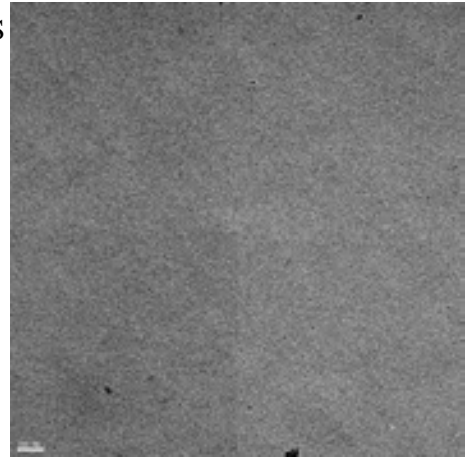
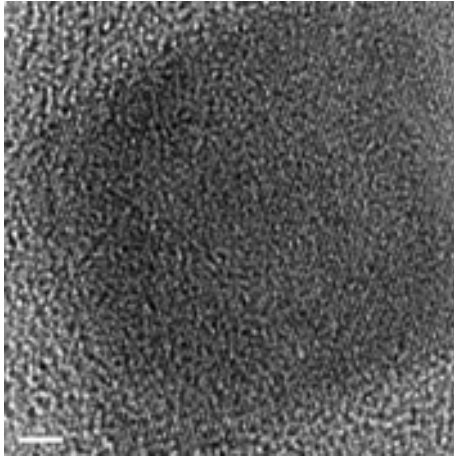


foto29
100nm

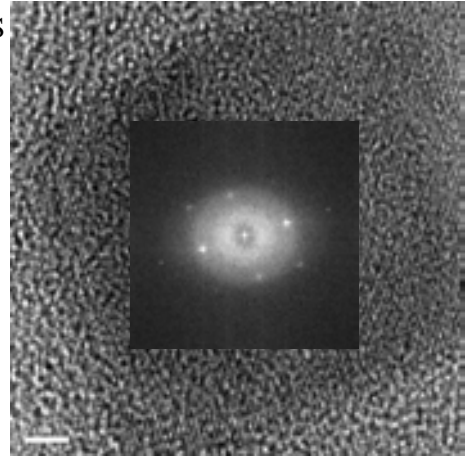
IMÁGENES
DE TEM



High
Resolution

Foto30
2nm

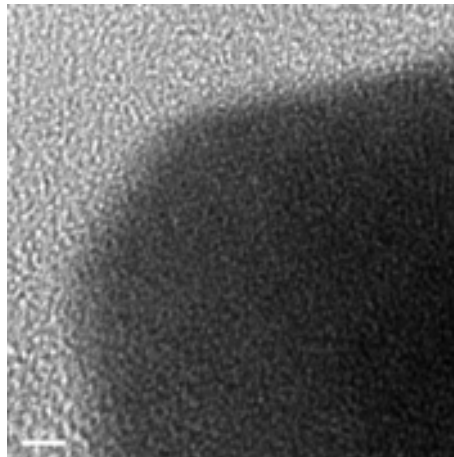
IMÁGENES
DE TEM



FFT

foto30
2nm

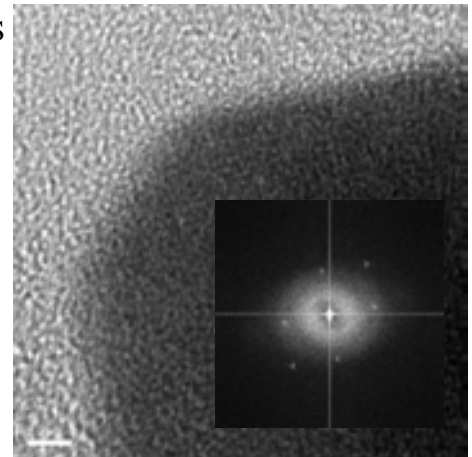
IMÁGENES
DE TEM



High
Resolution

foto31
2nm

IMÁGENES
DE TEM



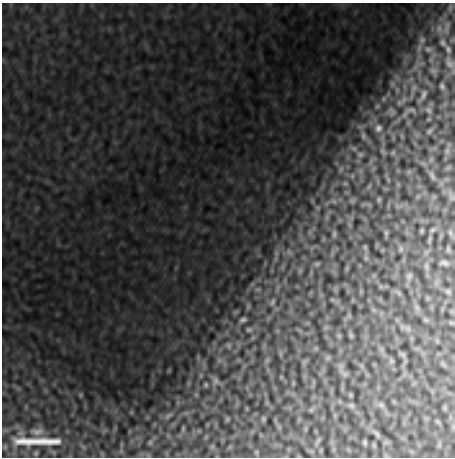
FFT

foto31
2nm

IMÁGENES DE TEM

High Resolution

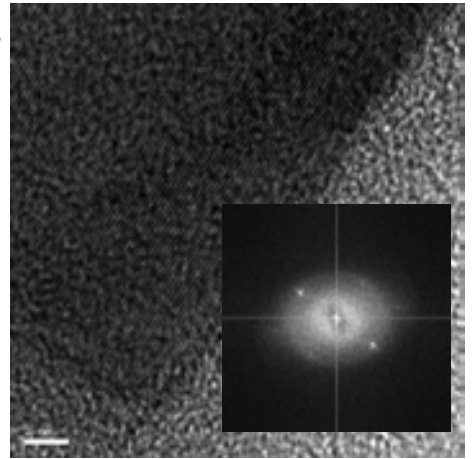
foto32
2nm



IMÁGENES DE TEM

FFT

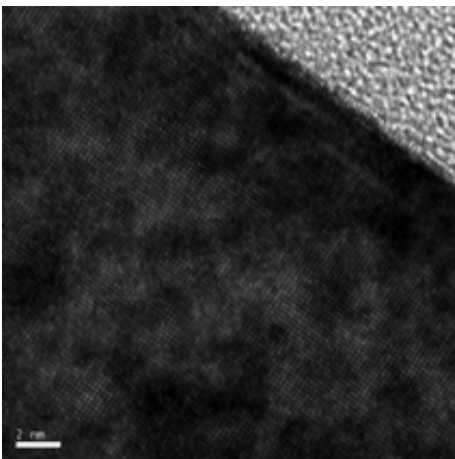
foto32
2nm



IMÁGENES DE TEM

High Resolution

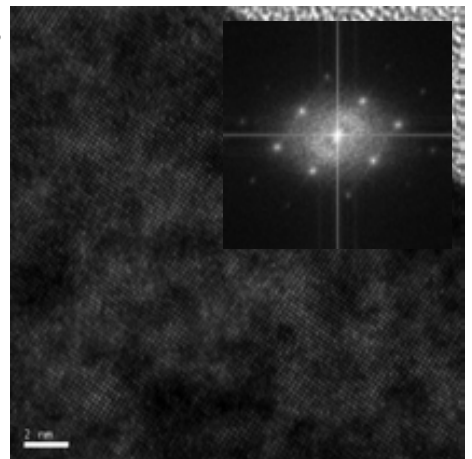
foto33
2nm



IMÁGENES DE TEM

FFT

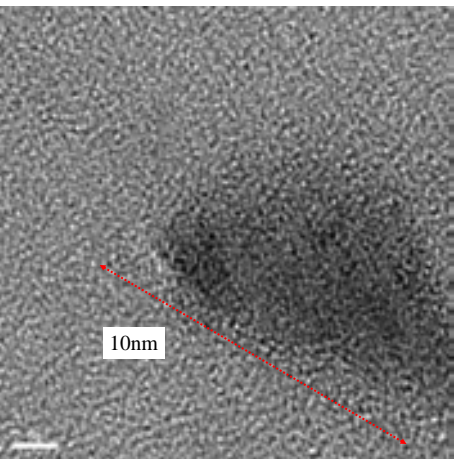
foto33
2nm



IMÁGENES DE TEM

High Resolution

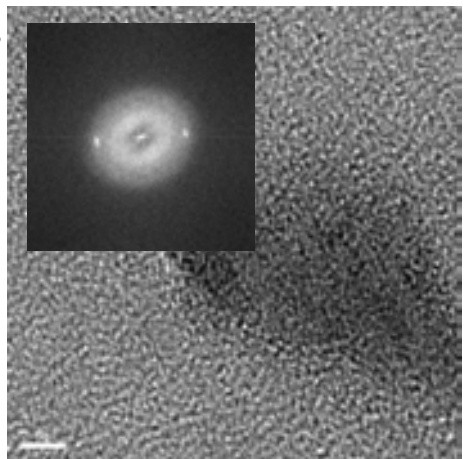
foto34
2nm



IMÁGENES DE TEM

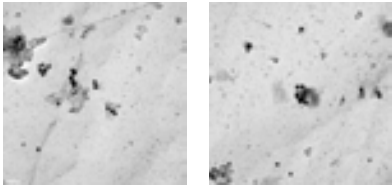
FFT

foto34
2nm



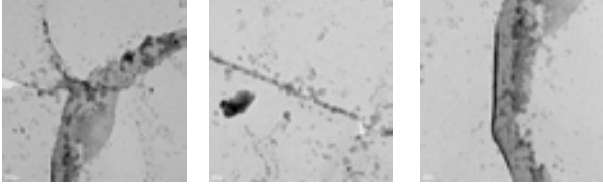
IMÁGENES DE TEM

Muestra preparada extrayendo la replica con nital



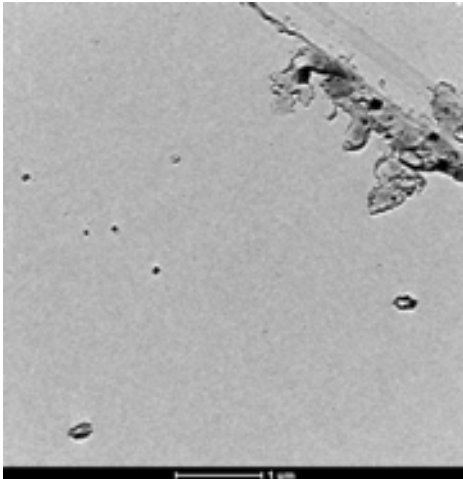
MUESTRA 1

FEI Tecnai G2
Scanning Transmission
Electron Microscope



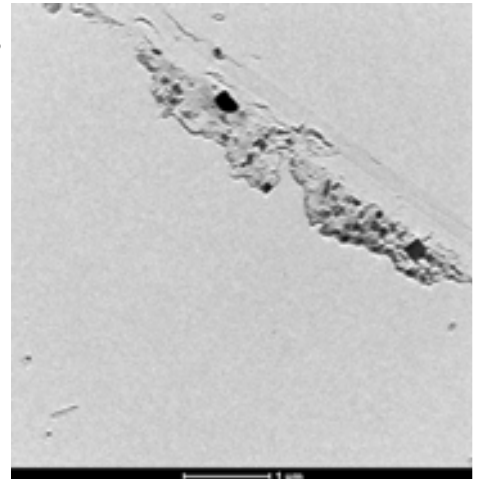
IMÁGENES DE TEM

foto1



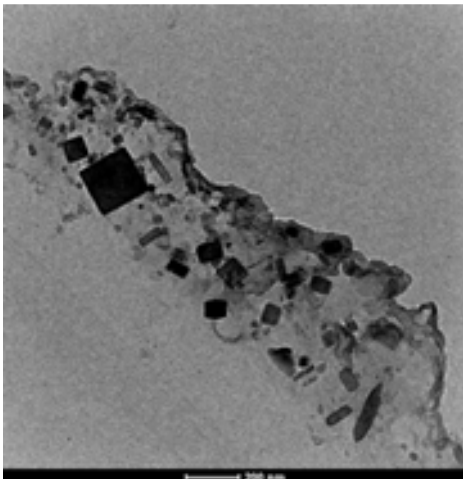
IMÁGENES DE TEM

foto2



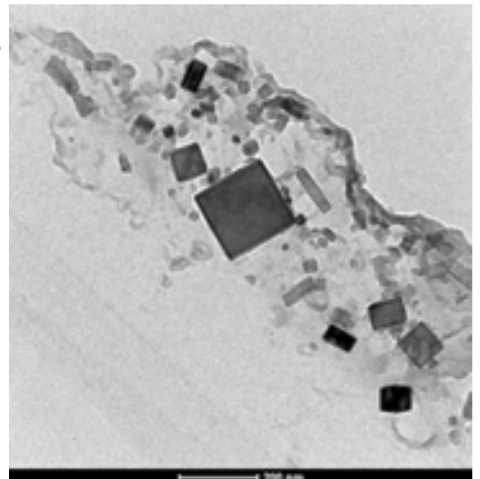
IMÁGENES DE TEM

foto3



IMÁGENES DE TEM

foto4



IMÁGENES DE TEM

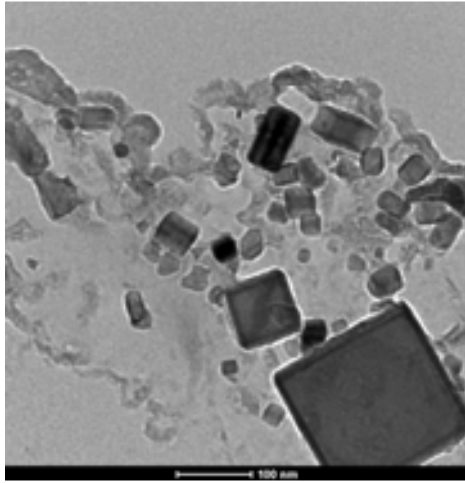


foto5

IMÁGENES DE TEM

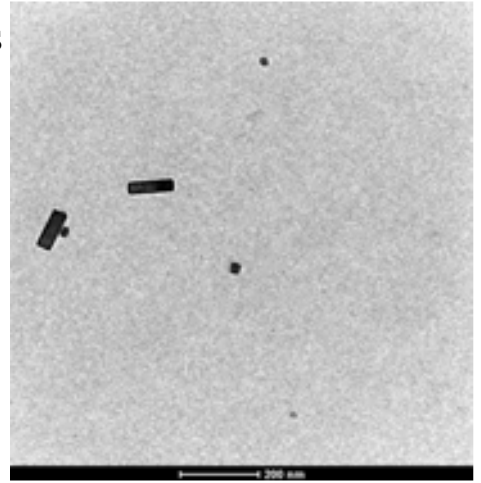


foto6

IMÁGENES DE TEM

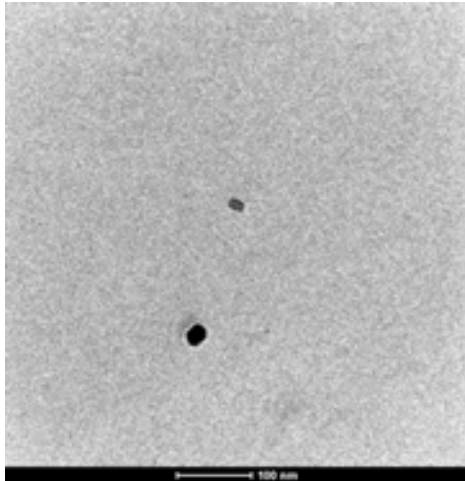


foto7

IMÁGENES DE TEM

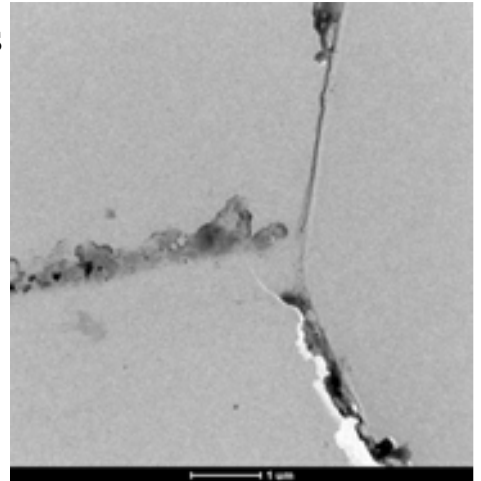


foto8

IMÁGENES DE TEM

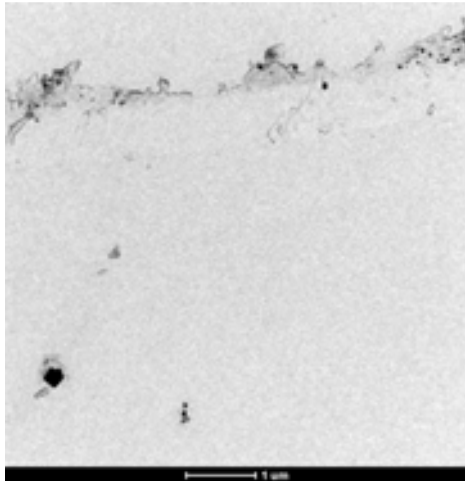
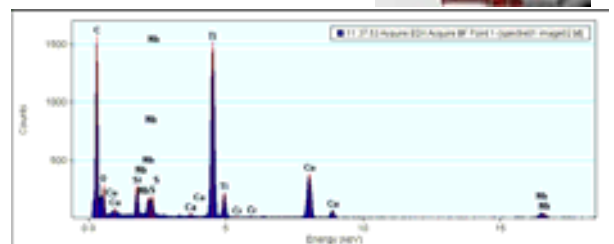
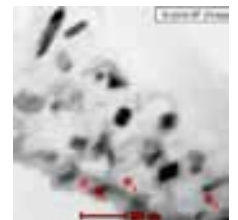


foto9

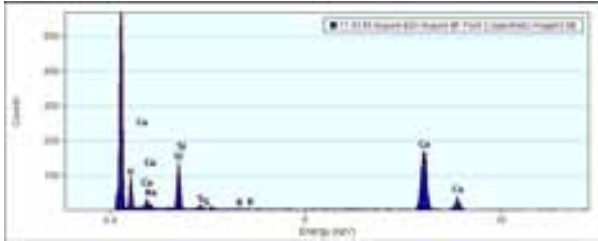
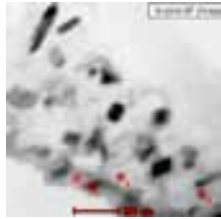
IMÁGENES DE STEM

1



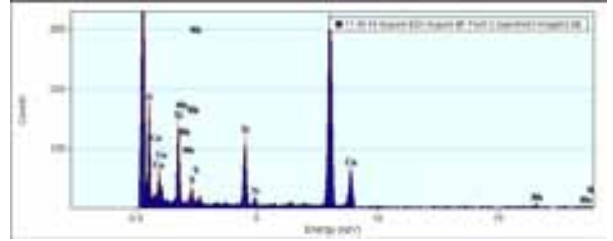
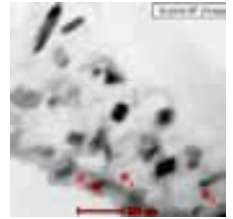
IMÁGENES DE STEM

2



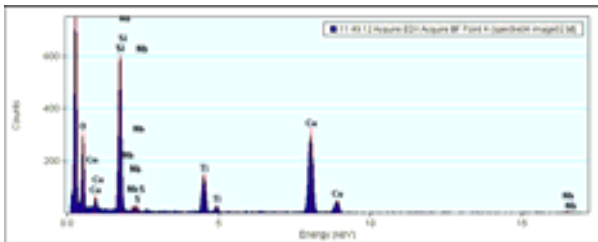
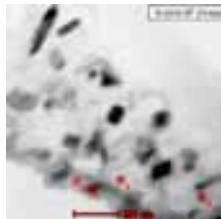
IMÁGENES DE STEM

3



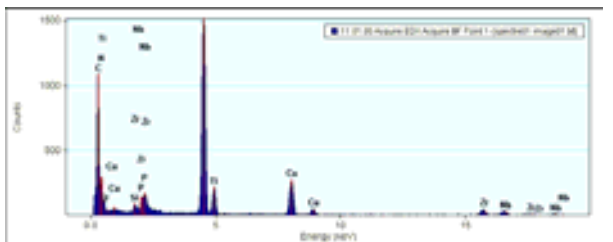
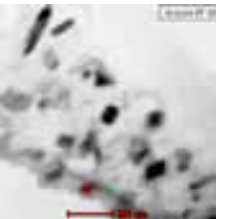
IMÁGENES DE STEM

4



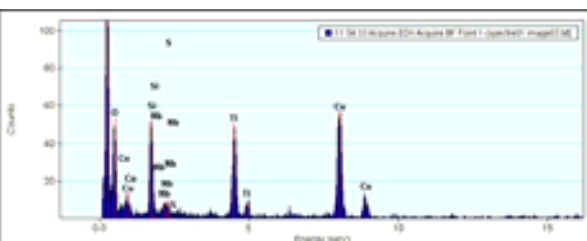
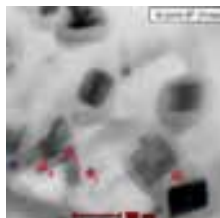
IMÁGENES DE STEM

3



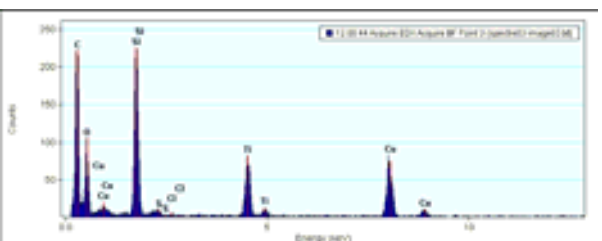
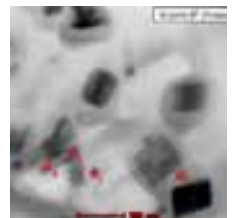
IMÁGENES DE STEM

1



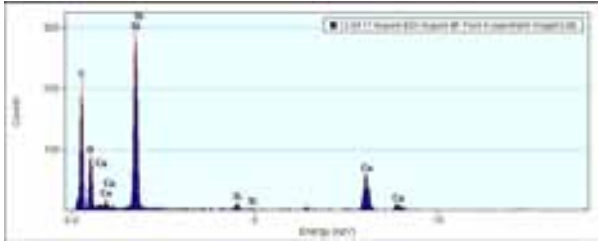
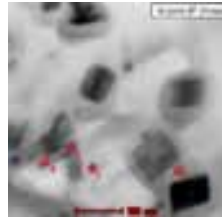
IMÁGENES DE STEM

3



IMÁGENES DE STEM

4

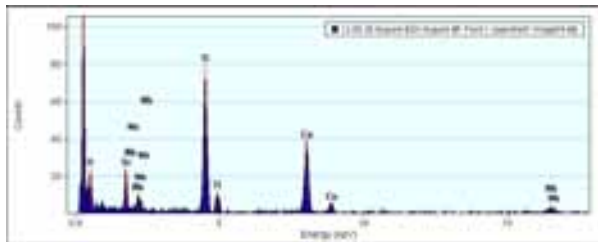


IMÁGENES DE STEM

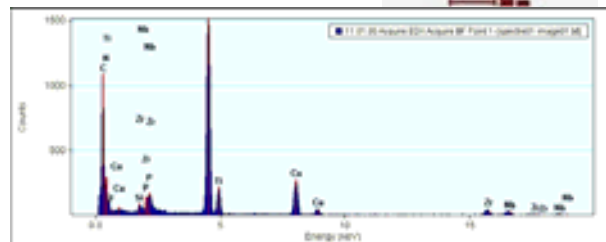
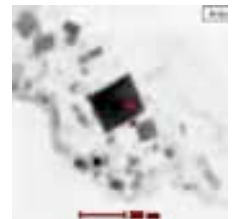


foto12

IMÁGENES DE STEM



IMÁGENES DE STEM



MUESTRA 2

IMÁGENES DE TEM

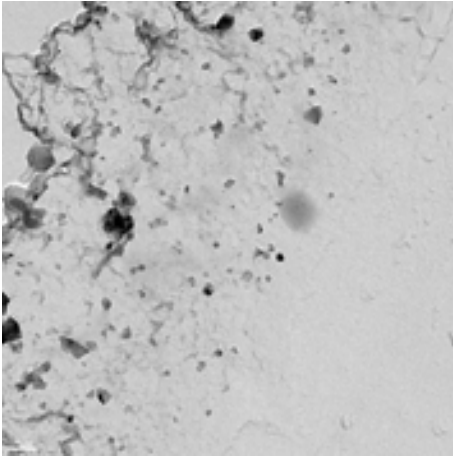
MUESTRA 2

JEOL JEM 2010F
Field Emission Electron Microscope

IMÁGENES
DE TEM

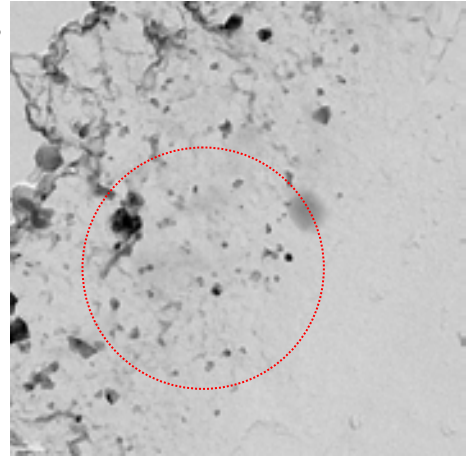
No se encuentran muchos precipitados en general. Predominio de los precipitados de tamaños medianos, entre 30 y 60 nm, sobre todo en las fronteras de grano. La mayoría de ellos pueden ser contaminación.

foto1
100nm



IMÁGENES
DE TEM

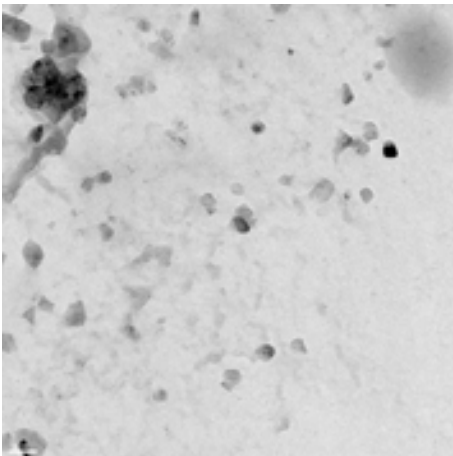
foto1
100nm



IMÁGENES
DE TEM

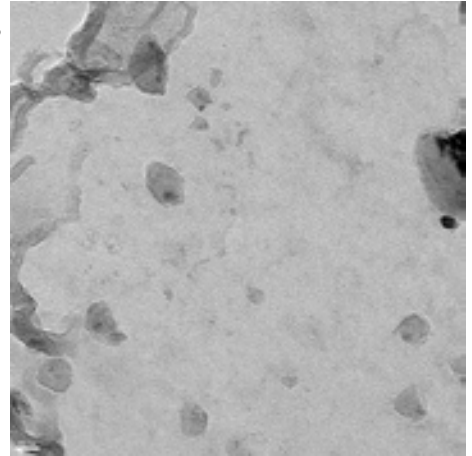
La forma predominante es redondeada. Posiblemente carburosulfuros de titanio

foto2
50nm



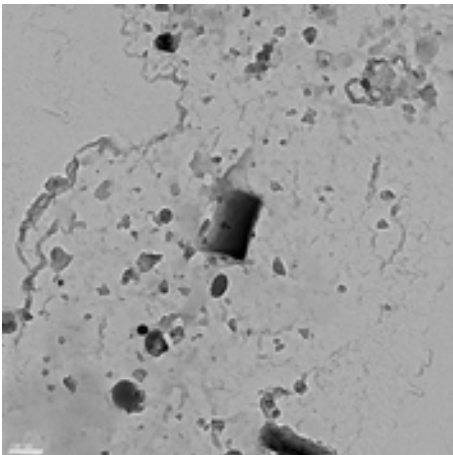
IMÁGENES
DE TEM

foto3
20nm



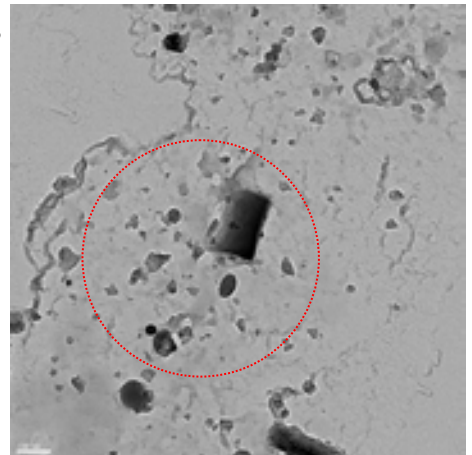
IMÁGENES
DE TEM

foto4
100nm



IMÁGENES
DE TEM

foto4
100nm



IMÁGENES DE TEM

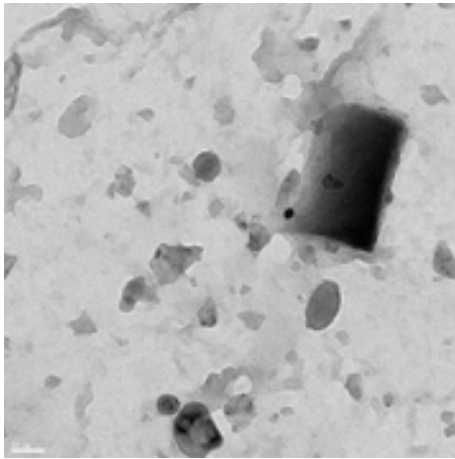
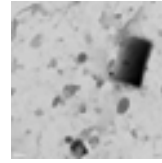


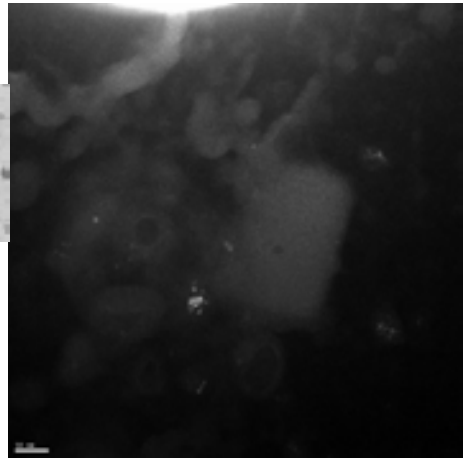
foto5
50nm

IMÁGENES DE TEM

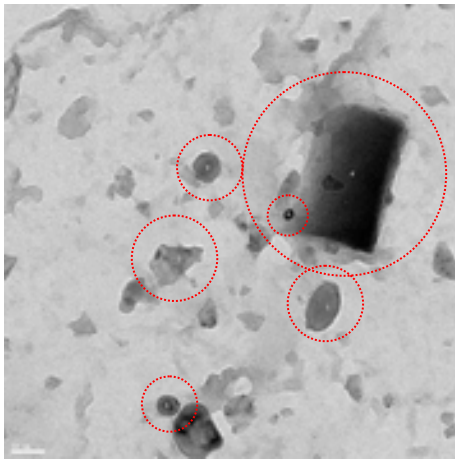


dark field

foto5
50nm



IMÁGENES DE TEM



EELS

foto5
50nm

IMÁGENES DE TEM

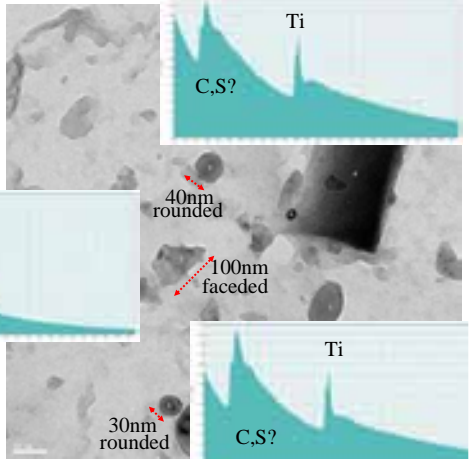


foto5
50nm

IMÁGENES DE TEM

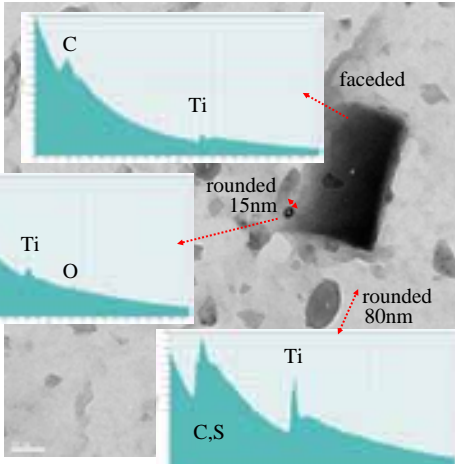


foto5
50nm

IMÁGENES DE TEM

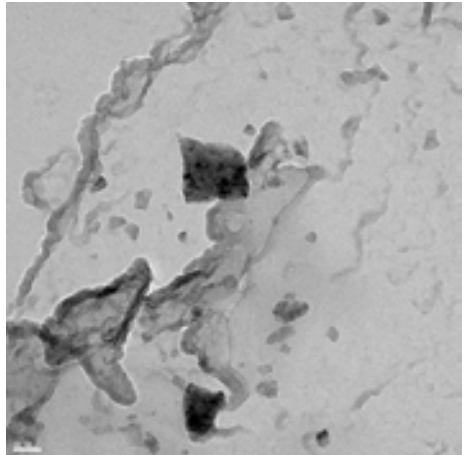
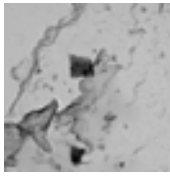


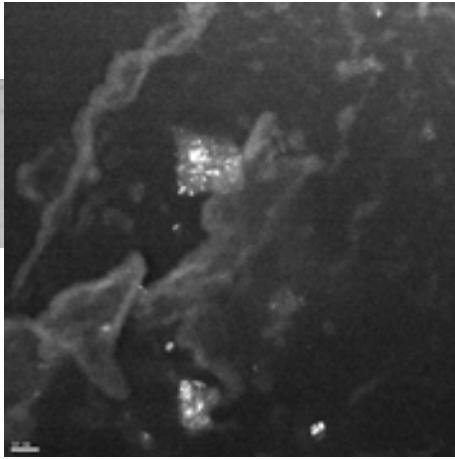
foto6
50nm

IMÁGENES DE TEM



dark field

foto6
50nm



IMÁGENES DE TEM

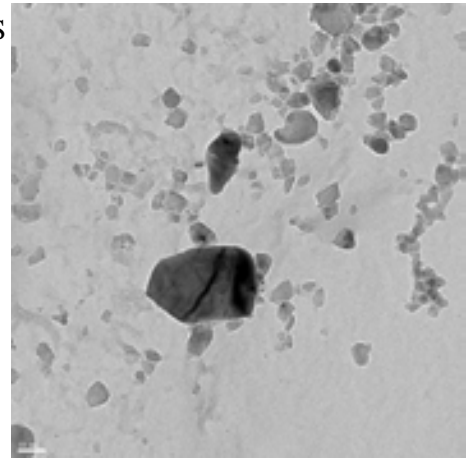


foto7
50nm

IMÁGENES DE TEM

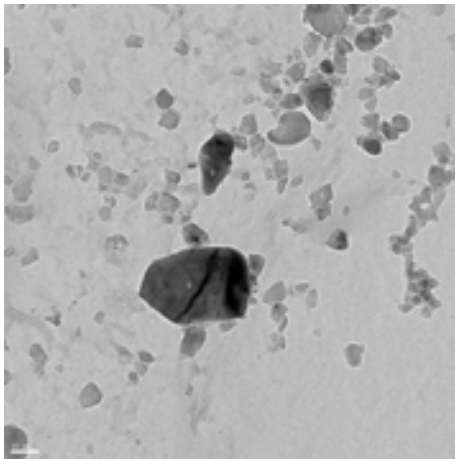
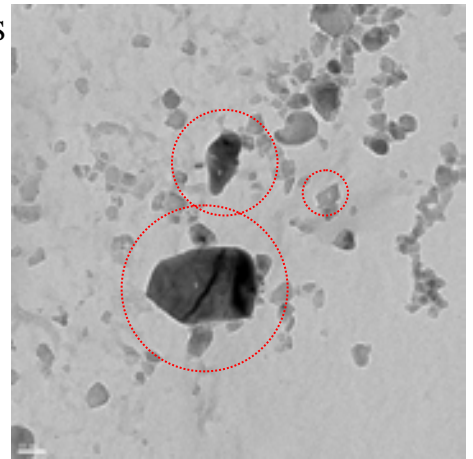


foto7
50nm

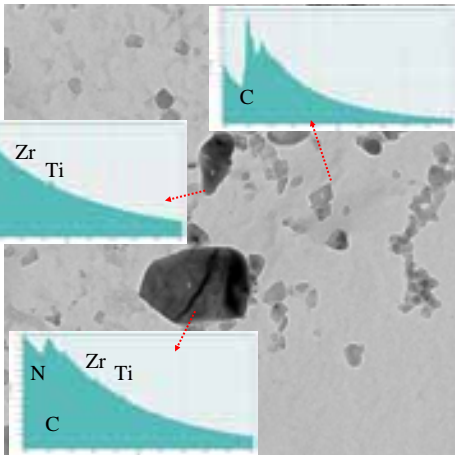
IMÁGENES DE TEM



EELS

foto7
50nm

IMÁGENES DE TEM



EELS

foto7
50nm

IMÁGENES DE TEM

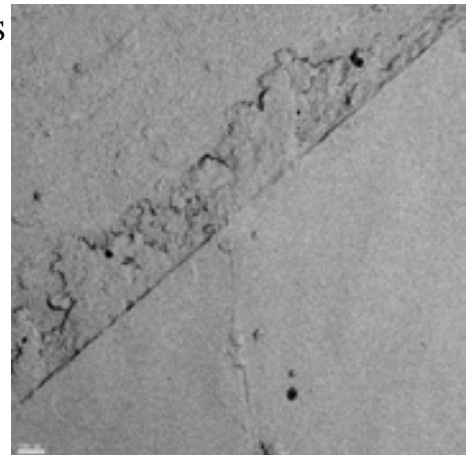


foto8
100nm

IMÁGENES
DE TEM

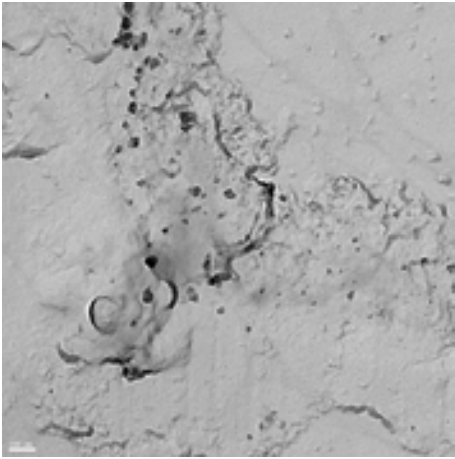


foto9
100nm

IMÁGENES
DE TEM

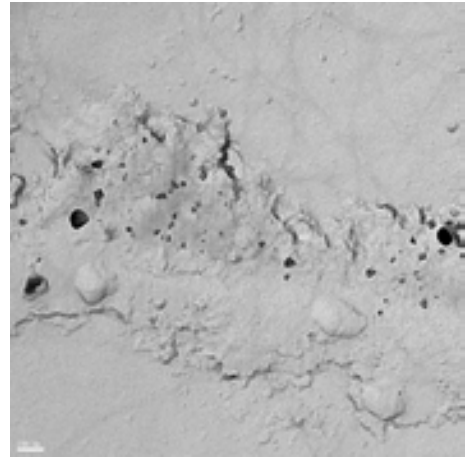


foto10
100nm

IMÁGENES
DE TEM

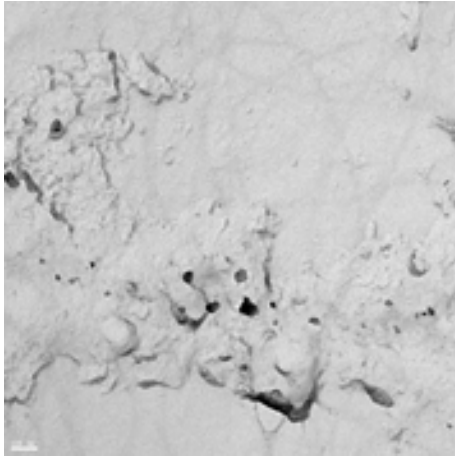


Foto11
100nm

IMÁGENES
DE TEM

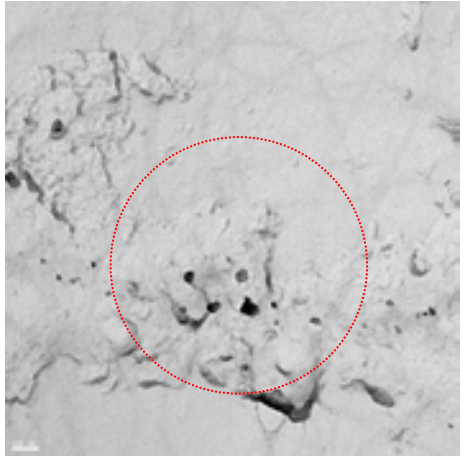


Foto11
100nm

IMÁGENES
DE TEM

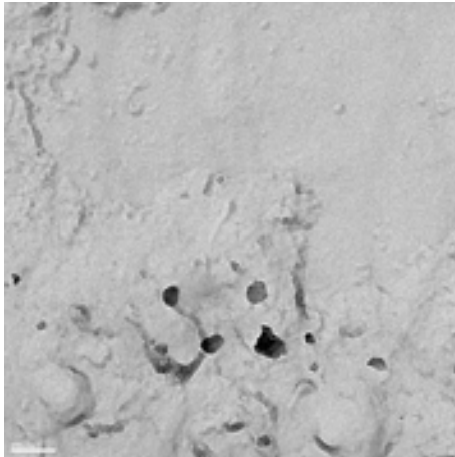


Foto12
100nm

IMÁGENES
DE TEM

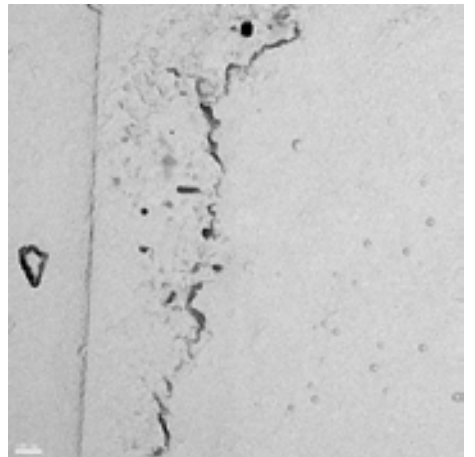


Foto13
100nm

IMÁGENES
DE TEM

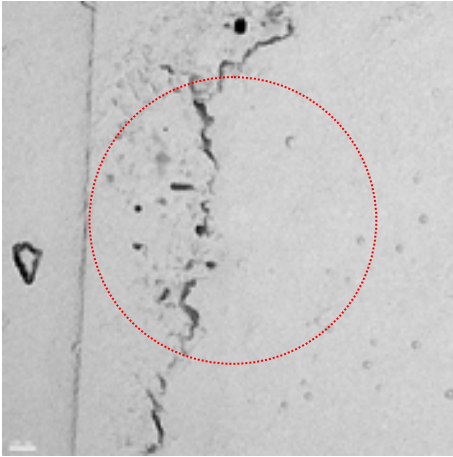


Foto13
100nm

IMÁGENES
DE TEM

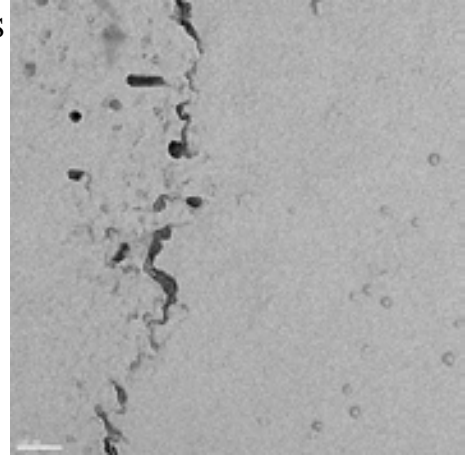


Foto14
100nm

IMÁGENES
DE TEM

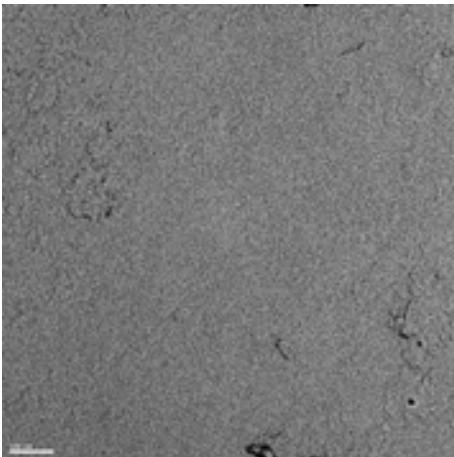


Foto15
100nm

IMÁGENES
DE TEM

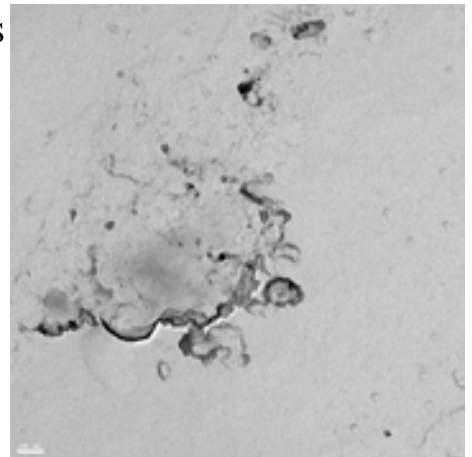


Foto16
100nm

IMÁGENES
DE TEM

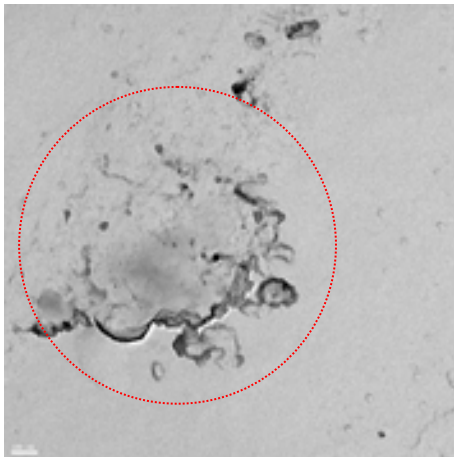


Foto16
100nm

IMÁGENES
DE TEM

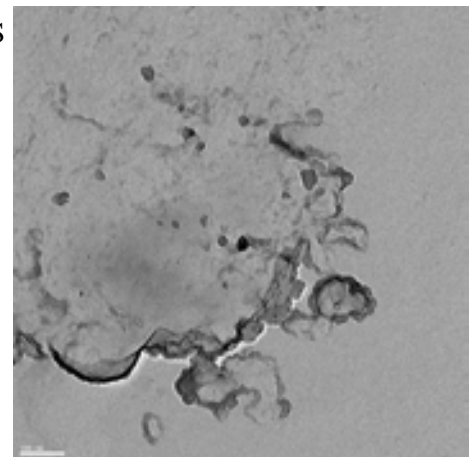
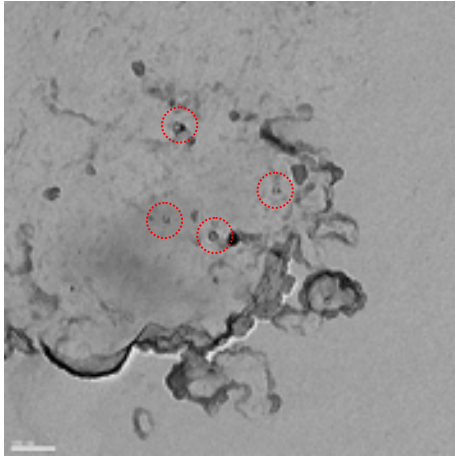


Foto17
100nm

IMÁGENES DE TEM

EELS

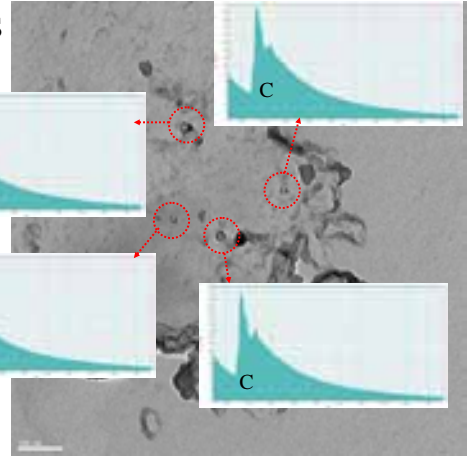
Foto17
100nm



IMÁGENES DE TEM

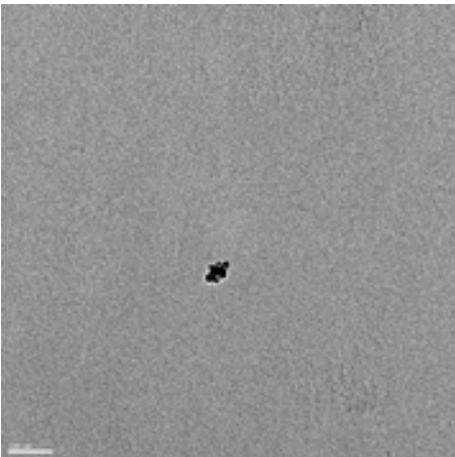
EELS

Foto17
100nm



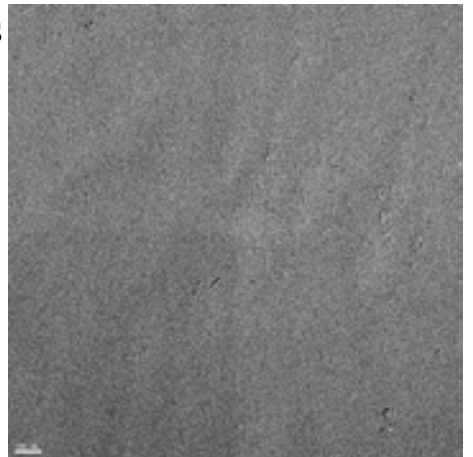
IMÁGENES DE TEM

Foto18
100nm



IMÁGENES DE TEM

Foto19
100nm

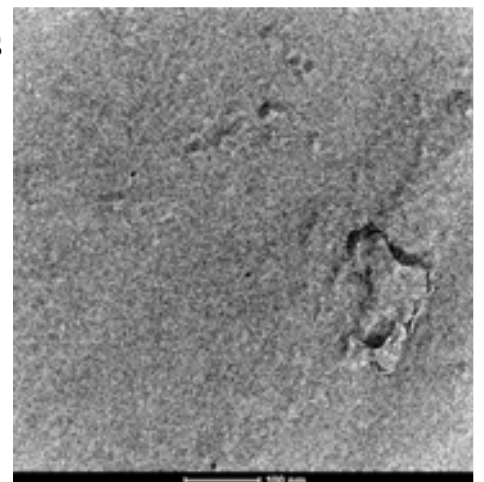


MUESTRA 2

FEI Tecnai G2
Scanning Transmission
Electron Microscope

IMÁGENES DE TEM

Foto1



IMÁGENES DE TEM

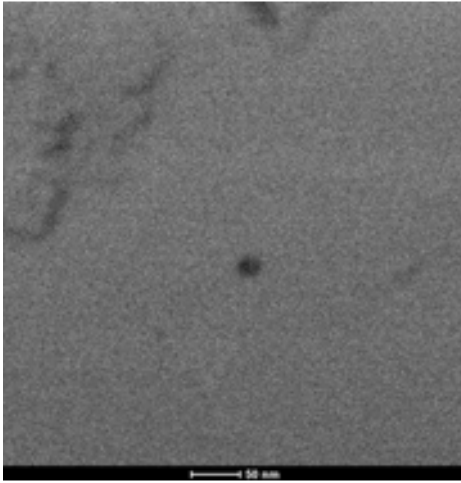


Foto2

IMÁGENES DE TEM

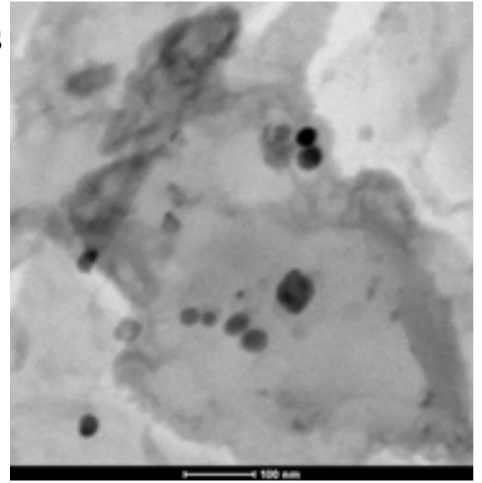
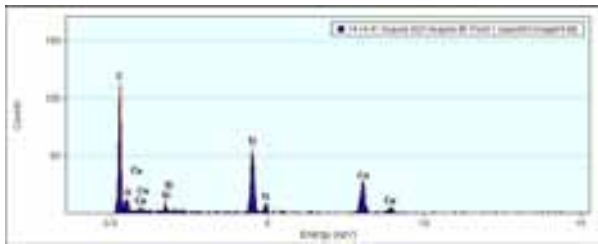
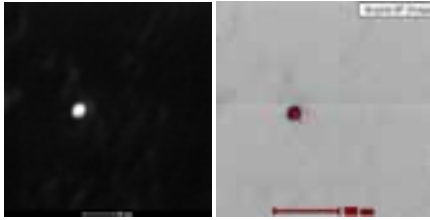


Foto3

IMÁGENES DE STEM



IMÁGENES DE STEM

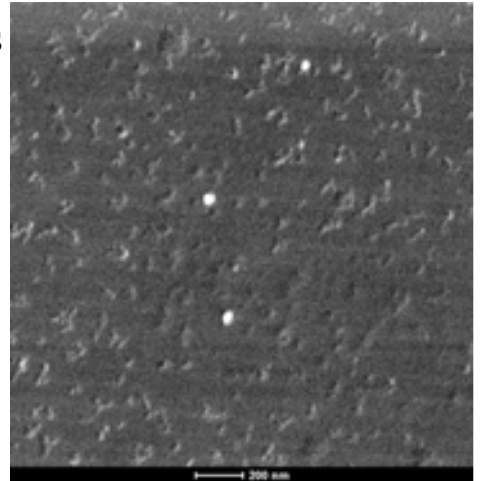
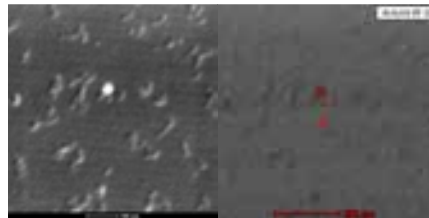


Foto5

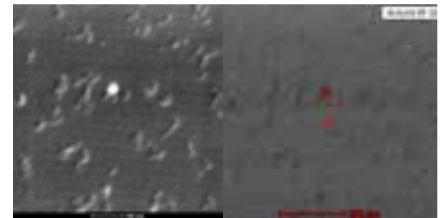
IMÁGENES DE STEM



1



IMÁGENES DE STEM

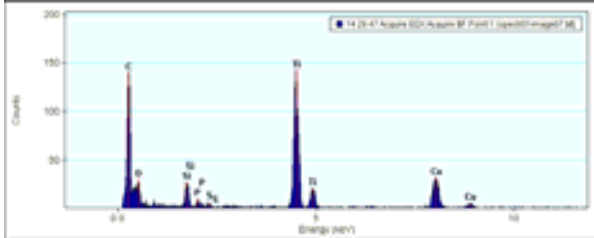
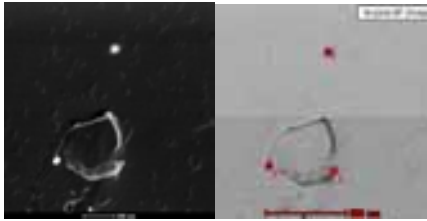


2



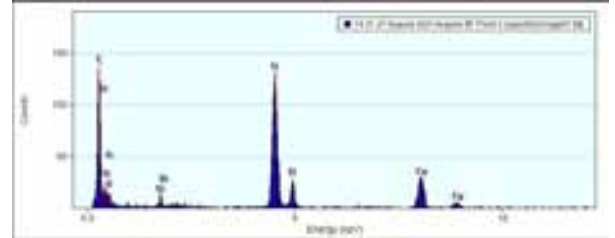
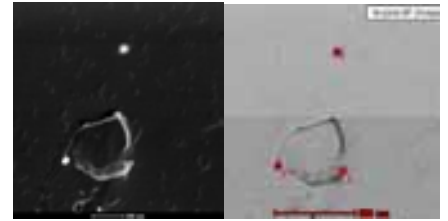
IMÁGENES DE STEM

1



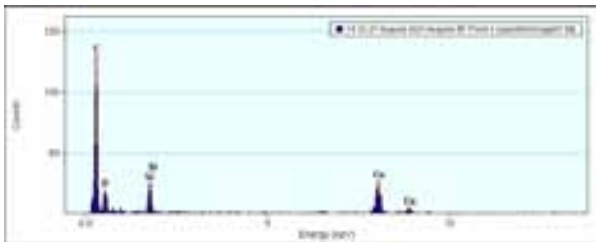
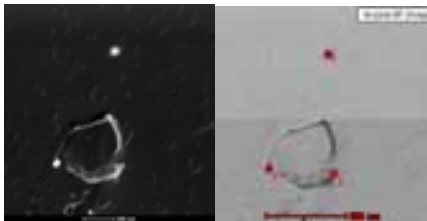
IMÁGENES DE STEM

2



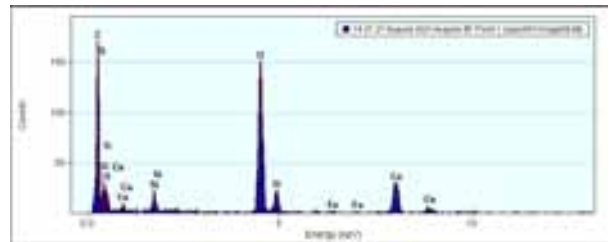
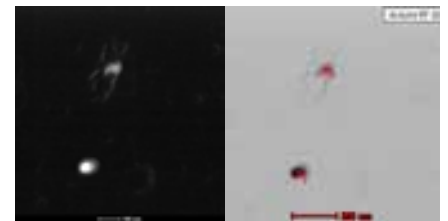
IMÁGENES DE STEM

3



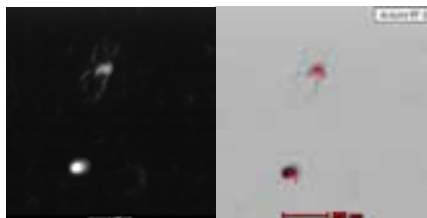
IMÁGENES DE STEM

1



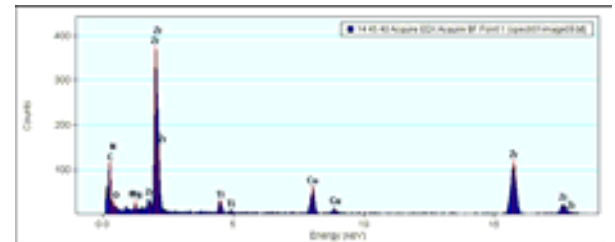
IMÁGENES DE STEM

2



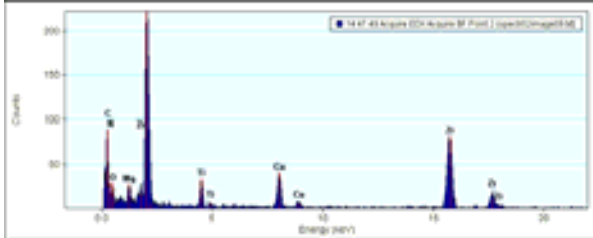
IMÁGENES DE STEM

1



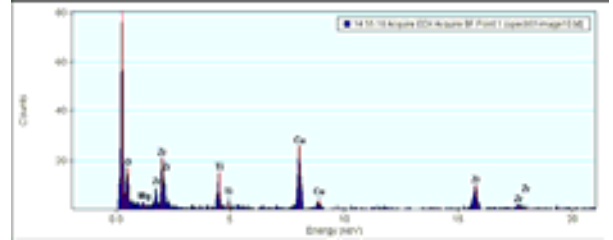
IMÁGENES DE STEM

2



IMÁGENES DE STEM

1



IMÁGENES DE STEM

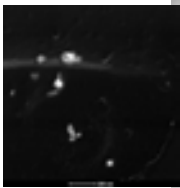
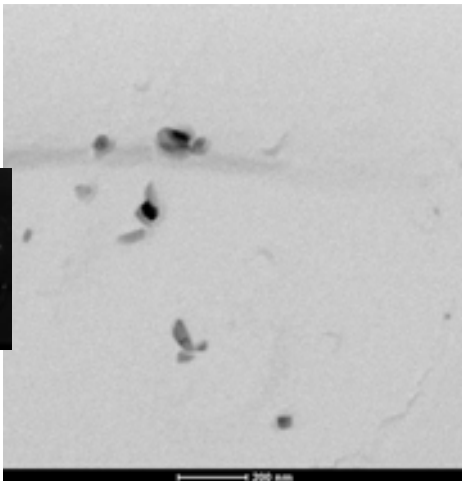
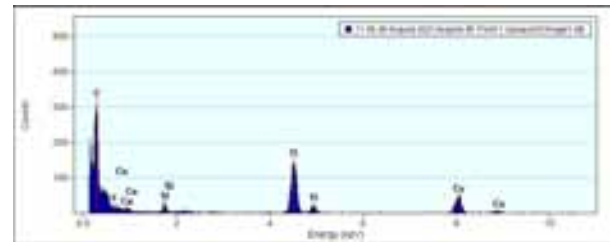
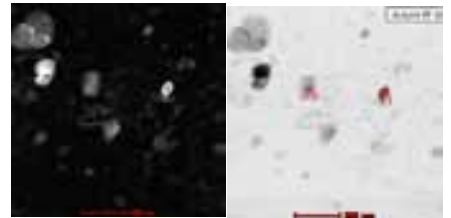


Foto11



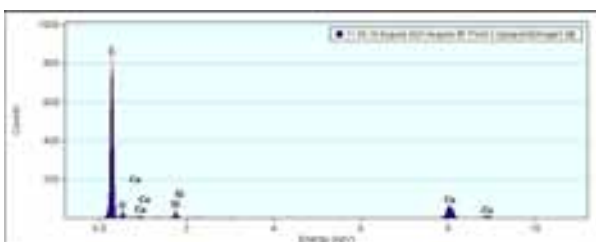
IMÁGENES DE STEM

1



IMÁGENES DE STEM

2

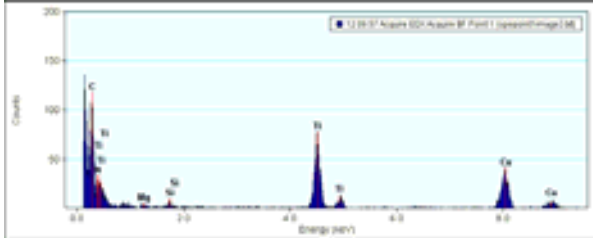


IMÁGENES DE STEM



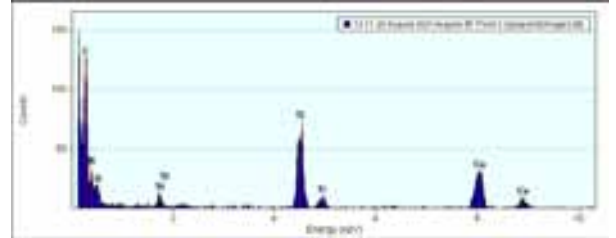
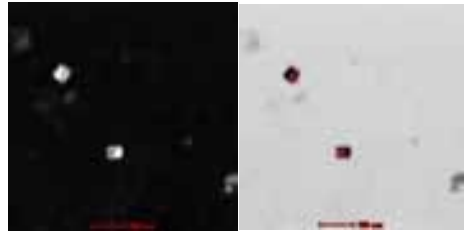
IMÁGENES DE STEM

1



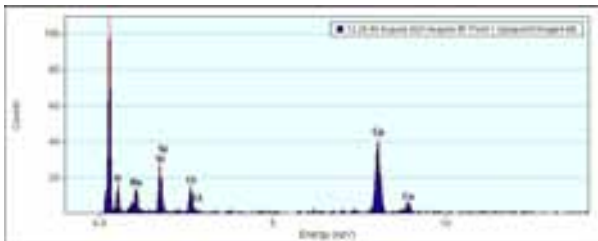
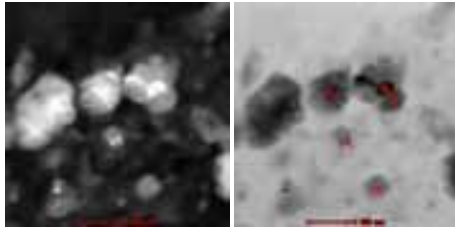
IMÁGENES DE STEM

2



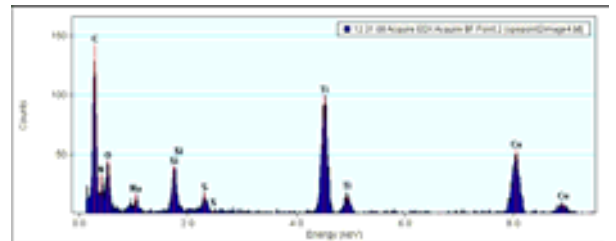
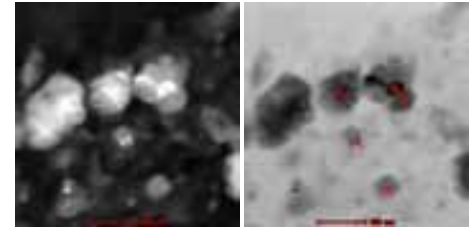
IMÁGENES DE STEM

1



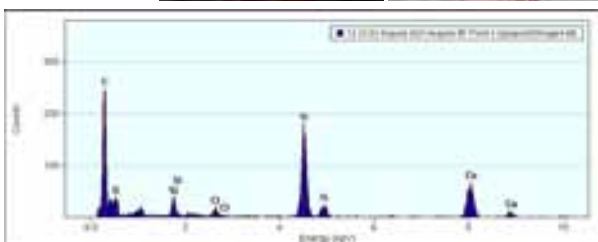
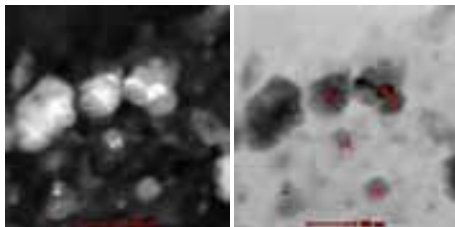
IMÁGENES DE STEM

2



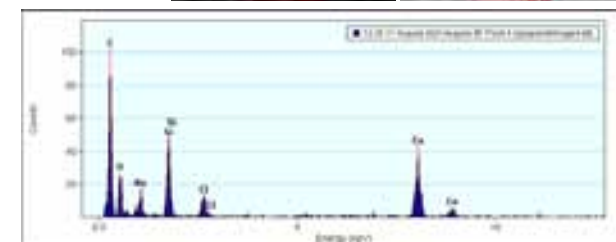
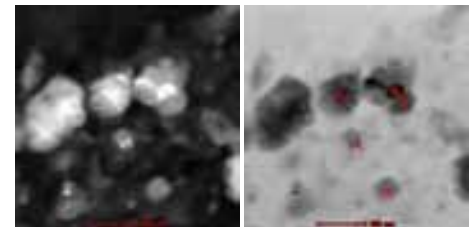
IMÁGENES DE STEM

3



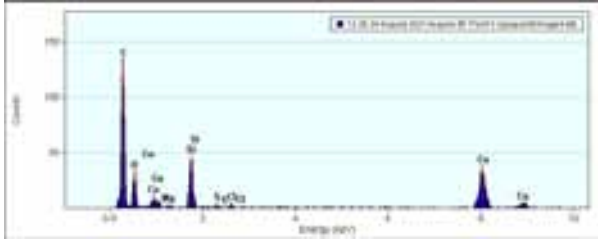
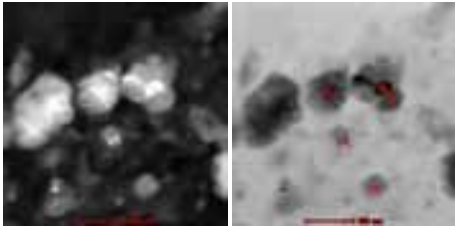
IMÁGENES DE STEM

4



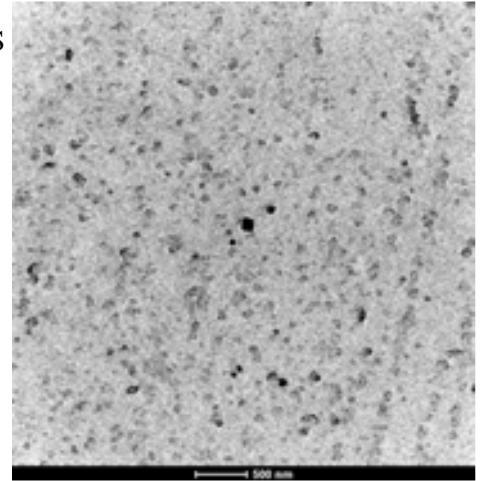
IMÁGENES DE STEM

5



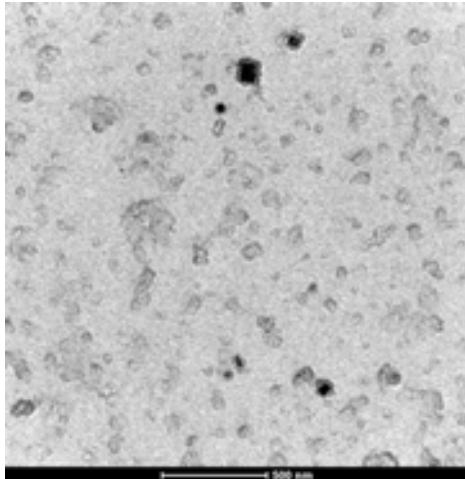
IMÁGENES DE TEM

Marsella Foto1



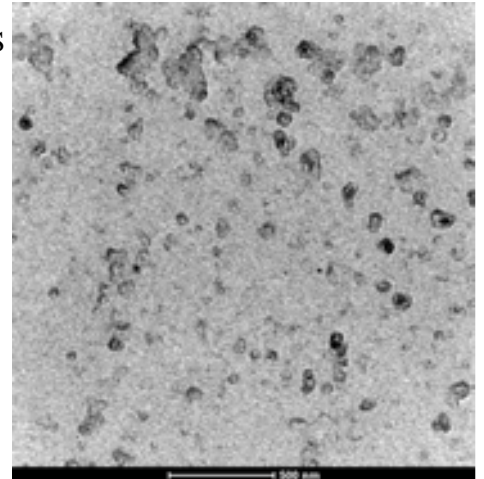
IMÁGENES DE TEM

Marsella Foto2



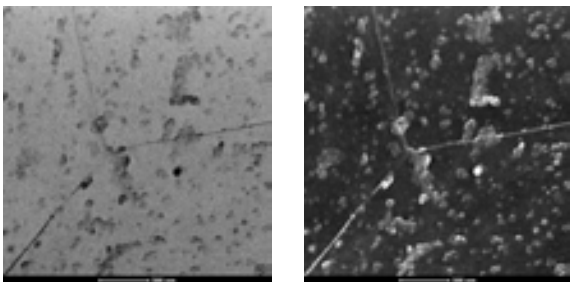
IMÁGENES DE TEM

Marsella Foto3



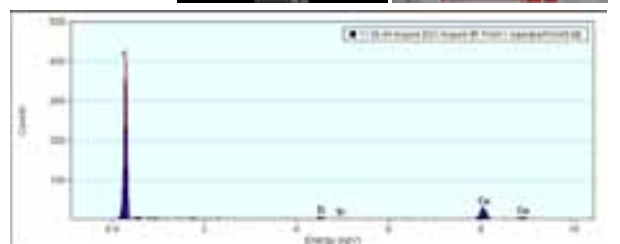
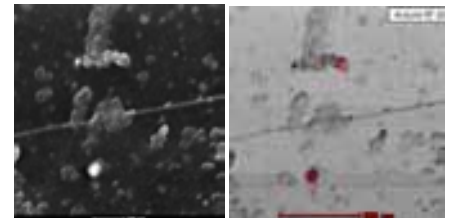
IMÁGENES DE STEM

Marsella Foto4



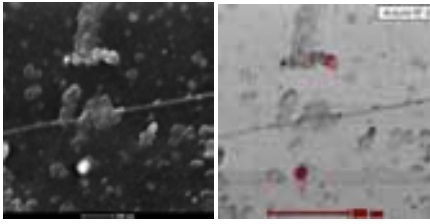
IMÁGENES DE STEM

1



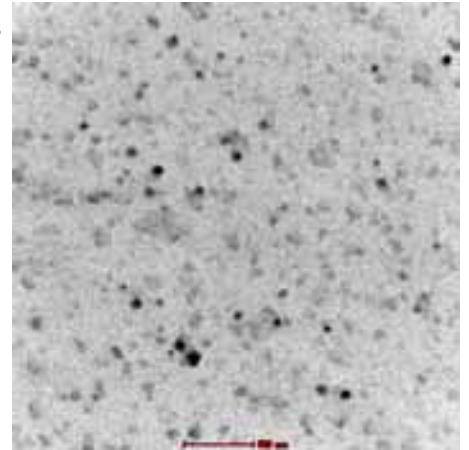
IMÁGENES DE STEM

2



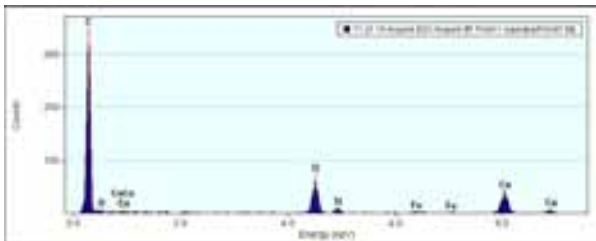
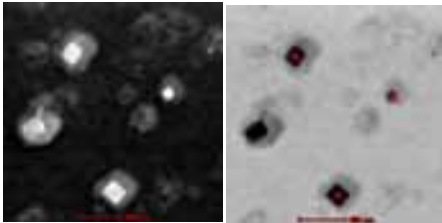
IMÁGENES DE TEM

Marsella
Foto6



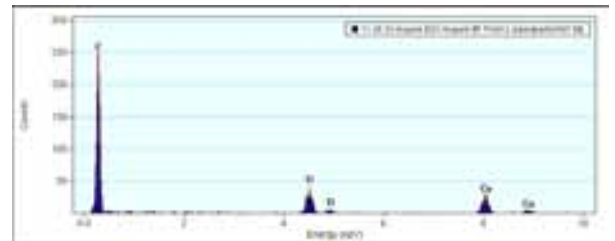
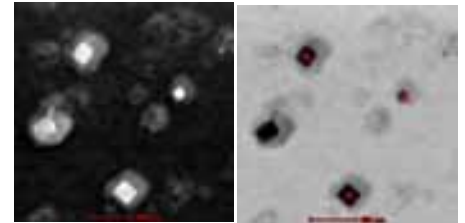
IMÁGENES DE STEM

1



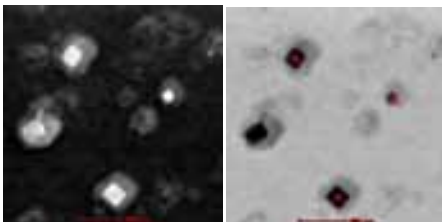
IMÁGENES DE STEM

2



IMÁGENES DE STEM

3



MUESTRA 4

IMÁGENES DE TEM

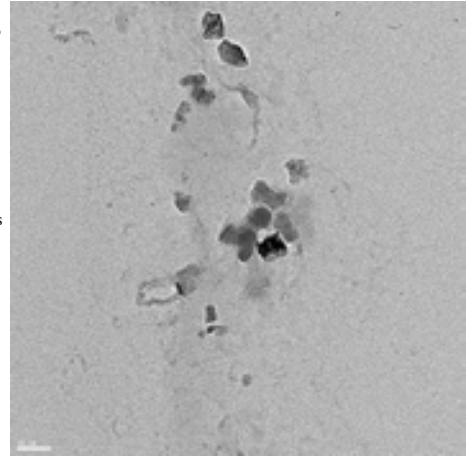
MUESTRA 4

JEOL JEM 2010F
Field Emission Electron Microscope

IMÁGENES DE TEM

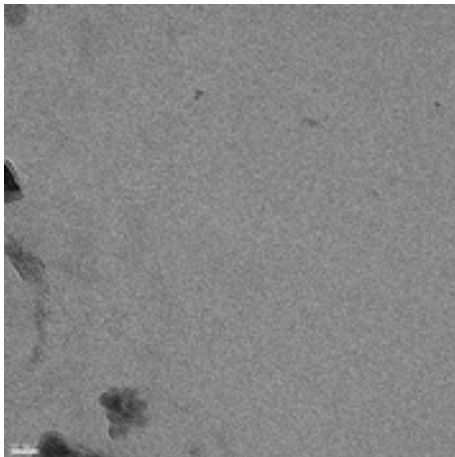
Gran cantidad de precipitados de tamaños pequeños, entre 2 y 10 nm, encontrándose en las fronteras y en el interior de los granos.

foto1
50nm



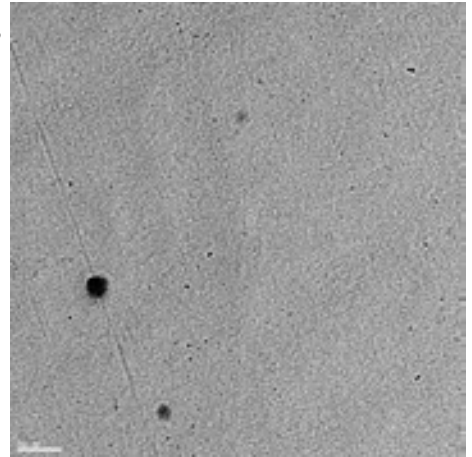
IMÁGENES DE TEM

foto2
20nm



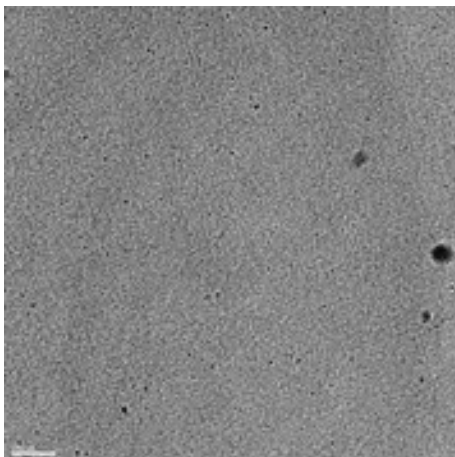
IMÁGENES DE TEM

foto3
100nm



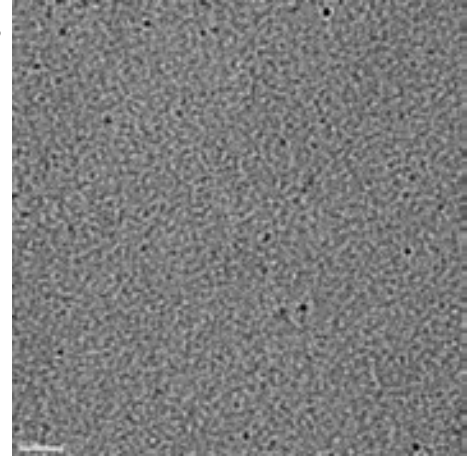
IMÁGENES DE TEM

foto4
100nm



IMÁGENES DE TEM

foto5
50nm



IMÁGENES
DE TEM

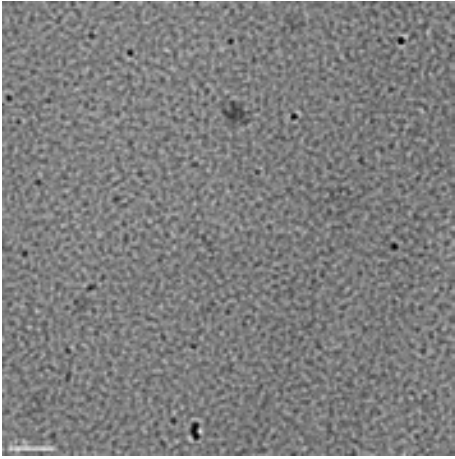


foto6
50nm

IMÁGENES
DE TEM

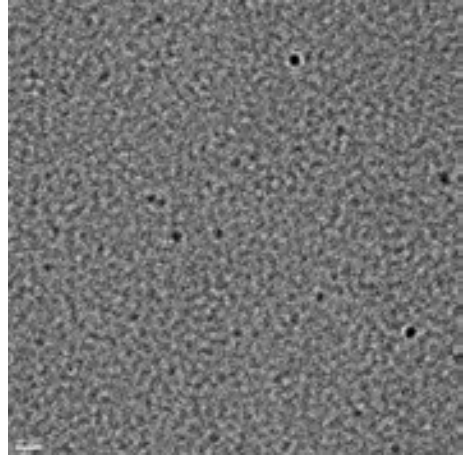


foto7
20nm

IMÁGENES
DE TEM

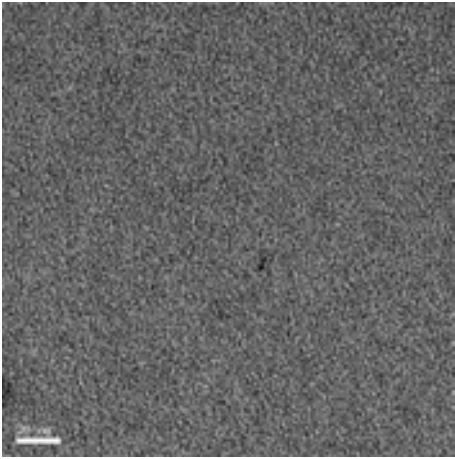


foto8
20nm

IMÁGENES
DE TEM

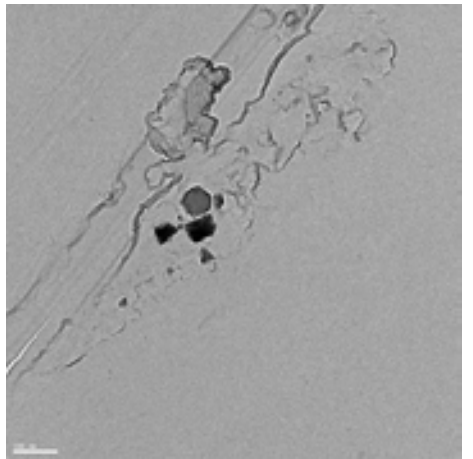


foto9
100nm

IMÁGENES
DE TEM

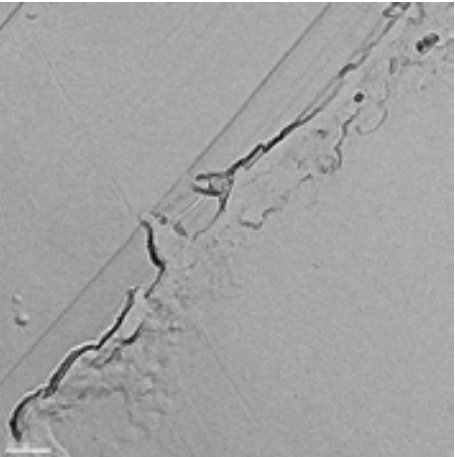


foto10
100nm

IMÁGENES
DE TEM

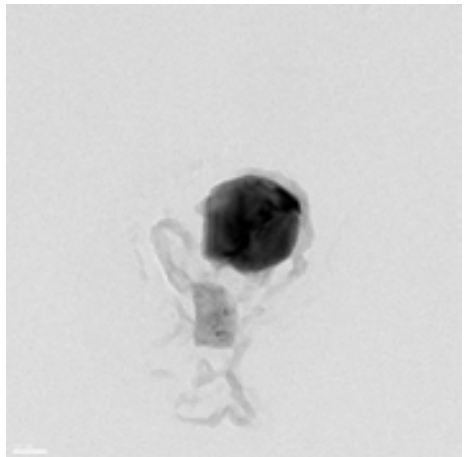
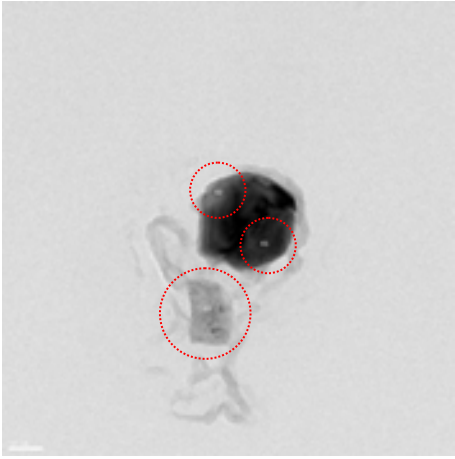


foto11
50nm

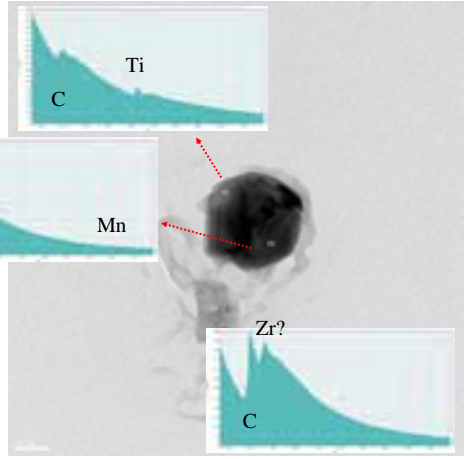
IMÁGENES DE TEM



EELS

foto11
50nm

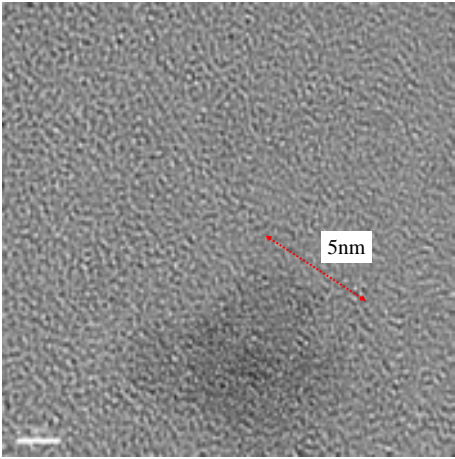
IMÁGENES DE TEM



EELS

foto11
50nm

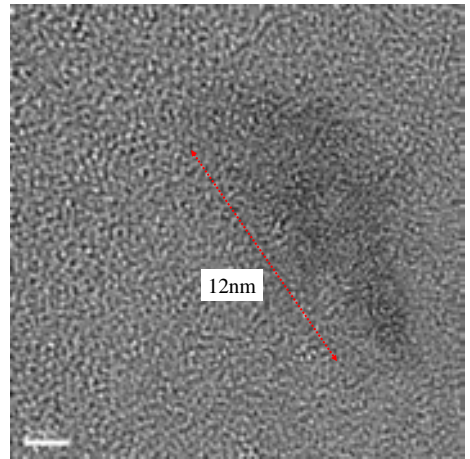
IMÁGENES DE TEM



High Resolution

foto12
2nm

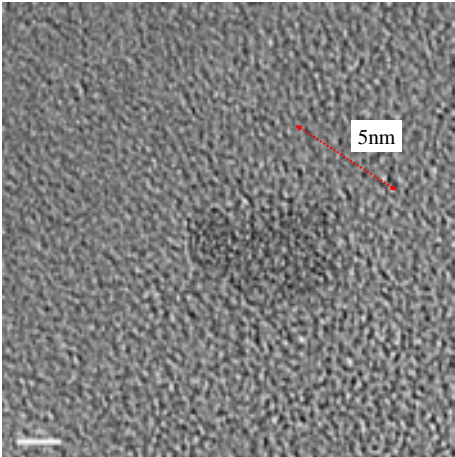
IMÁGENES DE TEM



High Resolution

foto13
2nm

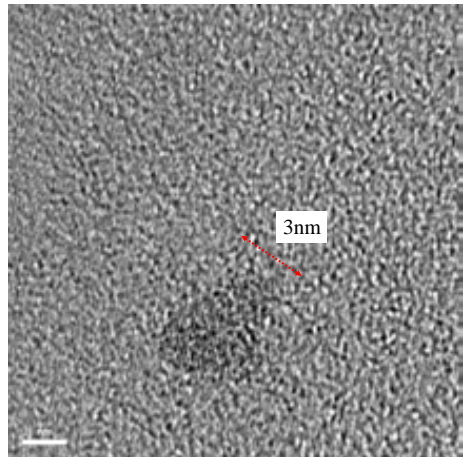
IMÁGENES DE TEM



High Resolution

foto14
2nm

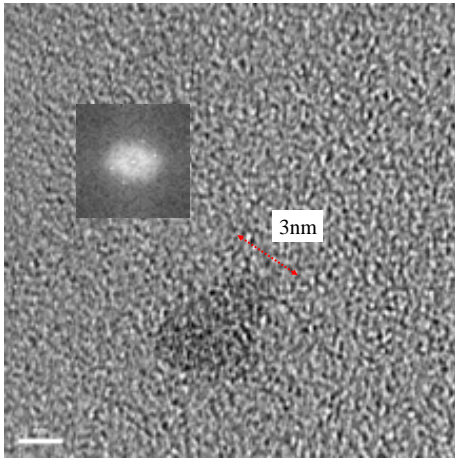
IMÁGENES DE TEM



High Resolution

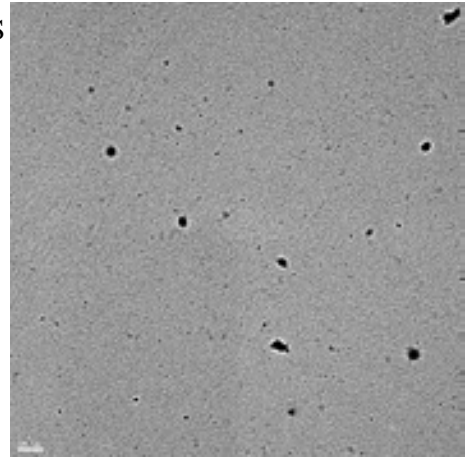
foto15
2nm

IMÁGENES
DE TEM

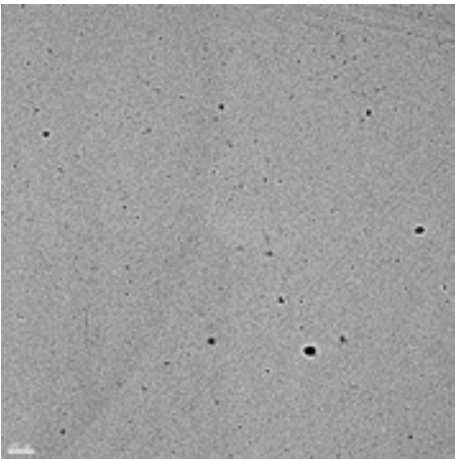


FFT

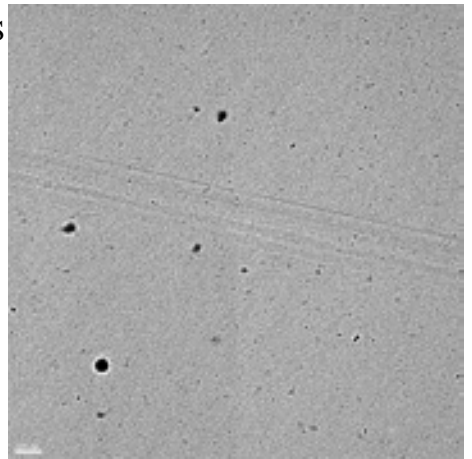
IMÁGENES
DE TEM



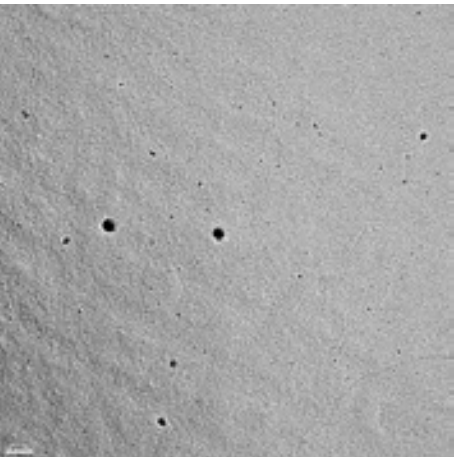
IMÁGENES
DE TEM



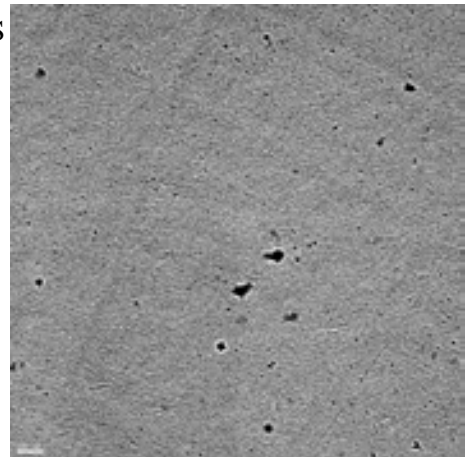
IMÁGENES
DE TEM



IMÁGENES
DE TEM



IMÁGENES
DE TEM



IMÁGENES
DE TEM

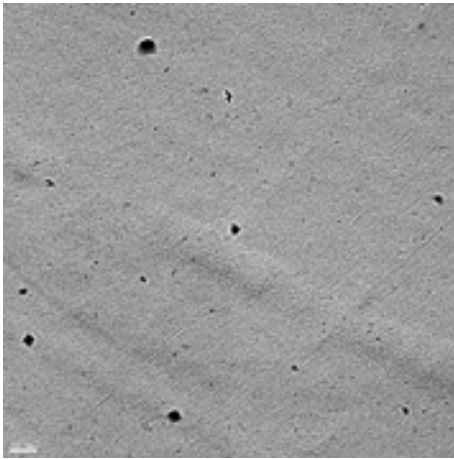


foto21
100nm

IMÁGENES
DE TEM

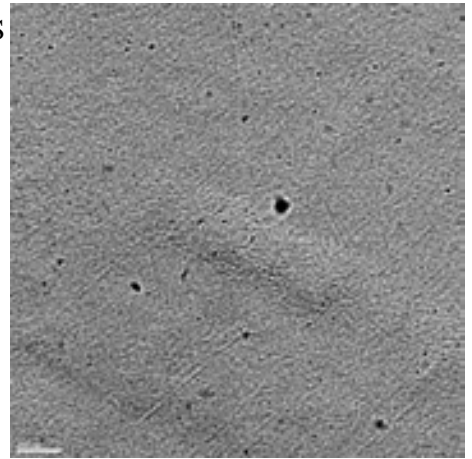


foto22
100nm

MUESTRA 5

IMÁGENES DE TEM

MUESTRA 5

JEOL JEM 2010F
Field Emission Electron Microscope

IMÁGENES
DE TEM

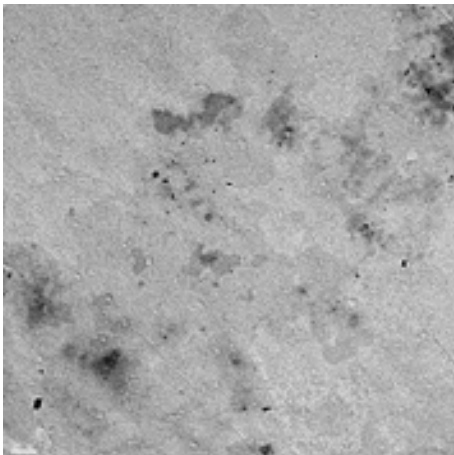


foto1
100nm

IMÁGENES
DE TEM

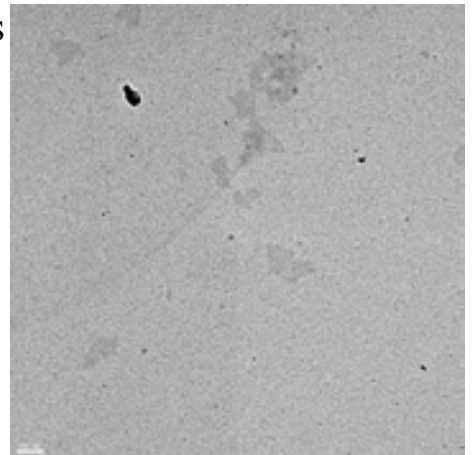


foto2
100nm

IMÁGENES
DE TEM

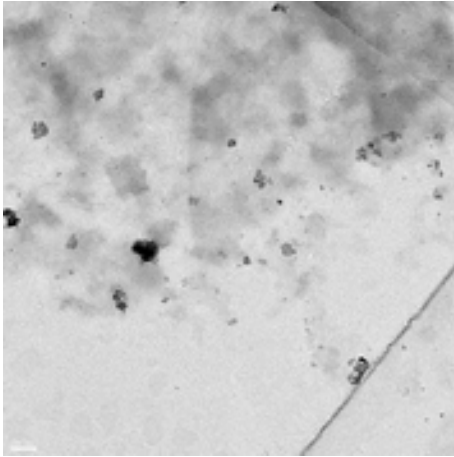


foto3
100nm

IMÁGENES
DE TEM

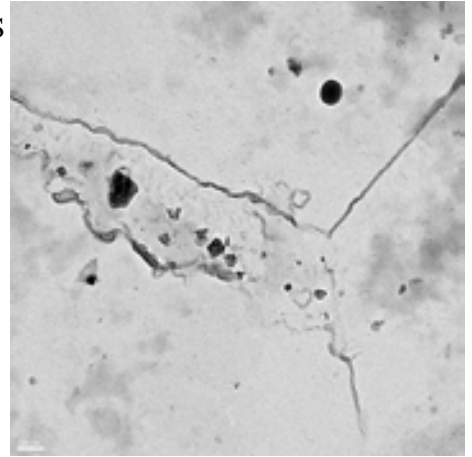


foto4
100nm

IMÁGENES
DE TEM

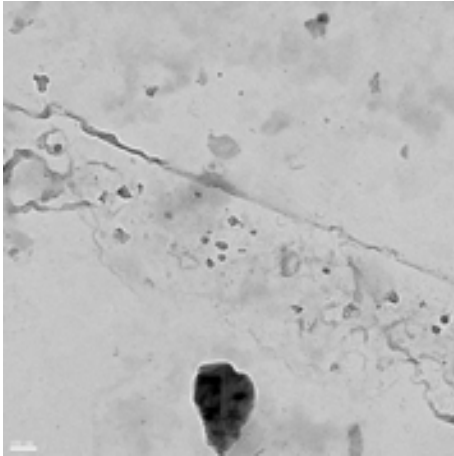


foto5
100nm

IMÁGENES
DE TEM

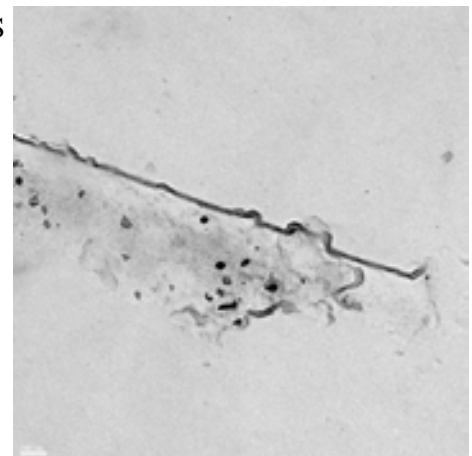


foto6
100nm

IMÁGENES
DE TEM

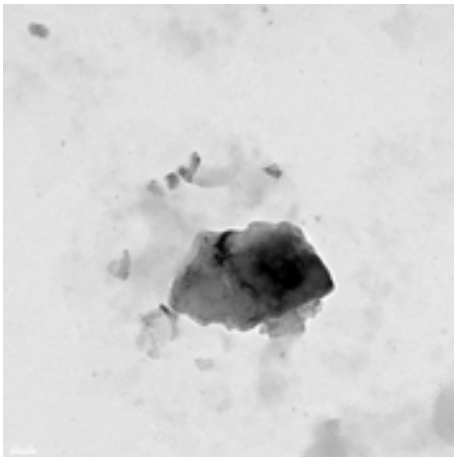


foto7
100nm

IMÁGENES
DE TEM

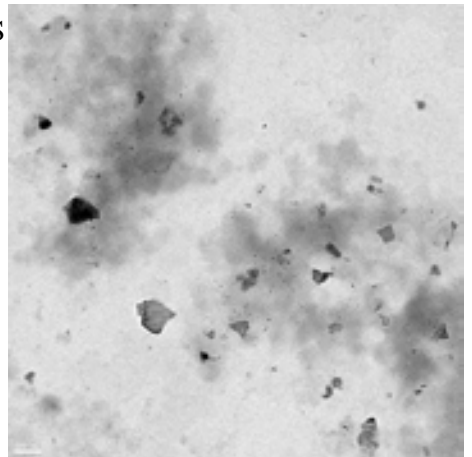


foto8
100nm

IMÁGENES
DE TEM

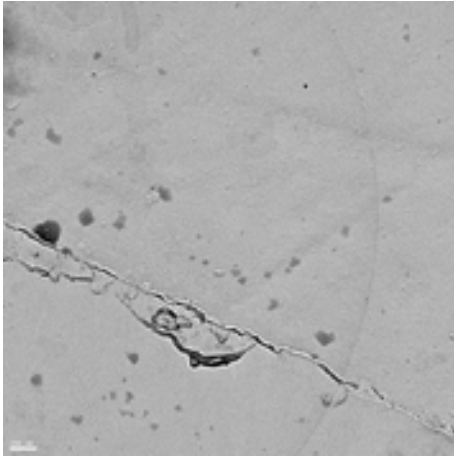


foto9
100nm

IMÁGENES
DE TEM

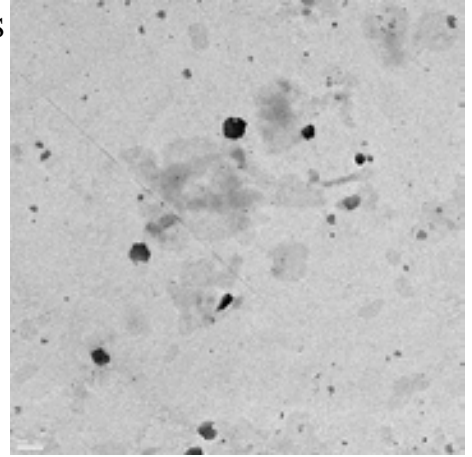


foto10
100nm

IMÁGENES
DE TEM

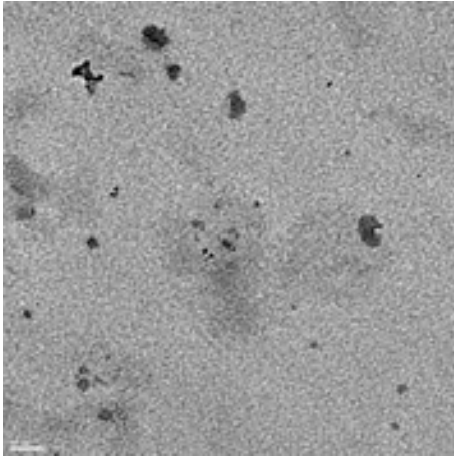


foto11
100nm

IMÁGENES
DE TEM

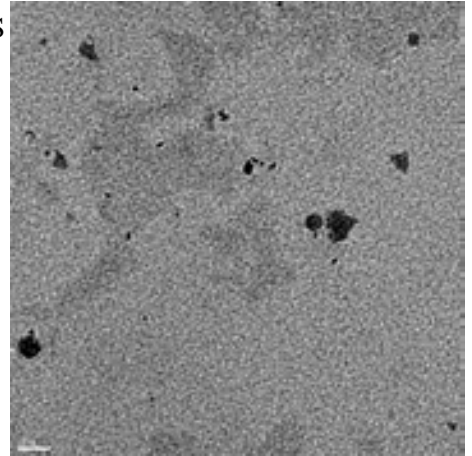


foto12
50nm

IMÁGENES
DE TEM

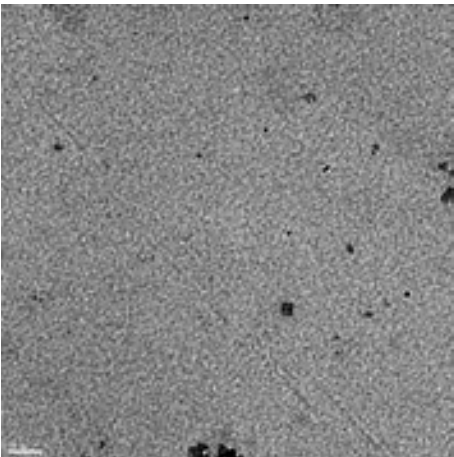


foto13
50nm

IMÁGENES
DE TEM

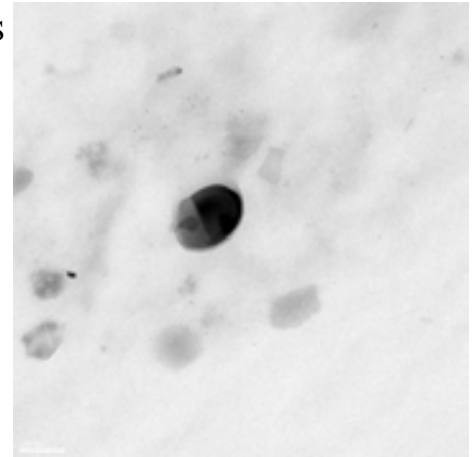


foto14
100nm

IMÁGENES
DE TEM

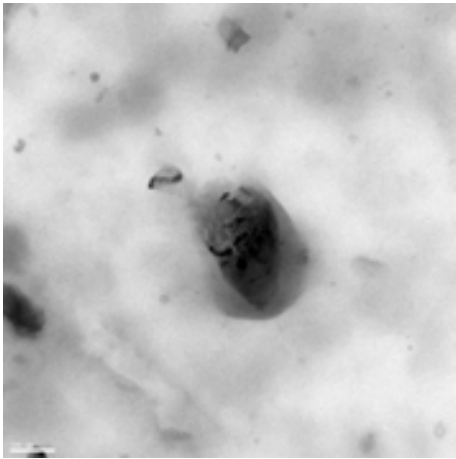
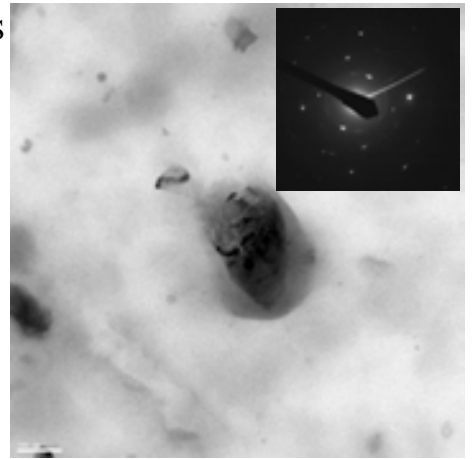


foto15
100nm

IMÁGENES
DE TEM



Difracción

foto15
100nm

IMÁGENES
DE TEM

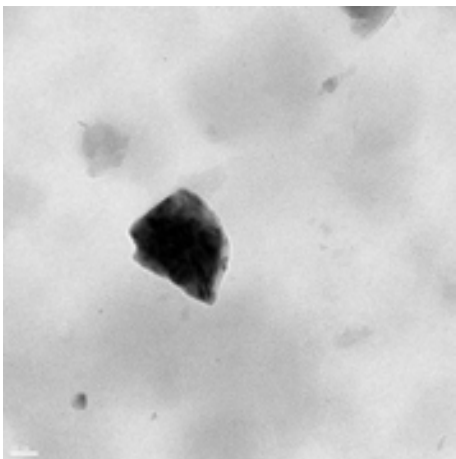
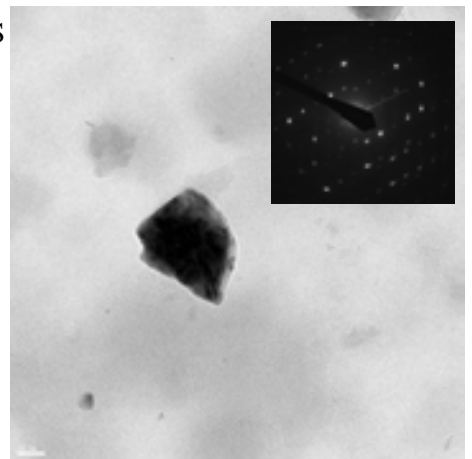


foto16
50nm

IMÁGENES
DE TEM



Difracción

foto16
50nm

IMÁGENES
DE TEM

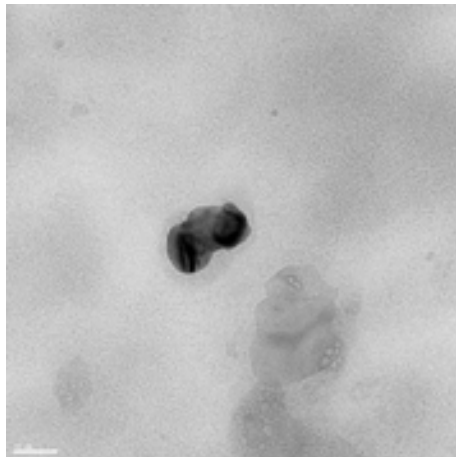
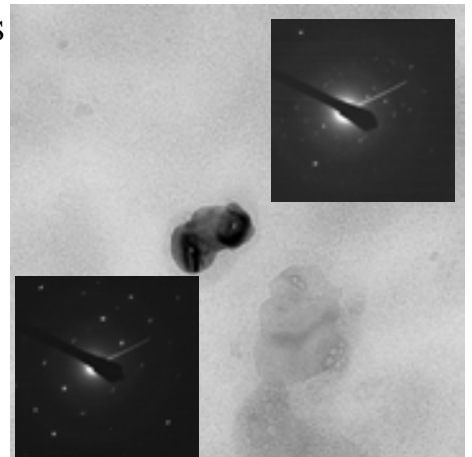


foto17
50nm

IMÁGENES
DE TEM



Difracción

foto17
50nm

IMÁGENES DE TEM

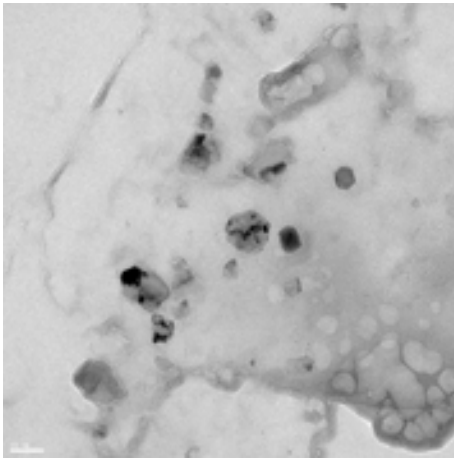


foto18
50nm

IMÁGENES DE TEM

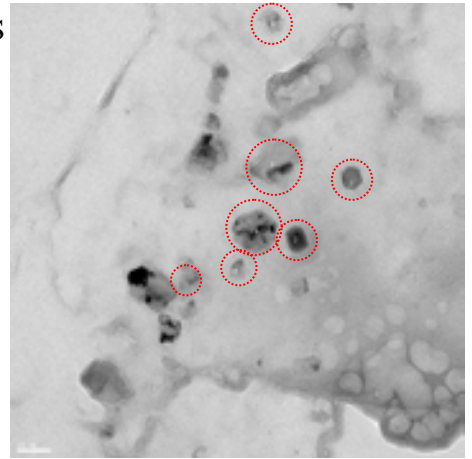
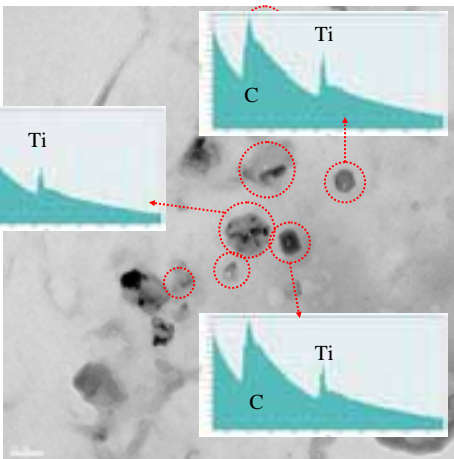


foto18
50nm

IMÁGENES DE TEM



EELS

foto18
50nm

IMÁGENES DE TEM

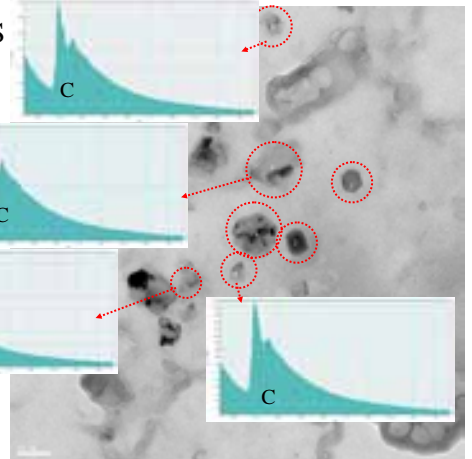


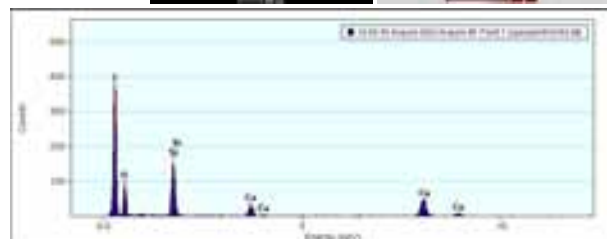
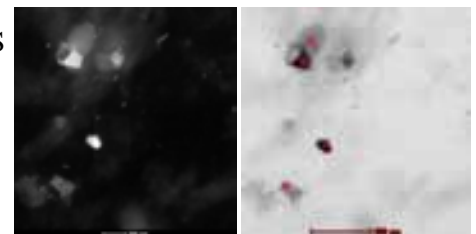
foto18
50nm

MUESTRA 5

FEI Tecnai G2
Scanning Transmission
Electron Microscope

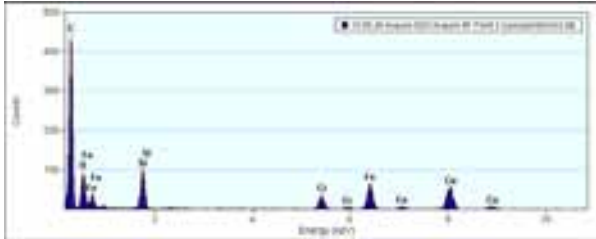
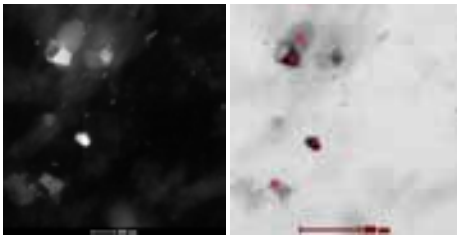
IMÁGENES DE STEM

1



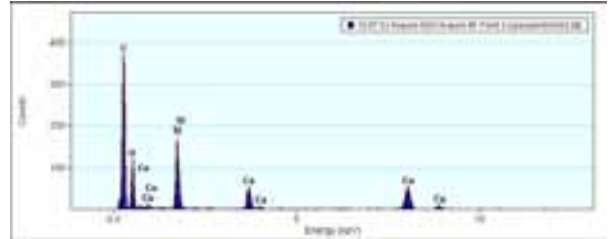
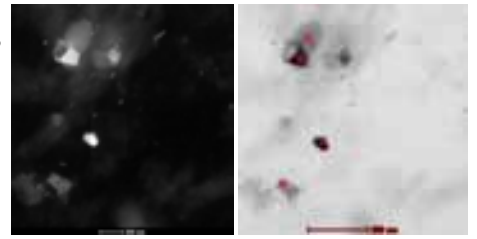
IMÁGENES DE STEM

2



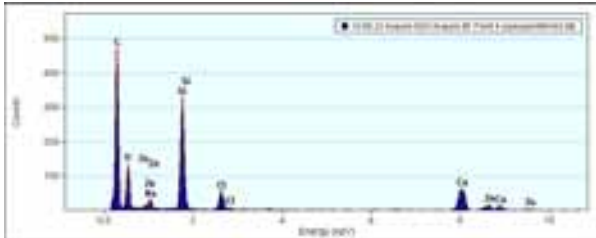
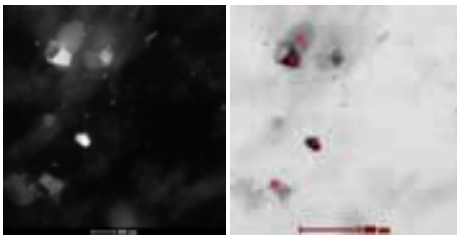
IMÁGENES DE STEM

3



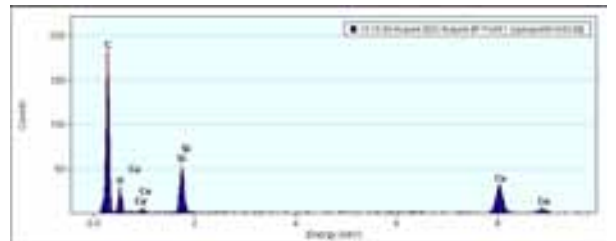
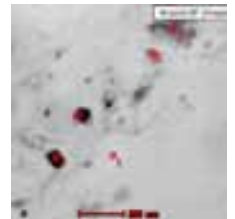
IMÁGENES DE STEM

4



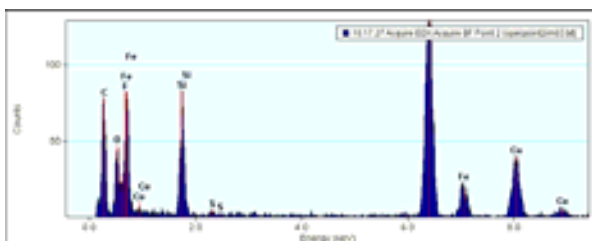
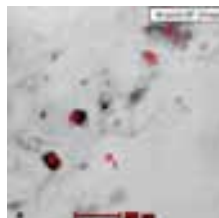
IMÁGENES DE STEM

1



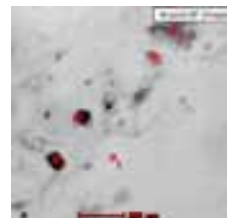
IMÁGENES DE STEM

2



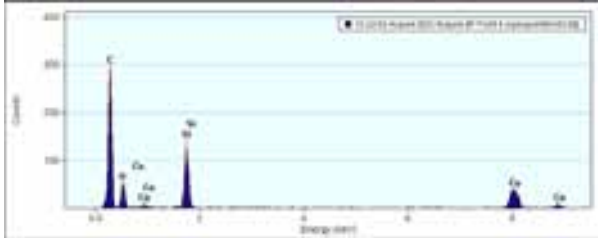
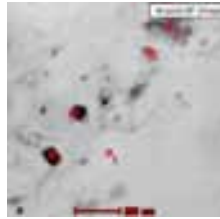
IMÁGENES DE STEM

3



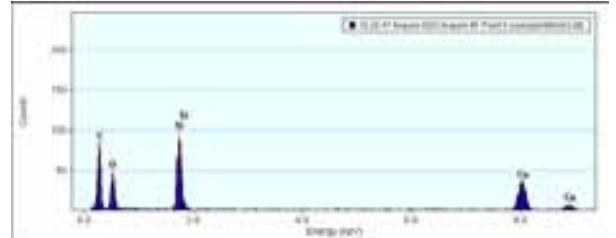
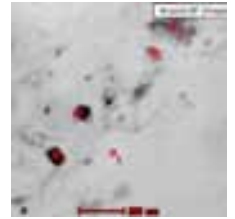
IMÁGENES DE STEM

4



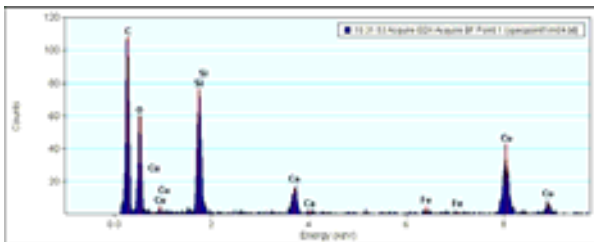
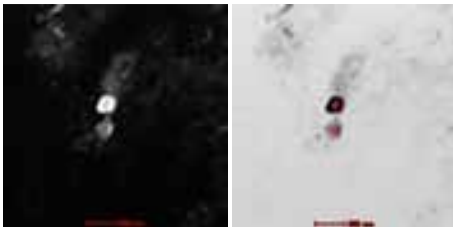
IMÁGENES DE STEM

5



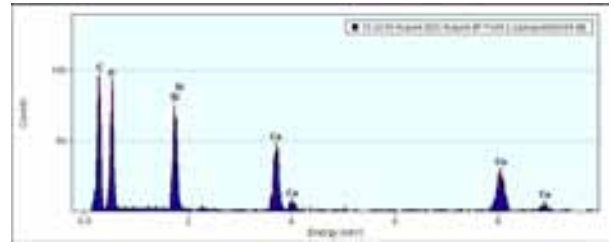
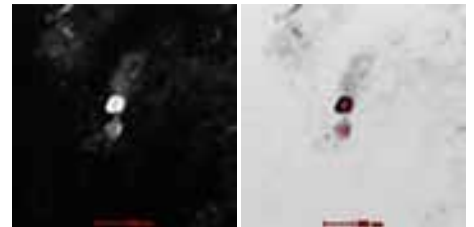
IMÁGENES DE STEM

1



IMÁGENES DE STEM

2



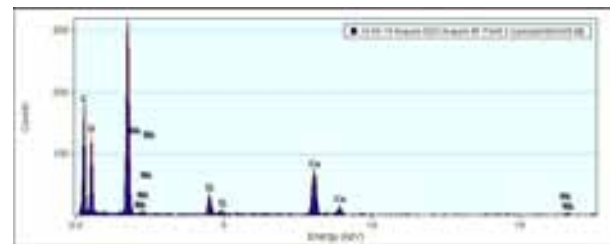
IMÁGENES DE STEM

1

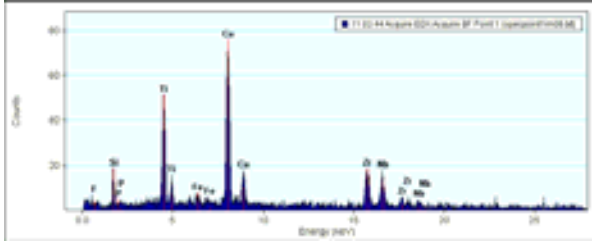
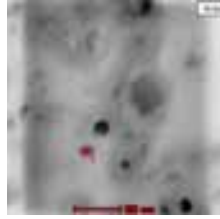


IMÁGENES DE STEM

2



IMÁGENES DE STEM



IMÁGENES DE STEM

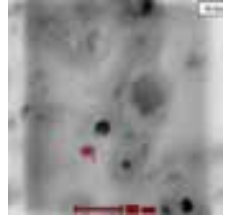
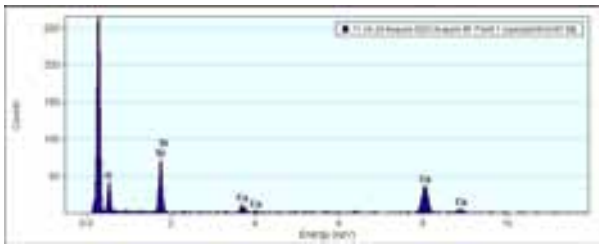
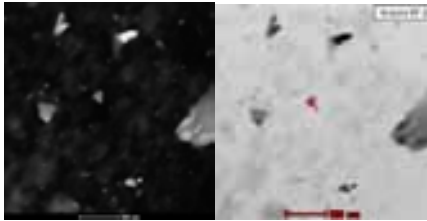
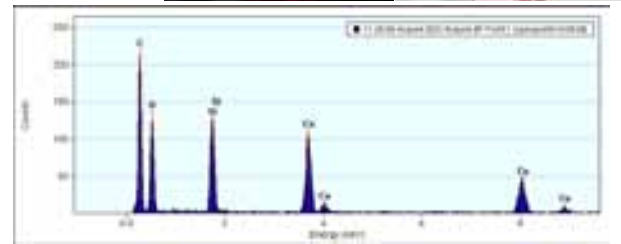


foto6

IMÁGENES DE STEM



IMÁGENES DE STEM



IMÁGENES DE TEM

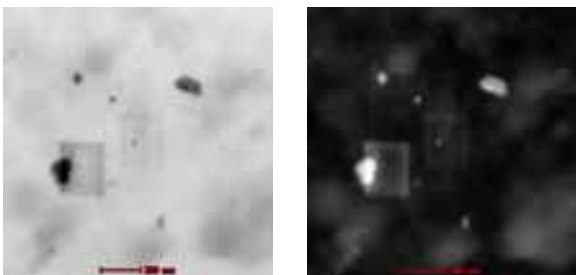


foto11

IMÁGENES DE TEM

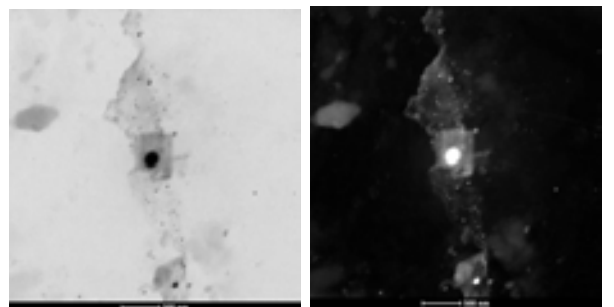


foto12

MUESTRA 6

IMÁGENES DE TEM

MUESTRA 6

JEOL JEM 2010F
Field Emission Electron Microscope

IMÁGENES
DE TEM

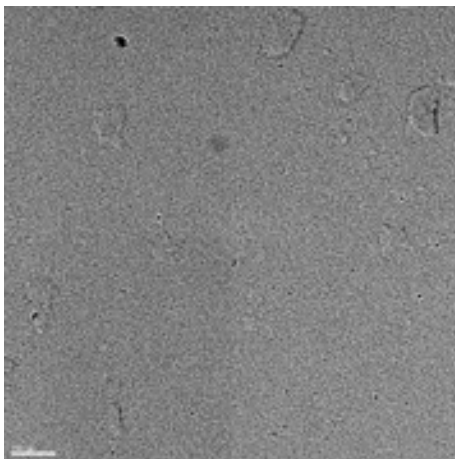


foto1
100nm

IMÁGENES
DE TEM

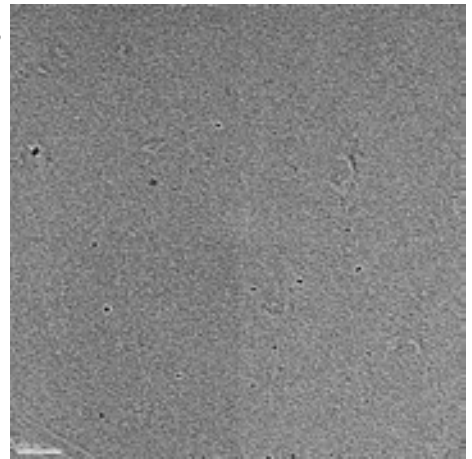


foto2
100nm

IMÁGENES
DE TEM

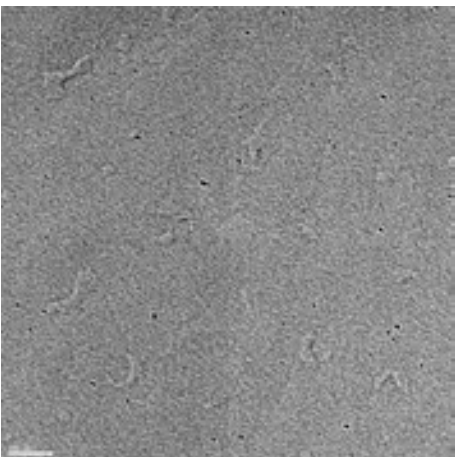


foto3
100nm

IMÁGENES
DE TEM

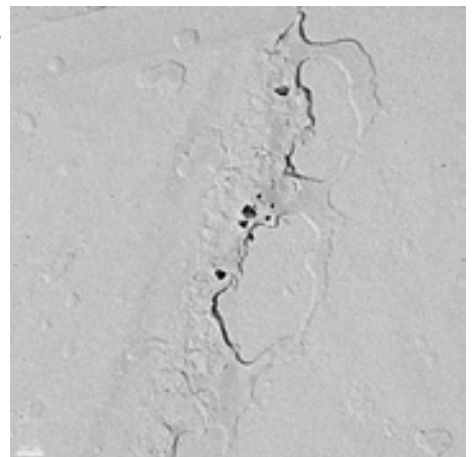


foto4
100nm

IMÁGENES
DE TEM

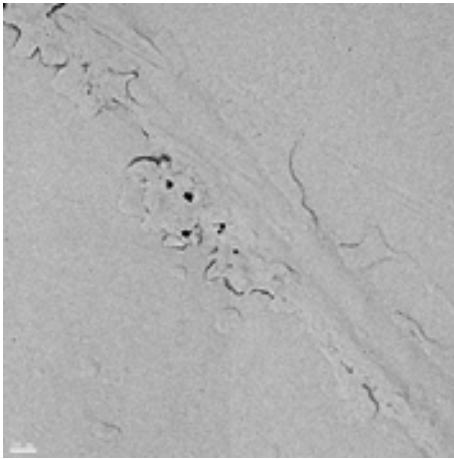


foto5
100nm

IMÁGENES
DE TEM

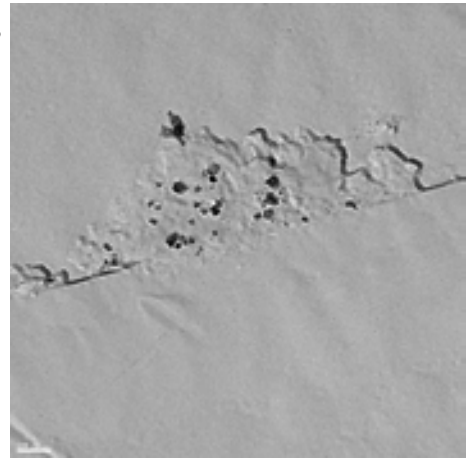


foto6
100nm

IMÁGENES
DE TEM

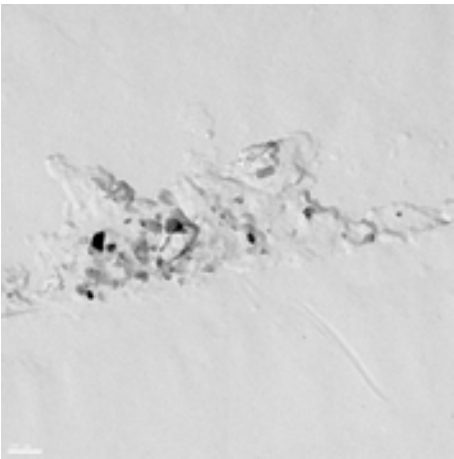


foto7
100nm

IMÁGENES
DE TEM

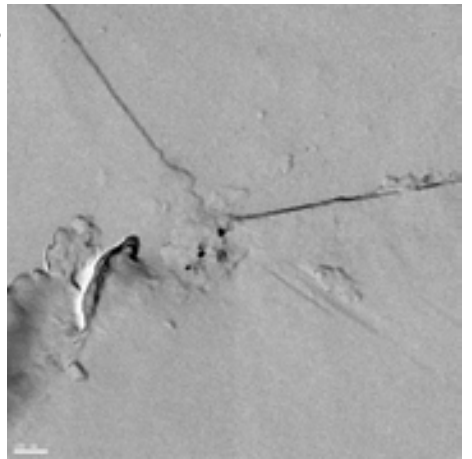


foto8
100nm

IMÁGENES
DE TEM



foto8
100nm

IMÁGENES
DE TEM

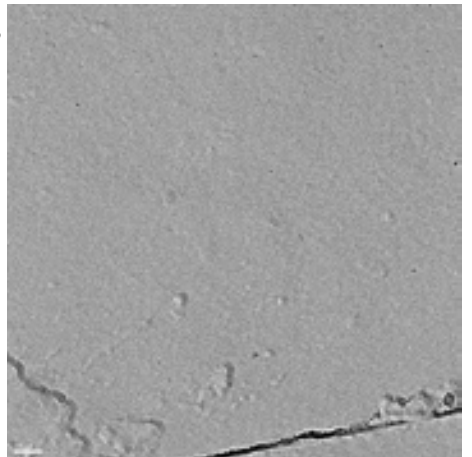


foto9
50nm

IMÁGENES
DE TEM

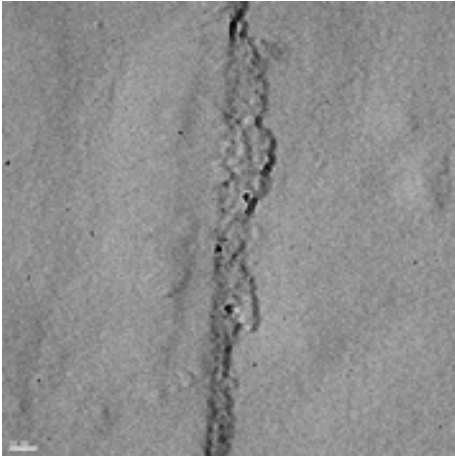


foto10
50nm

IMÁGENES
DE TEM

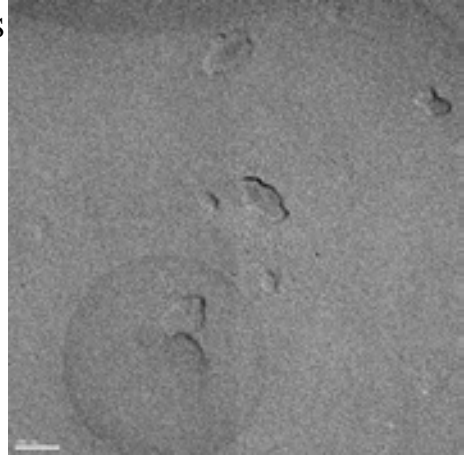


foto11
100nm

IMÁGENES
DE TEM

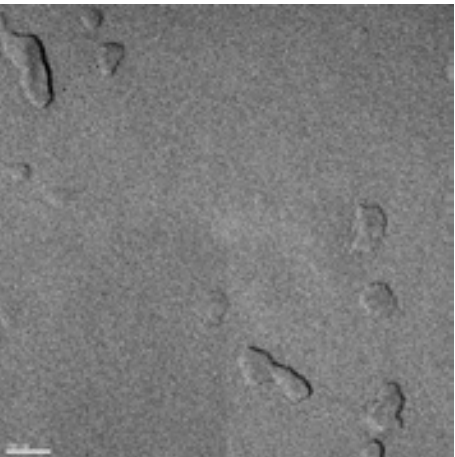


foto12
100nm

IMÁGENES
DE TEM

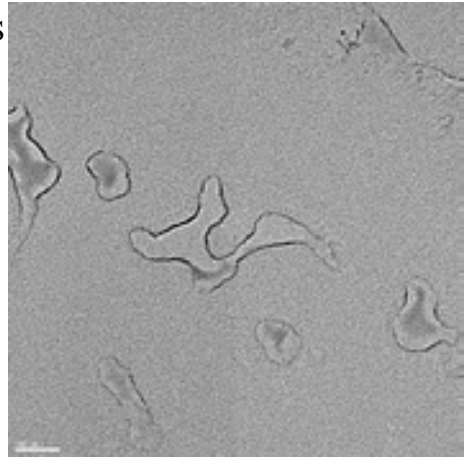


foto13
100nm

IMÁGENES
DE TEM

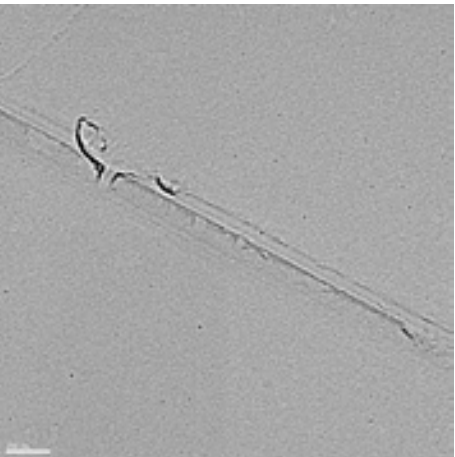


foto14
100nm

IMÁGENES
DE TEM

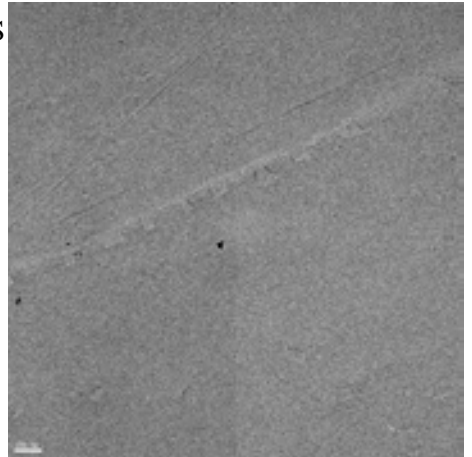


foto15
100nm

IMÁGENES
DE TEM

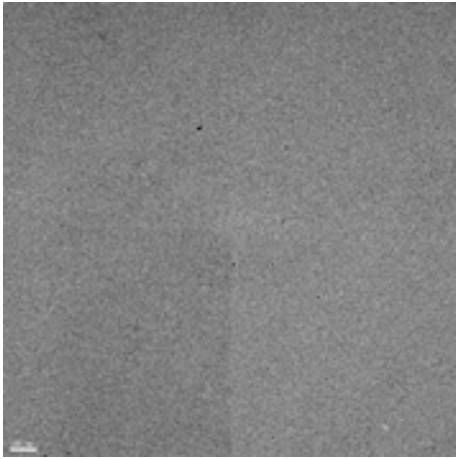


foto16
100nm

IMÁGENES
DE TEM

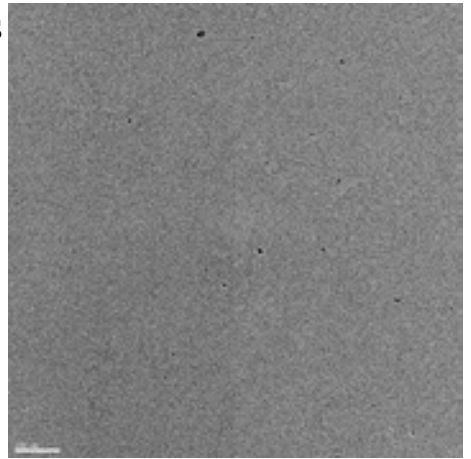


foto17
100nm

IMÁGENES
DE TEM

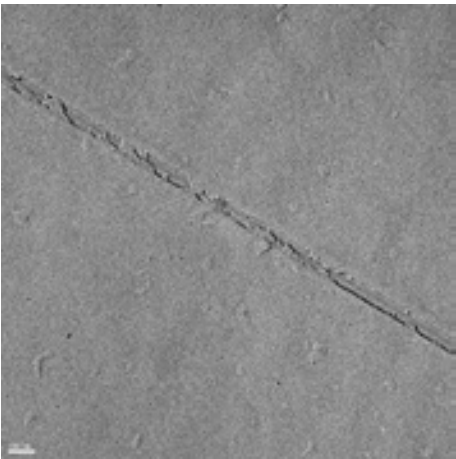


foto18
100nm

IMÁGENES
DE TEM

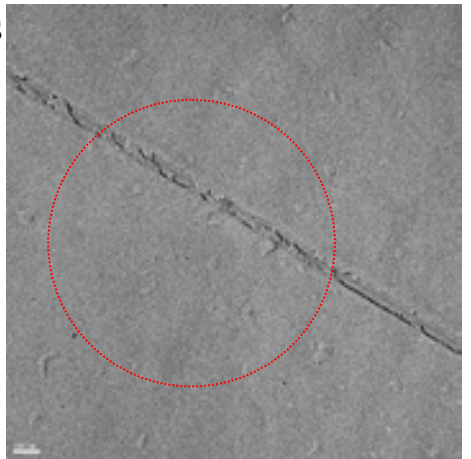


foto18
100nm

IMÁGENES
DE TEM

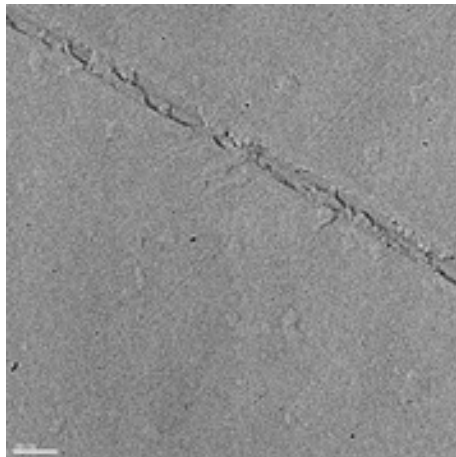


foto19
100nm

IMÁGENES
DE TEM

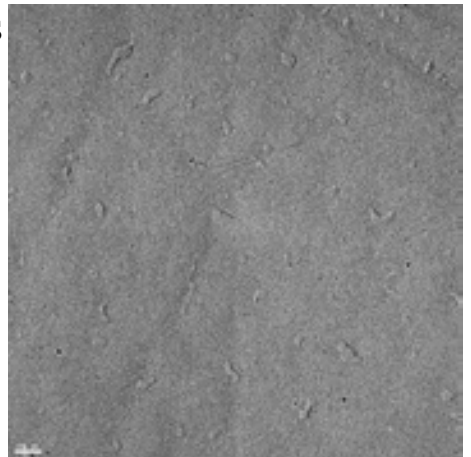


foto20
100nm

IMÁGENES
DE TEM

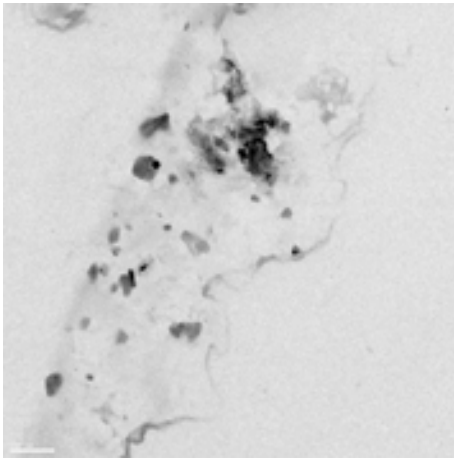
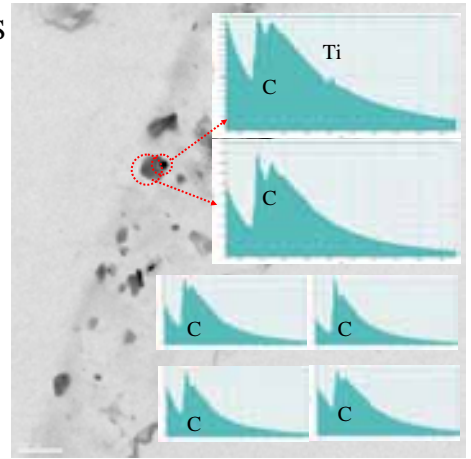


foto21
100nm

IMÁGENES
DE TEM



EELS

foto21
100nm

Muestra 1

- Precipitados de todos los tamaños, sobre todo en las fronteras de grano.
- La forma predominante es cuadrada o rectangular.
- Gran cantidad de nitratos de titanio. También pueden ser carburonitratos.
- Se encuentran carburos que no son de titanio. No se encuentra zirconio.
- En general no se encuentran precipitados en el interior de los granos.
- La muestra preparada con nital es posible que esté sobreatacada.

Muestra 2

- Predominio de los precipitados de tamaños medianos, entre 30 y 60 nm, sobre todo en las fronteras de grano.
- La forma predominante es redondeada.
- Gran cantidad de nitratos de zirconio de formas poligonales. También pueden ser carburonitratos.
- Se encuentran gran cantidad de carburos. (posiblemente contaminación de partículas de diamante)
- Poca cantidad de nitratos de titanio. Posiblemente el titanio sobrante forma carburosulfatos, de forma redondeada.
- Generalmente no se encuentran precipitados en el interior de los granos.

Muestra 4

- Predominio de los precipitados de tamaños pequeños, entre 2 y 10 nm, encontrándose en las fronteras y en el interior de los granos.
- Gran cantidad de carburos de zirconio de formas poligonales.
- Poca cantidad de nitratos de titanio.
- Poca cantidad de precipitados de tamaños grandes en el interior de los granos.

Muestra 5

- Predominio de los precipitados de tamaños pequeños, dentro y en los límites de los granos.
- No se encuentra gran cantidad de precipitados de tamaños grandes y medios.
- Formas generalmente redondeadas y poligonales.
- Gran cantidad de carburos de titanio.
- No se encuentran nitratos.

Muestra 6

- Predominio de precipitados de pequeño tamaño.
- En general no se encuentran precipitados de tamaños grandes y medios.
- Se encuentran nitratos de titanio y carburos.

Observaciones I

- No se puede determinar si se trata de nitratos o de carburonitratos en precipitados de pequeño tamaño de titanio, debido a que la muestra tiene C y al tamaño del haz.
- Una parte del silicio detectado en los análisis EDX puede ser depositado sobre la réplica en la evaporación de carbono debido al vidrio que cubre las muestras.
- Detección de cobre debido a la rejilla portamuestras.
- No fue posible la observación de las muestras enviadas a Marsella.

Observaciones II

- EELS: Electron Energy Loss Spectra.
- STEM: Scanning Transmission Electron Microscope.

Appendix 5: Guide for TEM observation procedures

START

During this process is not allowed to enter or remove the sample holder.
In the box at right below, we have to type the follow commands:

LOAD HT ↵ high tension
RUN ↵ start
160 ↵ initial voltage
200 ↵ final voltage
1000(v) ↵ rate
30(s) ↵

When this process is finished, the sample can be entered or changed.

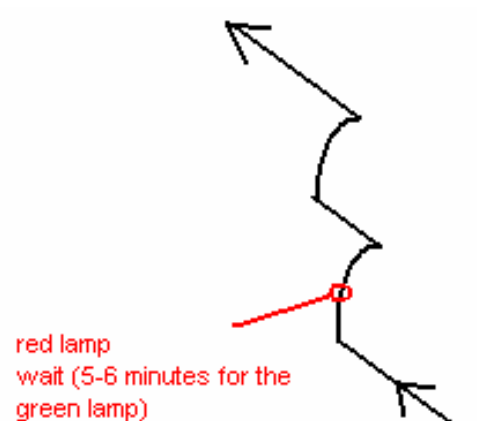
REMOVE OR INSERT THE SAMPLES

Before reach the current beam, we have to insert the sample. If the current beam is reached, it is needed to low to 0. The EDX detector has to be removed. To do it, to take out, it has to be turned in the right (horary) way; and in the left (antihorary) way to enter again.
Press **N** to go to (0,0,0)

Remove:



Insertion:



REACH THE BEAM CURRENT

The filament current usually is a half of the High Power of the microscopy. In this case, it is between 101 and 102 μA .

The currents is reached a few (1 point) etch 3 minutes approximately, between Off to 4 μA . After, the reached is slower, (1/2 point), until achieve 6 μA .

TO FIND THE VALID AREA

In thin foils the valid area is the hole, while in carbon replica the valid area is this film.

- 1- Go to low magnification: **Low Mag**.
- 2- To achieve more light, select less **spot size** until 1.
- 3- Find the valid area
- 4- Go to high magnification: **Mag 1**.

ALIGNMENT

Steps:

- Put DV (in the screen in the right) on 0. It is made with the *Focus*.
- Select x40K, with the *Selector*.
- Move X and/or Y *SHIFT* to put the beam in the middle.
- Make small the beam, with the *Brightness*. If it seems a concentric rings (amorphous) or dispersed spots (crystal), it means that the high is NOT OK, and is necessary to press Z control **↑** and **↓**.
- Open the beam, with the *Brightness*, and check if the circle is right. If not, the condensate aperture is NOT OK. (in the column). To make small the beam.
- Select *Spot size 1* and check if the point is still in the center. If not, press *Gun* (in the box of the right) and *Shift*, to move the point. Then, return to *Spot size 2* to check the same. In this case, it will be used the *Shift* of the high path. Try until the spot keeps in the center. Switch off the button *Gun* when it finished.

VOLTAGE

It is needed to select one particle and go to x120K magnification, press **HT** *wobbler* (right) and **BRIT TILT** (left). Then, with *Deflector Position* (Def) we can centered the point in the center until achieve no movement. When it is finished, unpress the buttons.

STIGMATISM

Press button **COND STIG** and to make the beam smallest. Then, move *Deflector Position X* and/or Y, to achieve a perfect circle.

PRECIPITATES SIZE

- Look for the magnification.

- Make the conversion using the table (cm → nm) (the scale in the screen is 1cm each 2 lines)

EDX

- Push **0** to remove the extra aperture.
- To insert the detector, it has to be turned until the end, in the left (antihorary) way.
- Push the button **EDS**.
- Center the beam on the particle.
- Choose the spot size. The spot size has to be as small as possible so 15 nm is the minimum spot size. If is too small, the sample can be transposed and it is needed to change to a bigger size spot.

DIFRACTION SOFTWARE

- Open the detector. If there are many iron, it is necessary to close quickly.
- Start: **●**
- Stop: **■**
- Save the spectrum (File→Save)
- Determinate elements: **?**
- See the spectrum: **Ⓜ** Choose the 0-8 range.
- Print: **🖨** Copy and paste (special paste) in a word file.

IMAGES SOFTWARE

Scale: press in the software: Image --> Scale Bar --> Draw to overlay

Contrast:

- Condenser aperture
- Objective aperture: push 1 or 2... to quit, push 0.

Focus:

- If the focus is higher than 20, is better to go to 0 and change the Z axis with **↑** and **↓**.
- If the image moves with the brightness, the focus are wrong.

FINISHING

- Temporally:
 - o Open the focus.
 - o Low the beam current until 4
 - o Take out the EDX detector (horary)
 - o Put the cover
 - o Low intensity of the right screen
- Permanently:
 - o Open the focus.
 - o Low the beam current until 0
 - o Take out the EDX detector (horary)
 - o Put the cover
 - o In the box at right below, we have to type the follow commands:
 - **ACCSET 160** acceleration settings
 - **RETURN**
 - o Low intensity of the right screen

Appendix 6: Photographic Gallery



Image 1: Pilot line of continuous annealing in St-Chely



Image 2: Embedding machine



Image 3: Embedding resin



Image 4: Polishing machine



Image 5: Diamond solution dispenser

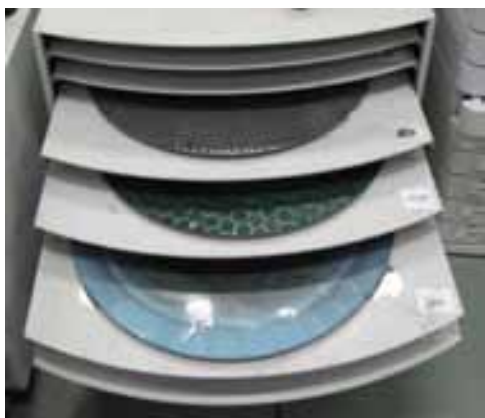


Image 6: Polishing dishes



Image 7: Carbon deposition device



Image 8: Micrometer



Image 9: Furnace

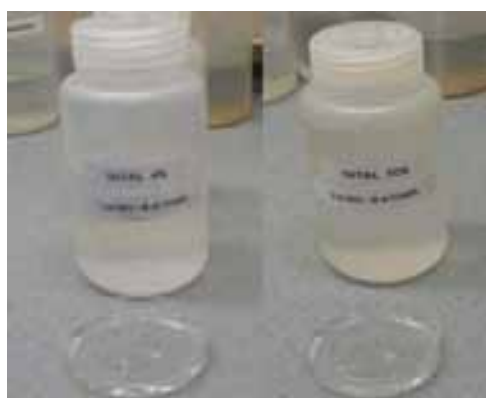


Image 10: Etching solutions



Image 11: Transmission Electron Microscope



Image 12: Optical microscope



Image 13: Guillotine



Image 14: Electrochemical etching device

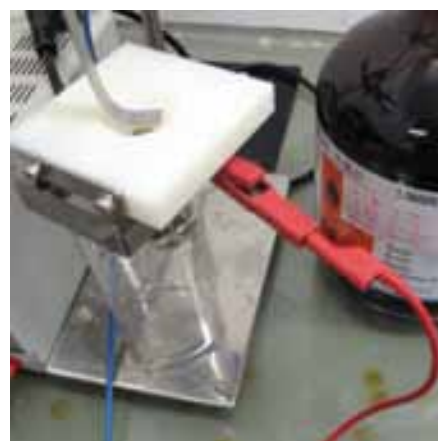


Image 15: Electrical steel samples



Image 16: TEM samples storage

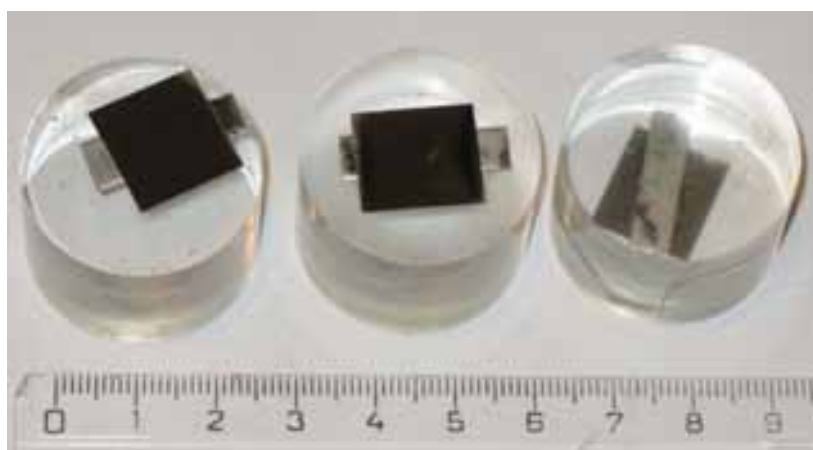


Image 17: TEM samples after polishing

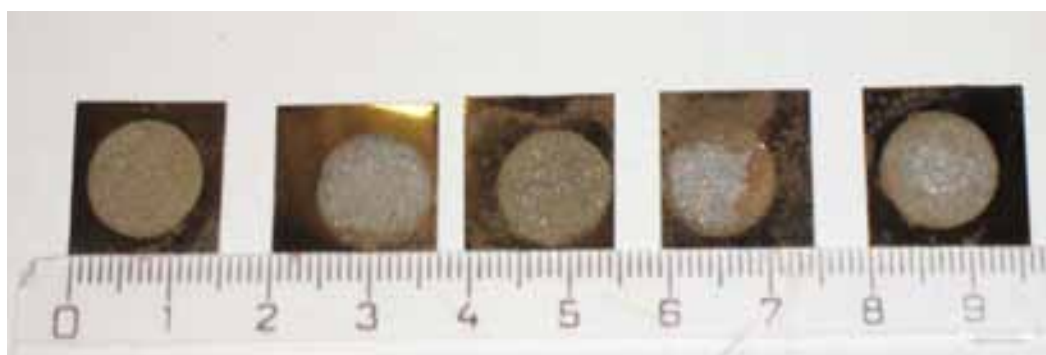


Image 18: TEM samples after electrochemical etching

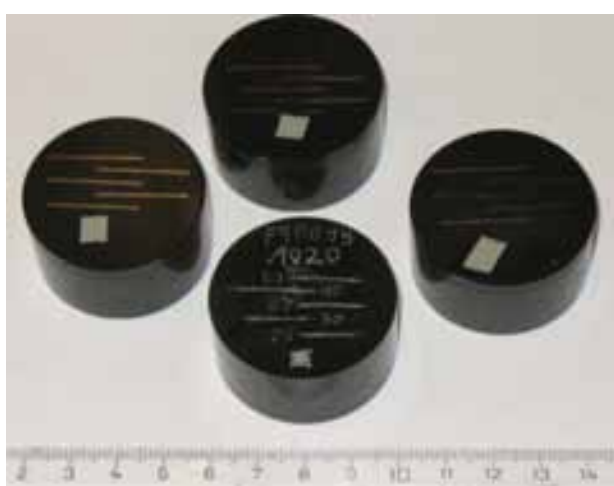


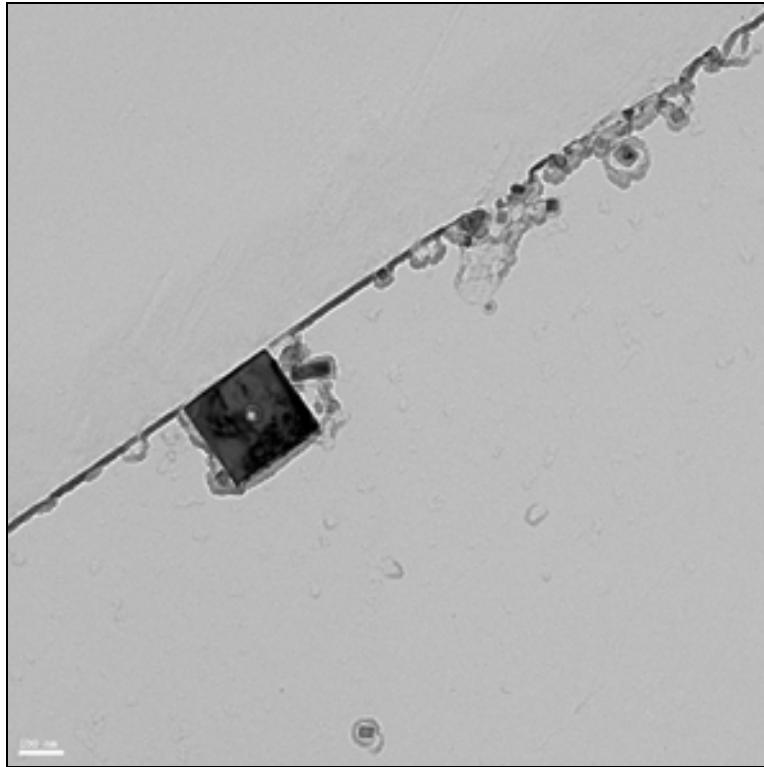
Image 19: Samples for grain size determination



Image 20: Magnetic measurements devices

MARGARITA MIRANDA DE LA TORRE

January, 2008



STUDY OF THE INFLUENCE OF GRAIN SIZE AND PRECIPITATES ON THE ELECTROMAGNETIC LOSSES IN DIFFERENT GRADES OF NON-ORIENTED FULLY PROCESSED ELECTRICAL STEEL

The study was performed in the installations of OCAS, a Steel Research Centre of ArcelorMittal. Taking M32 steel (3.25%Si+0.9%Al) as the basis chemical composition and three different thicknesses (0.35, 0.5 and 0.65mm), different annealing conditions (temperature and time) have been applied in the laboratory simulator at St.Chély, France. The aim was to link annealing parameters, grain size and energy loss. It was determined the optimum annealing parameters to reach the lowest power losses for three different grades of non-oriented fully processed electrical steel.

In addition, M250-50 samples having different magnetic behaviour (high and low losses) but the same grain size and texture, have been analyzed in terms of TEM observations of their precipitates, in the University of Marseille. The results reveal that a high amount of medium and big precipitates (>10 nm) worsen the magnetic properties of the material. The small precipitates (<10nm) do not have a strong influence on the magnetic properties. The presence of precipitates can have a great influence on the power losses and further work is clearly necessary.